UNIVERSITY OF PADOVA

DEPARTMENT OF INDUSTRIAL ENGINEERING

MASTER DEGREE IN CHEMICAL ENGINEERING AND INDUSTRIAL PROCESSES

Master Degree Thesis in
Chemical Engineering and Industrial Processes

DEVELOPMENT AND CHARACTERIZATION OF NANOCOMPOSITE MEMBRANES FOR GAS SEPARATION

Supervisor: Prof. Michele Modesti

Correlator: Prof. Vikas Mittal

Student: LUCA CERVELLIN

ACADEMIC YEAR: 2014-2015

Abstract

This thesis focuses on the development and characterization of poly(ether block amide) (PEBA) based membranes, with the aim of improving the properties of the material for potential gas separation applications.

The first part of the work has been based on the evaluation of the potential improvement of the physical properties of PEBA membrane by the introduction of graphene as reinforcing nanofiller.

The membranes were prepared by solution casting, dispersing graphene in the polymer solution. The samples obtained have been tested in terms of permeability to O_2, water vapor and CO_2, and the morphology has been explored by electron microscopy (SEM and TEM). To obtain a complete characterization, they were also conducted mechanical tests (tensile test), dynamic-mechanical (DMA), thermal analysis (DSC, TGA) and X-ray diffraction (XRD). The results obtained, have shown a reduction of gas permeability with increasing filler content (graphene), however, is very useful to increase the mechanical and thermal properties, improving them significantly.

In the second part of the work the introduction of ionic liquid inside the membranes, in order to obtain materials with an improved permeability. The disadvantage that has been noticed, is the decrease of the thermal and mechanical properties, because the ionic liquid, once introduced in the polymer matrix, acts as plasticizer, changing its domain. The samples prepared were analyzed using electron microscopy (SEM and TEM), mechanical (tensile test), dynamic-mechanical (DMA), thermal analysis (DSC, TGA) and X-ray diffraction (XRD). The results have shown that the ionic liquid added in the membranes has no interactions with graphene used as nanofiller.

In conclusion, on the basis of the study realized, it is possible to observe that, even though graphene and the ionic liquid have opposite effects on the properties of the membrane, when added together in the polymer matrix, there is an improvement of both the permeability.

Riassunto

Il progetto di tesi è stato realizzato ad Abu Dhabi, presso the Petroleum Institute, ed ha come obiettivo quello di fornire un sondaggio di tipo sperimentale con lo scopo di migliorare alcune caratteristiche del polyether block amide (PEBA), polimero oggetto di studi recenti, in modo da ottenere un materiale con proprietà utili per la separazione in fase gas.
Lo studio è stato diviso in due principali filoni di ricerca: nel primo, sono state preparate ed analizzate varie membrane a base di PEBA con l'aggiunta di grafene, il quale svolge una funzione di nanocarica, con l'obiettivo di migliorare le proprietà meccaniche e termiche del film. Successivamente, nel secondo filone di ricerca, sono stati realizzati i composti comprendendo anche il liquido ionico, con l'obiettivo di produrre membrane con un incremento delle proprietà permeanti.
Per quanto riguarda la prima linea di ricerca, le membrane sono state effettuate utilizzando un tipo di additivo: nanocarica industriale (grafene) a diverse concentrazioni (1,5%, 3% e 5% in peso). I campioni ottenuti sono stati caratterizzati da misure di permeabilità (O_2, CO_2 e vapore acqueo), analisi meccaniche (prova di trazione dinamometro), dinamico maccaniche (DMA), termiche (DSC e DMA), morfologiche (SEM e TEM) e raggi X (XRD).
Le misure di permeabilità hanno mostrato che l'aggiunta della carica determina una riduzione della permeabilità del film, questa riduzione è data dall'effetto barriera che il grafene provoca a spese del percorso delle molecole, andando a diminuire il coefficiente di diffusione (D) del gas all'interno del film. Per quanto riguarda i coefficienti di solubilità (S), rimangono invariati. Dal punto di vista morfologico, la carica è disposta nella matrice di PEBA come platelets, tipica morfologia delle nanocariche, aumentando così la tortuosità del percorso che le molecole di gas devono seguire durante la permeazione. Infatti, per le nanocariche, l'effetto barriera è legato al loro grado di esfoliazione all'interno della matrice polimerica e, il grafene, è caratterizzato da un buon grado di esfoliazione, giustificando in tal modo l'effetto barriera. Tuttavia, questo effetto potrebbe essere migliorato aumentando il tempo di sonicazione della soluzione grafene + solvente, o cambiare la metodologia sonicazione utilizzando strumenti più efficaci. Le prove meccaniche hanno rivelato che l'aggiunta di carica determina un aumento del modulo elastico sul materiale e una riduzione di duttilità, giustificata dalla diminuzione dell'allungamento a rottura. All’aumentare della percentuale di grafene, si vede un accentuamento degli effetti appena descritti. Dall'analisi DSC è stato possibile stabilire l'influenza del grafene all'interno della struttura cristallina di Pebax, infatti la presenza di questa carica risulta in un leggero aumento della temperatura di fusione. La presenza di grafene ha anche un effetto nucleante, questo si nota subito per piccole percentuali, in quanto favorisce la cristallizzazione del PEBAX e aumenta il grado di cristallinità del polimero finale

provato attraverso analisi di ΔHm_real. Inoltre, dalla DMA, si può vedere come il grafene ha effetto sulle temperature, in particolare la temperatura di transizione vetrosa è aumentata di qualche grado, come accade per la temperatura di fusione nella DSC. Dalle due analisi TGA, in atmosfera inerte la prima e la seconda con ambiente ossidativo, si vede come il grafene aumenti leggermente la stabilità della base PEBAX. Questo accade più nell'analisi di ossidazione, anche se si notano temperature inferiori alla TGA per ambiente inerte, confrontando i dati per la stessa percentuale di massa degradata. Le ultime analisi, utili per comprendere appieno il grado di esfoliazione di grafene, sono SEM, TEM e XRD: dall' analisi SEM non si vede molto e si può concludere dicendo che il film è molto compatto ed omogeneo. Invece, dalle altri due, si vede come il grafene ha subito una esfoliazione parziale: le immagini TEM mostrano dei punti in cui la dispersione è molto buona ed altri in cui non è praticamente presente, il grafico XRD infine, mostra che aumentando la percentuale di grafene, essa ha un minor grado di esfoliazione.

Invece, per quanto riguarda la seconda linea di ricerca, le membrane sono state create aggiungendo liquido ionico (Bmim-TSFI) al 5% in peso. Sono state create tante membrane quante erano quelle già state prodotte con il grafene. I campioni ottenuti sono stati caratterizzati mediante misure di permeabilità (O_2, CO_2 e vapore acqueo), analisi meccanica (dinamometro), dinamico-maccaniche (DMA), termiche (DSC e DMA), morfologica (SEM e TEM) e X -ray (XRD). Le misure di permeabilità hanno mostrato che l'aggiunta del liquido ionico aumenta la permeabilità dei film, questo effetto è dovuto ad un aumento dei coefficienti di solubilità (S), rimanendo invariati i coefficienti di diffusione (D) rispetto alle membrane già analizzate nella prima linea di ricerca. Pertanto, il liquido ionico è responsabile dell'aumento della permeabilità perché, avendo una conformazione chimica affine al passaggio delle molecole di gas, consente l'aumento dell'assorbimento delle molecole di CO_2 e di O_2. Dal punto di vista morfologico, il liquido viene probabilmente disposto, nella matrice di PEBAX, come forma di piccole gocce, intaccando il dominio del polimero. Le prove meccaniche hanno rivelato che l'aggiunta di liquido ionico risulta in una diminuzione del modulo elastico del materiale e una riduzione di duttilità, giustificata dalla diminuzione dell' allungamento a rottura. Questi effetti sono tutti dovuti perché il liquido ionico non è un plastificante come i polimeri. Dall'analisi DSC è stato possibile stabilire che la presenza di liquido provoca una diminuzione della temperatura di fusione. Inoltre, dalla DMA può essere visto come vi sia un effetto sulla temperatura, in particolare la temperatura di transizione vetrosa diminuisce di pochi gradi, come avviene per la temperatura di fusione DSC. Dalle due analisi TGA, in atmosfera inerte e ossidativa, vediamo come il liquido ionico diminuisce la stabilità del PEBAX base, sempre per lo stesso motivo menzionato prima (materiale non plastificante). Questo accade più nell'analisi di ossidazione, anche se comunque si notano temperature inferiori nella TGA in ambiente inerte, confrontando i dati per la stessa percentuale di massa degradata. Dalle ultime analisi, SEM, TEM e XRD, non possiamo dire

molto. Immagini SEM e TEM non mostrano chiaramente la presenza del liquido ionico, che può essere invece visto nel grafico XRD: ci sono picchi che provengono dal liquido, ma va a variare solo lo sfondo che dà la base polimerica come risposta alla analisi ai raggi X.
Infine, si può dire che l'effetto del liquido ionico è bilanciato dall'effetto del grafene: il primo aumenta considerevolmente la permeabilità ai gas, con lo svantaggio che le proprietà meccanico-termiche del polimero di base subiscono un calo. D'altra parte il grafene è utile per migliorare tali proprietà, avendo un effetto barriera quasi trascurabile rispetto all'aumento di permeabilità dovuta dal liquido ionico. In sintesi, l'aggiunta della nanocarica migliora la struttura e la resistenza della membrana mentre il liquido ionico diminuisce le proprietà, tuttavia, aumentando la permeabilità.

Possibili sviluppi futuri potrebbero essere quelli di effettuare un'analisi di permeabilità al CH_4 e H_2S, per capire quali sono le migliori applicazioni per tali membrane, nonché effettuare un'analisi di selettività con apposito strumento per capire come la separazione avviene in un flusso non puro. Quando questi dati saranno disponibili, sarà possibile verificare le prestazioni di tali membrane per capire se procedere o meno con la costruzione di un piccolo impianto pilota.
Possibili applicazioni future, a seconda dei dati in uscita, potrebbero essere la depurazione dell' aria o la purificazione del gas naturale, ciò dà senso allo studio appena fatto.

Summary

Introduction

The Petroleum Institute (PI) is an engineering school financed and governed by the Abu Dhabi National Oil Company (ADNOC). This company has a lot of chemical plants inside UAE (United Arab Emirates), it gives many projects to PI for the development.

An important and actual topic is the separation of the impurities from natural gas.

Right now, the process needs a large amount of energy in order to cool down or compress the gas or use chemical reactions, in order to achieve a liquid phase easier to separate. On the other side there is a new method through membranes that doesn't need energy and the separation is a physical process due to a "molecular sieve" effect, enhanced by weak chemical bonds.

At the same time, an increase of the concerns related to the climate change, has developed the interest in a more sustainable lifestyle that has led to a growing demand for alternative solutions. One of such solutions is related membranes, which favor an implementation of the process used to reduce the energy consumption. They can be used in various processes in addition to the gas purification, such as purification of air, flue gas, etc.

The purpose of this thesis is to improve the properties of PEBAX based membranes for gas separation, using two different combined approaches: the addition of a nanofiller to improve the general properties of the polymer and the subsequent addition of ionic liquid to improve the gas permeability. The blends were prepared by mixing PEBAX and a nanofiller (graphene) at different weight percentages, and subsequently adding a ionic liquid at 5% by weight.

The study has been organized according to the following chapters:

- Chapter 1: It describes the polymer and illustrates the solution-diffusion model and the most important factors that affect the permeation through the polymeric film;
- Chapter 2 describes the physical and chemical properties of all the materials employed for the preparation of the membrane, object of study;
- Chapter 3 shows the processes and tools used for samples preparation and analysis of their properties;
- Chapter 4 presents and discusses the results of the characterization tests carried out on the membranes.

Chapter 1

Polymer and gas permeation

The interest towards a more sustainable lifestyle is one of the key concepts that has developed in recent years, becoming a shared goal by world public. The attention to the environmental and economic implications of the world growth has been reflected in many areas, especially towards the research of new techniques and new materials .

1.1 Membranes: generality and gas separation

For many years, several technologies for gas treatment in the petrochemical industry have been employed, including absorption towers, packed and plate columns. Although these conventional processes are being used up to date, these methods possess many disadvantages such as flooding, foam formation, and demand of high capital and operating costs. Therefore, many researches have been seeking new technologies to eliminate these drawbacks while sustaining low operative costs. Membranes have emerged as a promising and potential large scale technology for gas absorption, and for this reason the development of new membranes is one of the most active research fields nowadays..

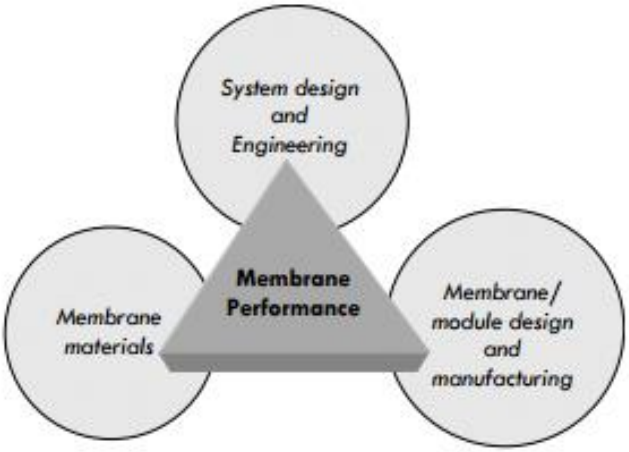

Figure 1.1. *Main topics involved in membrane performance development* [1].

Membrane separations can be efficiently and successfully used for the purification of gases [1]. This technology offers several benefits, including lower energy consumption and flexibility in operation. Membrane technology can be effectively applied for the removal acid gases (i.e. CO_2, H_2S, water vapor) present in a gas streams. The membrane technology has proven to be

technically feasible and has impacted the market by its many advantages over the standard amine processes, in terms of:

a) Smaller and lighter streams;
b) Simultaneous removal of CO_2, H_2S and water vapor;
c) Reduced energy consumption;
d) Lower operating and capital cost;
e) High process flexibility;
f) Ease of installation;
g) Ability to treat gas at wellhead.

For example, membranes modules with hollow fiber or spiral wound design are capable to reduce the carbon dioxide content in natural gas to less than 2%.

Although since more than one century ago gas diffusion and mass transport principles through polymer films are known, only in the last 30 years membranes have been applied on an industrial scale for gas separation (GS) [2]. Since the first large industrial application of Prism membranes by Permea (Monsanto) for hydrogen separation from the purge gas stream of ammonia plants, membrane-based GS has grown exponentially.

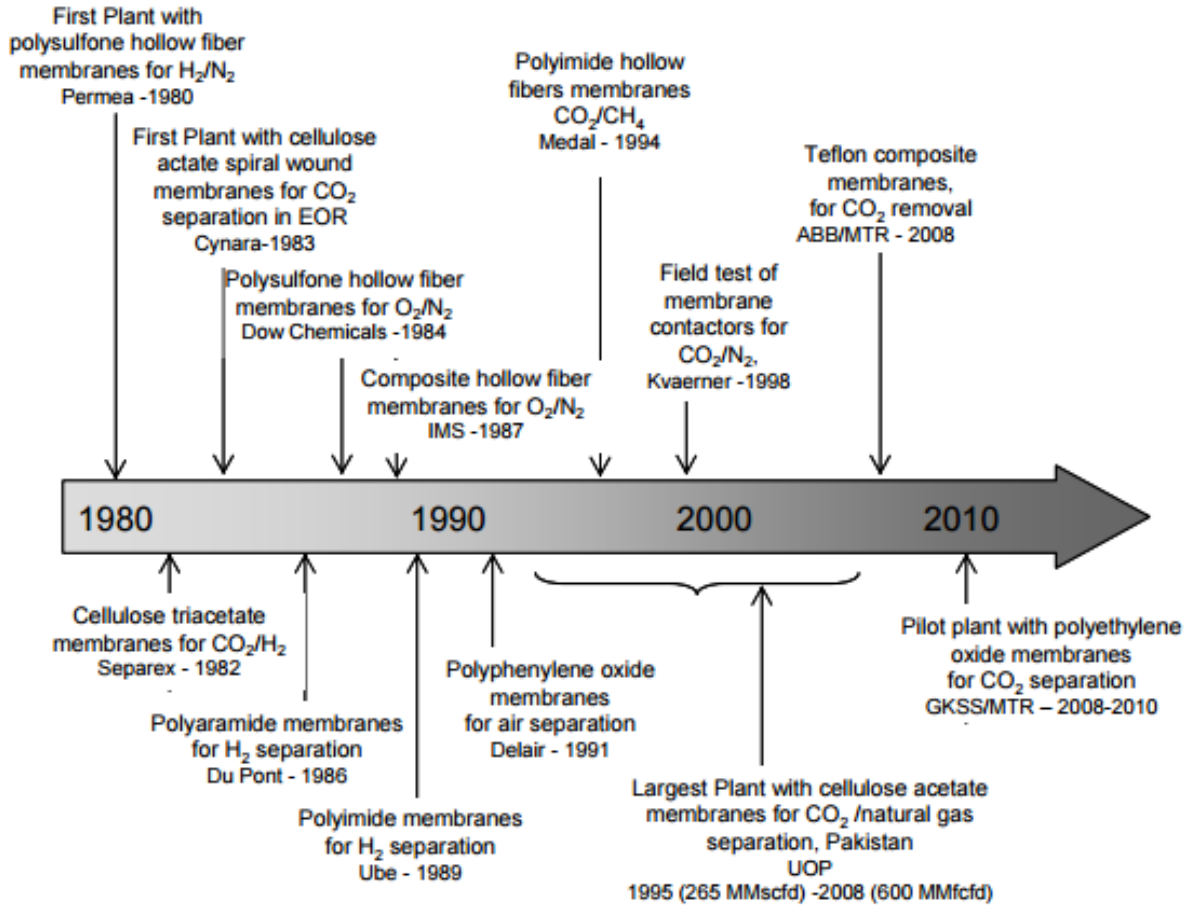

Figure 1.2. *Milestones in the industrial application of membrane gas separation systems* [1].

1.2 Permeation of gases through polymeric membranes: The solution-diffusion model

The first theory for the description of gas permeation through polymeric membranes was developed in 1866, when Thomas Graham formulated the solution-diffusion model [3]. According to this model the permeation of a gas through a film is achieved by a process divided into three phases: the dissolution of the gas species penetrating the upper surface of the film, followed by its diffusion through the membrane to end with the dissolution from the lower surface of the film. Other important observations made at that time were:

- The permeation was independent of pressure,
- The increase in temperature led to a decrease of the solubility of the penetrant, but made the membrane more permeable,
- Prolonged exposure to elevated temperatures influenced the retention capacity of the membrane,
- Differences in permeability could be exploited to obtain the separation of a gas,
- A variation in the membrane thickness altered the permeation rate, but not the separation characteristics of the polymer.

Towards the end of the 70s (XIX century) Stefan and Exner showed that the permeation, P, through a membrane of soap was proportional to the product of the solubility coefficient, S, and the diffusion coefficient , D [3]. On the basis of these discoveries Von Wroblewski built a quantitative solution to the solution-diffusion model of Graham. The dissolution of the gas was based on the the Henry's law of solubility, where the concentration of the gas in the membrane was considered directly proportional to its pressure.

$$P = D \cdot S \tag{1.1}$$

where:

$$\mathrm{P} = \frac{(\text{gas quantity}) \times (\text{membrane tickness})}{(\text{membrane area}) \times (\text{time}) \times (\text{pressure})} \qquad \left[\frac{\mathrm{cm^3 mm}}{\mathrm{m^2\ day\ atm}}\right] \tag{1.2}$$

$$\mathrm{D} = \frac{\text{membrane area}}{\text{time}} \qquad \left[\frac{\mathrm{mm^2}}{\mathrm{s}}\right] \tag{1.3}$$

$$\mathrm{S} = \frac{\text{gas quantity}}{(\text{polymer volume}) \times (\text{pressure})} \qquad \left[\frac{\mathrm{cm^3}}{\mathrm{cm^3 atm}}\right] \tag{1.4}$$

Von Wroblewski subsequently showed that, under steady state conditions, and assuming that the diffusion and solubility coefficients are independent of the concentration, the flow of the permeating gas can be expressed as:

$$J = \mathrm{D} \cdot S\left(\frac{p_f - p_p}{l}\right) = P\left(\frac{\Delta p}{l}\right) \tag{1.5}$$

where p_f and p_p are the upstream and downstream pressures on the membrane, (Δp / l) is the pressure gradient applied along the thickness of the membrane (s) and P is defined as the gas permeability of the membrane. In 1920, Daynes showed that it was impossible to determine both the diffusion and solubility coefficients by permeability experiments at steady state. He presented a mathematical solution using Fick's second law of diffusion in order to calculate the relative coefficient, assuming that they were independent of concentration. This "time lag" experiments is the most common method for the estimation of the diffusion and solubility coefficients of a gas through a membrane of material.

1.2.1 The time-lag method

This method is based on the fact that the permeation process can be divided into two components, the transient and the steady states [4-5]. The dynamic or transient component can be represented by a time-lag parameter, obtained by measuring the time required penetrating goes in the membrane and the time at the flow rate of the diffusing species within the closed volume reaches a steady state permeation. This technique was originally conceived in 1920 by Daynes, who modeled the mass transport through a rubber membrane and obtained a solution for the time-lag observed as a function of the diffusion coefficient. The starting point for the development of this method is based on the resolution of the Fick's second law of diffusion. Adolf Fick in 1855 developed the work of Graham saying that distribution could be described using the same mathematical models used for the description of Fourier's law of heat conduction or Ohm's law of electric conduction. Both of these relationships define a ratio of the speed of energy transport (heat and electricity, respectively) and the distance covered by this energy. The quantity of gas, Q(t), which passes through the membrane, in the time t, is given by the series expansion employed to approximate the integration of the Fick's second law:

$$\frac{Q(t)}{lC_1} = \frac{Dt}{l^2} - \frac{1}{6} - \frac{2}{\pi^2}\sum_{n=1}^{\infty}\frac{(-1)^n}{n^2} exp\left(-\frac{Dn^2\pi^2 t}{l^2}\right) \tag{1.6}$$

where D is the diffusion coefficient, l the film thickness, C_1 is the concentration of the penetrant on the upper side of the film, in equilibrium with the partial pressure of the

penetrating upstream of the film. When t tends to a very long time, the steady state is reached and the exponential term becomes negligible. The curve which represents Q(t) as a function of time (figure 1.3) is then a straight line represented by the following relation:

$$Q(t) = \frac{\mathrm{D}C_1}{l}\left(t - \frac{l^2}{\mathrm{D}}\right) \tag{1.7}$$

The intercept of this line and the x-axis is equal to:

$$\theta = \frac{l^2}{6\mathrm{D}} \tag{1.8}$$

where θ is called a "*time lag*".

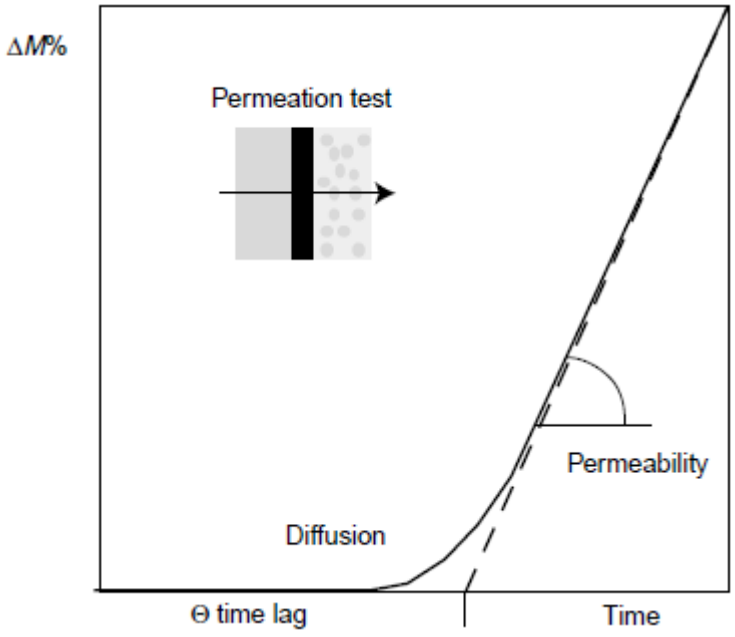

Figure 1.3. *Results of a theoretical curve for an gas permeation experiment of a polymeric membrane* [4].

Under steady-state conditions, this equation can be employed to estimate the diffusion coefficient and then proceed to quantify of the solubility coefficient from the ratio of the permeability constant of the polymer and the calculated diffusion coefficient .

1.3 Factors affecting the permeation

Numerous factors can affect the diffusion of gaseous species through a polymer membrane [5-7]. Based on the theoretical solution-diffusion model it can be observed that the solubility coefficient, S, is dependent on the gas-polymer interaction, from molecule penetrating packing and from the cohesive energy density (CED) of the polymer. Conversely, the diffusion coefficient, D, is influenced by the size of the penetrating molecule, the degree of crystallinity, from the free volume of the polymer and the stiffness of the polymer chains.

1.3.1 Nature of the polymer

The behavior of a given penetrating species changes from one polymer to another. The transport properties depend on the free volume within the polymer, and the mobility of the segments of the polymer chains. This mobility is influenced by the degree of unsaturation of the polymer, its degree of crosslinking, the degree of crystallinity and the nature of the substituents present.

1.3.1.1 Free volume

The theory of the molecular free volume postulates that the movement of gas molecules is dependent of the available free volume in the polymer matrix, as well as, it is dependent from the energy of gas molecules sufficient to overcome the attractive forces between the chains[5-7]. The concept of free volume has been used to describe the unbalanced nature of the polymer. In 1960 Fujita suggested the presence of free volume in a polymer. The concept is based on the presence of three components for the specific volume of each polymer: volume occupied by macromolecules, interstitial free volume and free volume of the cavity that is large enough to allow the transport of gas. The dependence of the transport properties of a penetrant species in a polymer from the packing chains is often described using correlations involving the fraction of free volume (Fraction of Free Volume, FFV) polymer. It is constituted by the total quantity of voids created due to the static inefficient packing of the chains or empty transients created by thermally induced rearrangements of chain. More numerous and larger are these preferential paths to the spread, the faster the molecules migrate through the polymer. The fraction of free volume is defined as:

$$FFV = \frac{V_{SP} - V_0}{V_{SP}} \tag{1.9}$$

where V_{SP} is the specific volume of the bulk of the polymer, while V_0 is the volume occupied by the polymer chains. The occupied volume is usually estimated by means of the method of Bondi [5-7] as follows:

$$V_{SP} = 1{,}3V_0 \tag{1.10}$$

with V_0 volume of Van Der Waals, determined with the method of contribution to groups (Van Krevelen, 1990). FFV was related to the diffusion coefficient from the equation of Doolittle [5-7]:

$$D = A \exp\left(\frac{-B}{FFV}\right) \tag{1.11}$$

where A and B are empirical constants. When FFV increase, the diffusion coefficient increases as well. The dependence of the solubility of FFV is usually weaker than the dependence of the diffusivity, especially in amorphous polymers. For this reason, often the permeability follows a similar dependence on the free volume of the diffusivity of the penetrating species.

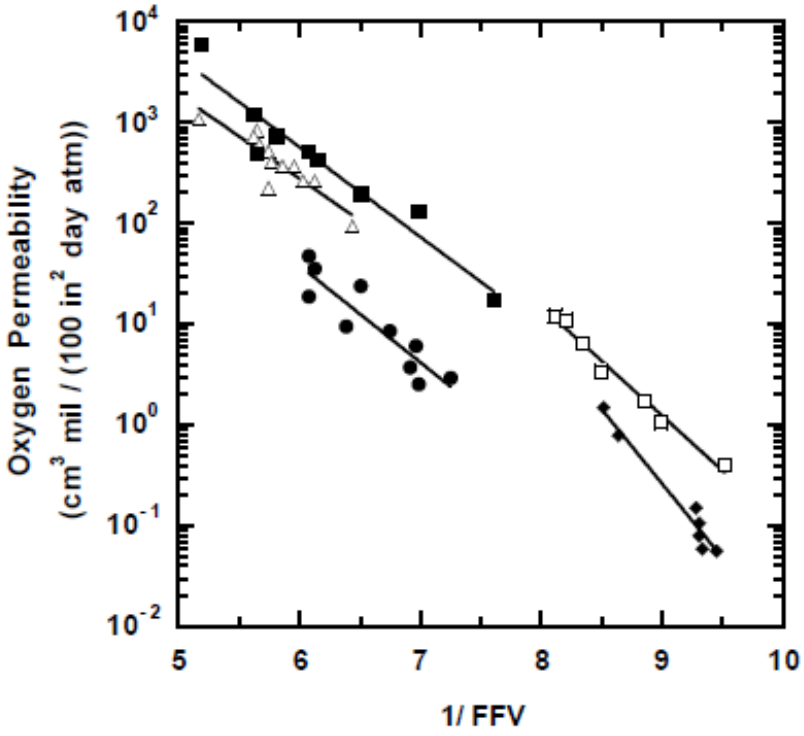

Figure 1.4. *Correlation of the oxygen permeability with the fraction of free volume of the polymer for different families of amorphous , glassy and liquid crystal polymers[5-7]. (■) Polystyrene (35 ° C), (Δ) Polycarbonate (35 °C), (●) Polyesters (30 °C), (□) Polyamides (25 °C), (♦) Polymers LCD.*

Several attempts have been conducted to correlate the FFV of the polymers with the gas permeability. As shown in Figure 1.3, a linear correlation was identified between the logarithm of the coefficient of oxygen permeability and the reverse of FFV in different families of amorphous, glassy and liquid crystal polymers with high barrier properties.

Many barrier polymers are glassy materials, since their temperature of use is below their glass transition temperature. In glassy polymers, non-equilibrium materials, the free volume can be altered to a certain degree by the thermal history of the sample. For example, high cooling rates create a high free volume in the glassy state, and vice versa. A more meaningful way to alter the free volume is to vary the chemical structure, for example, by the addition or removal of pendant groups on the main chain of the polymer. The presence of polar groups with low specific volumes can reduce the free volume facilitating a more efficient packing of the polymer chains due to stronger interactions between them [7] .

1.3.1.2 Glass transition temperature

One of the most important parameters that affect the mobility of the chains and consequently the permeability of a polymer is the glass transition temperature (Tg) [5-7]. This is due to the fact that during the transition from the glassy to the rubbery state there is a significant increase in the free volume within the polymer. In fact, being the glass transition a second order transition, it determines a discontinuity in the specific volume of the polymer that allows cooperative movements of large segments of the chain, promoting the increase of the gas permeation into the polymers. The presence, or the introduction of bulky substituent groups or polar chain often increases the rigidity of the chain, leading to: an increase of the glass transition temperature, an improvement of mechanical properties and an increase of the packing density of the chains. Bulky side groups such as aromatic groups decrease the flexibility of the chain, increases the Tg and, therefore, reduce the diffusion coefficient of the penetrant. Others flexible groups as ethers or methylene, produce the opposite effect. The relaxations of chain below the glass transition are another indication of the molecular motion, and correlations were observed permeability of O_2 and CO_2 with relaxations of this type within families of amorphous polyesters and copolyesters. However, the exact nature of molecular motions that control the diffusion of the penetrant are complex and not clear, then the Tg and the relaxation to the rubbery state do not provide predictive correlations with the diffusivity of the penetrant. Changes in the molecular structure of the polymer often change more than a single factor that affects the permeability and the overall effect can be hard to anticipate. For example, as already stated previously, the incorporation of bulky side groups may stiffen the polymer chains, from which one would expect a reduction of the diffusion coefficients. However, the same change can also decrease the packing density of the chains in the amorphous phase and reduce the level of crystallinity in the polymer, that should increase diffusion coefficients. Consequently, the net result of these competitive effects can be difficult to predict from the beginning.

1.3.1.3 Cohesive Energy Density (CED)

Conventional barrier materials such as polyacrylonitrile (PAN) or polyvinyl alcohol (PVOH) have very low permeability to oxygen as result of the restricted movements of their chain and the high interaction between the chains due to the presence of polar groups [5-7]. The interaction between the polymer chains can be quantified through the energy density of cohesion (CED), which has a strong influence on the permeation of the penetrant. The CED of a polymer is the square root of its solubility parameter and characterizes the attraction force (or interaction) between the polymer chains. It can be estimated using group contribution techniques.

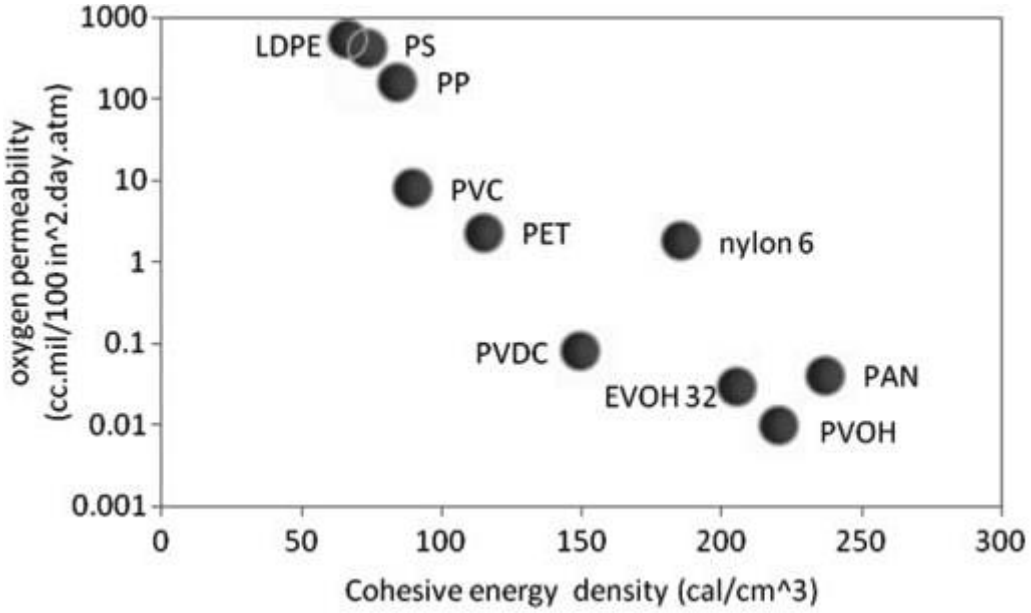

Figure 1.5. *Relation between oxygen permeability (measured at 23 °C and 0% relative humidity) and CED of some polymers.*

Polyethylene (PE), for example, with its flexible chains has a low CED. The molecular matrix provides a low resistance to the diffusion of the gas, so the polymer is characterized by a high oxygen permeability. For this reason, a method for reducing the flexibility of the chains and thus the permeability of the polymer is to add substituent groups to the hydrocarbon chain. Non-polar substituents such as methyl group determine a hindered motion of the chains and thus lower permeability. However, despite a decrease of the permeability of about three times the value of PE, PP still possesses reduced barrier properties. The inclusion of the methacrylate group within the polypropylene origines polymethylmethacrylate (PMMA) which has a higher CED to the PE and PP. This polymer, thanks to less flexibility of the chain has a lower oxygen permeability. The introduction of a polar ester group, however, increases the CED, resulting in a reduction of the free volume. However, it also serves as a site for

hydrogen bonding with the polar molecules of water, by which there is a reduction of the moisture resistance of the polymer. The replacement of highly polar halogen groups on the hydrocarbon chains gives rise to polymers such as polyvinyl chloride (PVC) and the polyvinyl fluoride (PVF). Both these polymers have high interactions between the chains resulting in a greater rigidity, a low packing density, low permeability and good water resistance despite the presence of polar groups.

1.3.1.4 Cristallinity

The increase of crystallinity in a polymer usually decreases the permeability of the gas (Table 1.1). The crystallinity affects both the solubility coefficient and the diffusion coefficient[5-7]. For most of the polymers and penetrants species of interest, the crystalline regions, which are far denser and ordered than the amorphous one, prevent the sorption of the penetrant and reduces, therefore, the solubility. Furthermore, the presence of crystallites in a polymer matrix generates a diffusion barrier, by increasing the path length that the gas must perform and, in some cases, by increasing the rigidity of the chain, a factor which in turn contributes to the reduction of the coefficient diffusion [5-7] .

Table 1.1. *Effect of Crystallinity on the permeability of the polymers.*

Polymer	**Morphology**	**Oxygen permeability [cc·mil/(100 in^2·day·atm)]**
EVOH[1]	58% of cristallinity (not oriented)	0.71
	68% of cristallinity (uniaxially oriented)	0.25
	70% of cristallinity (biaxially oriented)	0.15
LDPE[2]	50% of cristallinity	480
	75% of cristallinity	110
PET[2]	10% of cristallinity	10
	50% of cristallinity	5
PP[2]	Atactic (low crystallinity)	250
	Isotactic (high crystallinity)	150

While the size, shape and orientation of the crystallites usually do not have a significant effect on the solubility of the gas in the polymer, these factors may be important in the diffusion of gaseous penetrants. Duncan et al. [5-7] have expressed the effect of crystallinity on the diffusion coefficient of a penetrating species using the following model:

[1] Data measured at 20 ° C and 100% relative humidity for an EVOH with 32 mol% ethylene
[2] Data measured at 23 ° C and 50% relative humidity

$$D = \frac{D_a}{\tau\beta} \tag{1.12}$$

where Da is the diffusion coefficient of the amorphous phase of the polymer, τ is the geometric impedance (tortuosity) and β is a factor which accounts for the immobilization of the chains. The crystalline waterproof regions force the penetrating to follow tortuous paths through the permeable amorphous regions. This effect is described by the factor τ, which is the ratio between the average distance from a molecule of penetrating and the thickness of the sample. τ can be a complex function of the crystalline content as well as of the size, shape and orientation of the crystallites. The crystallites may also restrict segmental mobility acting as physical vulcanizing (physical crosslinks). This effect is accounted by the β factor and is generally more pronounced in flexible rubbery polymers such as PE. In glassy polymers such as PET, the inherent rigidity of the chain requires a greater impedance to the mobility compared to crystalline and then β is equal to 1. A two-phase model is often employed to describe the solubility of the penetrant in a semi-crystalline polymer:

$$S = S_A\varphi_A \tag{1.13}$$

where S_A is the solubility coefficient in the amorphous regions of the polymer and φ_A is the volume fraction of the amorphous phase. This model assumes that the solubility of the crystalline regions is zero and that the presence of crystallites doesn't affect the solubility coefficient of the amorphous phase. For polymers that are used in packaging applications with high barrier properties, neglecting the solubility in the crystalline regions is generally acceptable. The second assumption according to which the solubility of the amorphous phase is independent from the crystalline content is not necessarily checked, especially in glassy polymers whose structural organization of the amorphous phase can be significantly affected by common protocols process (e.g. orientation, stretching, aging, contact with agents that induce crystallization, etc.) However, the simplest and most common model for expressing the effect of crystallinity on the permeability of the stationary state is based on these assumptions and is expressed by the following relation:

$$P = (S_A\varphi_A)\left(\frac{D_A}{\tau\beta}\right) \tag{1.14}$$

In glassy polymers, the approximations more commonly used for τ and β are $\tau = \varphi_A^{-1}$ and $\beta = 1$.

1.3.1.5 Chain orientation

The orientation is an industrial technique commonly used to increase the crystallinity of a polymer and consequently to improve the mechanical properties and, under certain conditions, the barrier properties [5-7]. During the operation of orientation of the polymer, the chains are stretched in specific directions. If a polymer is subject to an external stress immediately after the crystallization of the polymer, the chains are aligned preferentially in the direction of the stress because the intrinsic properties of the polymer chain are strongly dependent on the direction. Stretching is usually done at temperatures slightly below the melting point, when the crystals are partially melted and the desired shape is maintained during cooling. The orientation can be uni-axial, if the material is stretched in one direction (that of the machine), or bi-axial, if the material is stretched in two mutually orthogonal directions (machine direction and transverse direction). The degree of orientation achieved by the chains is dependent on the stretching ratio and other process conditions. The orientation is usually characterized by birefringence and quantified by the Herman function of orientation , f:

$$f = \frac{1}{2}(3\ cos^2\theta - 1) \tag{1.15}$$

where θ is the mean angle between the axis of the chain of the polymer and stretch direction (draw direction). Being function of the mode of deformation and the physical process that occurs during the orientation, the permeability can either increase or decrease with the increase of the orientation. The polymer waterproof crystallites can become oriented like lamellar structures during deformation, and this process usually decreases the diffusivity due to increased tortuosity of the path that the penetrating has to make. Furthermore, the drawing of semicrystalline polymers can improve the barrier properties through the crystallization and orientation induced by the stress of the remaining amorphous phase. So, the reduction in permeability caused by the orientation of crystallizable polymers may be greater than the one of non-crystallizable polymers. For other systems, however, have also been reported increases in permeability as a result of biaxial orientation.

1.3.1.6 Copolymerization

The copolymerization is an important tool for combining the desirable properties of two or more materials in the same polymer[5-7]. The polyvinyl alcohol (PVOH), for example, has one of the lowest oxygen permeability reported in the literature, in conditions of absence of moisture. This is due to the significant chain-chain interactions generated by the formation of hydrogen bonds and crystalline domains that allow to obtain a high packing density of the polymer. The polymer, however, loses its barrier properties at high relative humidity values,

and also dissolves in water. The water molecules have a high affinity for the polymer matrix, resulting in the cessation of secondary interactions between the polymer chains and plasticized the polymer. In this state, the polymer chains become flexible and the permeability increases by a few orders of magnitude. The plasticization takes place when the concentration of the penetrant in the polymer matrix is sufficiently high to promote diffusive jumps of a penetrating molecule thanks to the local presence of another molecule penetrating. The reduction of the concentration of chemical groups capable to give hydrogen bonds in the chain, reduces the concentration of water molecules in the polymer. An example of the material developed according to this approach is the ethylene-co-vinyl alcohol (EVOH) copolymer.

The non-polar ethylenic fraction of the polymer is used to reduce the possible hydrogen bonding interactions in the polymer matrix and thus to reduce the solubility of water in the polymer. The EVOH greater resistance to water absorption is an improvement compared to the PVOH, but the permeability are still dependent on the relative humidity. The oxygen permeability of EVOH is greater than that of dry PVOH, but significantly less than that of PE. By increasing the ethylene content in the copolymer the dependence on the relative humidity is reduced; however, this component also provides greater flexibility to the polymer chain, increasing its permeability to gases. By varying the relative content of ethylene and vinyl alcohol monomer it is possible to optimize the gas barrier properties and the resistance to moisture absorption of the material. In a similar manner, an improvement of the barrier properties of PVC can be obtained by copolymerization with vinyl chloride. The polyvinylidene chloride (PVDC) homopolymer has a low oxygen permeability with excellent resistance to moisture, but it is not generally employed as a homopolymer. Despite some reduction of the barrier properties, the copolymerization with PVC seems to be preferred to balance the mechanical and barrier properties of the resulting polymer. Decreasing the fraction of vinyl chloride to obtain a better permeability to oxygen and water. The copolymerization of olefins and carbon monoxide in the presence of metal catalyst leads to the formation of polyketones which have excellent barrier properties combined with a high Tg. The polymer has strong polar groups that determine very ordered chains. While, sometimes the addition of a small fraction of the propylene copolymer is used to reduce the melting point and the temperature of processing.

1.3.2 Fillers

The diffusion and transport in filled polymers depend on the nature of the filler, on its aspect ratio[3], degree of adhesion and by their compatibility with the polymer matrix [5,6]. If the inert filler employed is compatible with the polymer matrix, it will occupy the free volume within the polymer matrix and create a tortuous path for the permeant molecules. The degree of tortuosity depends on the fraction of filler and by the shape and orientation of the particles.
The higher is the aspect ratio and more tortuous will be the path that the gas has to perform and, therefore, longer will be the diffusion process.
By contrast, when the filler is incompatible with the polymer, voids at the interface will form, which lead to an increase in the free volume of the system and consequently to an increase in the permeability of the polymer.

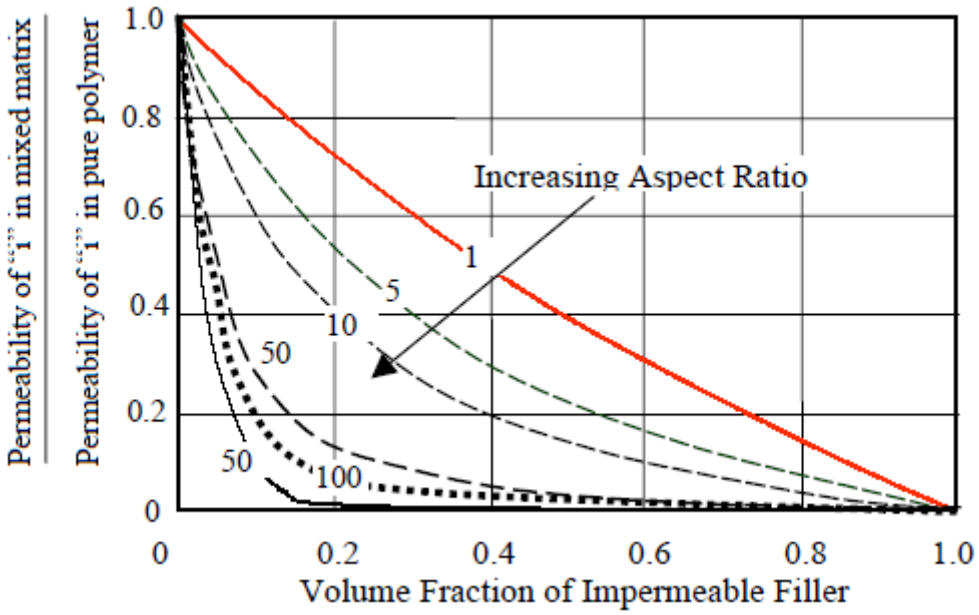

Figure 1.6. *Effective permeability of a polymer loaded with impermeable particles with different ratios of the form.*

[3] The aspect ratio of inorganic fillers or waterproof components present in a polymer matrix is defined as the ratio between the lateral dimension and the thickness which characterizes them.

1.3.3 Temperature

The effects on the thermal diffusivity and solubility show opposite trends[5,6]. In general, for the adsorption of gases, the solubility decreases with the increase of the temperature as the packing of the penetrant decreases with temperature. Diffusivity and permeability are usually modeled using an Arrhenius relationship:

$$D = D_0 \, exp\left(-\frac{E_D}{RT}\right) \tag{1.16}$$

$$P = P_0 \, exp\left(-\frac{E_P}{RT}\right) \tag{1.17}$$

where E_P and E_D are the activation energies for the permeation and diffusion and P_0 and D_0 are pre-exponential factors. The effect of temperature on solubility is usually expressed by a relation of Van t' Hoff type:

$$S = S_0 \, exp\left(-\frac{\Delta H_S}{RT}\right) \tag{1.18}$$

where S_0 is a pre-exponential factor and ΔH_S is the absorption heat of penetrating into the polymer. The solubility in thermodynamic terms is considered a two-stage process. The first involves the condensation of the gas molecule in the polymer, followed by the creation of an empty molecular size to accommodate this gas molecule. These two individual stages contribute to the total enthalpy of sorption, represented mathematically as:

$$\Delta H_S = \Delta H_{cond} + \Delta H_{mix} \tag{1.19}$$

where ΔH_{cond} is the enthalpy of gas condensation and ΔH_{mix} is the partial molar heat of mixing between the gas and the polymer. For weak interactions, ΔH_{mix} is positive and it can be calculated using the following equation:

$$\Delta H_{mix} = V_1(\delta_1 - \delta_2)^2 \varphi_2^2 \tag{1.20}$$

where V_1 is the partial molar volume of the gas, φ_2 is the volume fraction of the polymer, δ_1 and δ_2 are the solubility parameters of the gas and polymer, respectively. For supercritical gases whit low molecular weight, low packability means that the stage of mixing is the one that controls the sorption properties of the polymer. In case of weak interactions between the gas molecule and the polymer, the variation of the enthalpy of mixing is positive, which leads to an increase in solubility with increasing of temperature. For the case of gases and condensable vapors, the enthalpy for the condensation change and became negative and

dominant, showing a decrease in solubility with increasing temperature. At steady state the permeability is the product of the diffusivity and solubility, then the activation energy of permeation may be defined as the sum of the activation energy of the diffusion and heat of sorption:

$$E_P = E_D + \Delta H_S \tag{1.21}$$

E_D is always positive and ΔH_S can be positive or negative for light gases (such as H_2, O_2, N_2, etc.) as well as for more soluble and larger penetrating (such as C_3H_8, C_4H_{10}, etc.). As noted above, the diffusion of penetrant is a temperature activated process . At temperatures far from those of the main transitions (e.g. glass transition, melting point, etc.), the Arrhenius relationship is satisfied, and with an activation energy of the diffusion known, E_D, the diffusion coefficient of a penetrant in a polymer can be estimated at each temperature. In the case where E_D is not reported, it can be estimated using known correlations between D_0 and E_D:

$$ln\, D_0 = a\frac{E_D}{RT} - b \tag{1.22}$$

where a and b are independent of the type of penetrating. The parameter a is independent of the type of polymer and has a universal value of 0.64; b has a value of 9.2 (-ln (10^{-4} cm^2 / s)) for rubbery polymers (i.e. polymers above their Tg) and 11.5 (-ln (10^{-5} cm^2 / s)) for glassy polymers (i.e. polymers below their Tg). This equation is often called the "linear free energy" relation. When this is combined with the relation for the diffusivity is obtained:

$$D = exp\left[-b - (1-a)\frac{E_D}{RT}\right] \tag{1.23}$$

By knowing a single value of the diffusion coefficient at a given temperature, E_D can be estimated from this equation. In parallel, it allows to estimate the diffusion coefficient at other temperatures, provided that these two temperatures do not cross a thermal transition (such as the glass transition) and also the morphology of the polymer is not modified in any other way. In the case of glassy polymers, all three parameters of transport of the gas decreases with temperature increase. Some exceptions are observed at high temperatures where, due to the low solubility, more errors in the curve fitting of the dual mode sorption are introduced.

1.3.4 Pressure

The dependence of the coefficients P, D and S by the pressure of the penetrating gas is very different depending at the temperature, it can be below or above the Tg of the polymer[5-6].

When the polymers are in the rubbery state the pressure dependence of these coefficients depends on the solubility of the gases in the polymers. For example, if the penetrating gases are poorly soluble and do not significantly plasticize the polymer, the coefficient P as well as D and S are independent on the pressure of the gas penetrating. This is the case of supercritical gases with very low Tc (e.g. H_2, O_2, N_2, CH_4, etc.) in which the gas concentration in the rubbery polymer is within the limit of the Henry's law also at high pressures. Subcritical gases, such as organic vapors, are much more soluble in the polymer and, consequently, the above behavior occurs only at very low pressures. As the pressure of the penetrant is increased and the plasticized polymers are increasingly penetrating from the gas, the coefficients P, Q and S increase rapidly and in some cases also exponentially with the increase in the pressure. On the other side, these coefficients for glassy polymers are highly non-linear functions of the pressure of the penetrating gas. Such behavior is also observed when the polymer is not excessively plasticized by the penetrating gas. This behavior is satisfactorily described by the "dual mode" model that attributes to the heterogeneity of glassy polymers. In agreement with this model P and S decrease and D increases as the pressure of the penetrant increases; all three of these coefficients reach asymptotic values at pressures high enough. The dual-mode sorption model also shows that the coefficients of permeability, diffusion and solubility must become independent of the pressure at sufficiently low pressures. This type of behavior has been observed experimentally for a number of gases, in many glassy polymers. When the concentration of the penetrating gas in glassy polymers becomes high enough to be laminated polymers, the coefficients P, D and S will deviate with respect to the behavior of the dual-mode sorption and will increase as the pressure increases.

1.3.5 Concentration (or partial pressure) of the penetrating species

The influence of the concentration of a penetrating species on the solubility, diffusivity and, consequently, on the permeability varies in dependence of the system-penetrating polymer[5-6]. Glassy and rubbery polymers typically show reduced or no dependence of the solubility, diffusivity and permeability on concentration for light gases such as H_2, N_2, O_2 etc. Consistently with this statement, Figure 1.7 (A) below shows the absence of any trend of the pressure of H_2 with the permeability of PE. Gases like CO_2 that are more soluble than light gas, typically have a response pressure-permeability in glassy polymers that is similar to the one shown in Figure 1.7 (B).

The permeability decreases monotonically with increasing pressure as predicted by the dual-sorption model. The magnitude of the permeability decreases as a function of the quantity of the excess volume of non-equilibrium in the polymer, which can increase with the increase of the Tg, the affinity of the penetrant for the excess volume of non-equilibrium and the mobility of the penetrating into the excess volume of non-equilibrium with respect to mobility within

the balance of free volume. The permeability of a rubbery polymer to an organic vapor often shows the behavior shown in Figure 1.7 (C). The monotonic increase in permeability is often due to the increase in the solubility of the penetrating species with the increase of pressure, coupled with an increase in diffusivity if increase the pressure. The response shown in Figure 1.7 (D) is typical for strongly interacting penetrating species (e.g. organic vapors) in glassy polymers at sufficiently high partial pressures of the penetrating species. The sharp increase in the permeability begins when the penetrating species plasticizes the polymer. The plastification occurs when molecules of the penetrating species dissolve in the polymer matrix in concentrations sufficient to force the separation of segments of chains, increasing the free volume, and accordingly, facilitating the motion of the polymer segments. This increased mobility, observable by the depression of the Tg, determines an increase of the diffusion of the penetrant species and, consequently, the permeability.

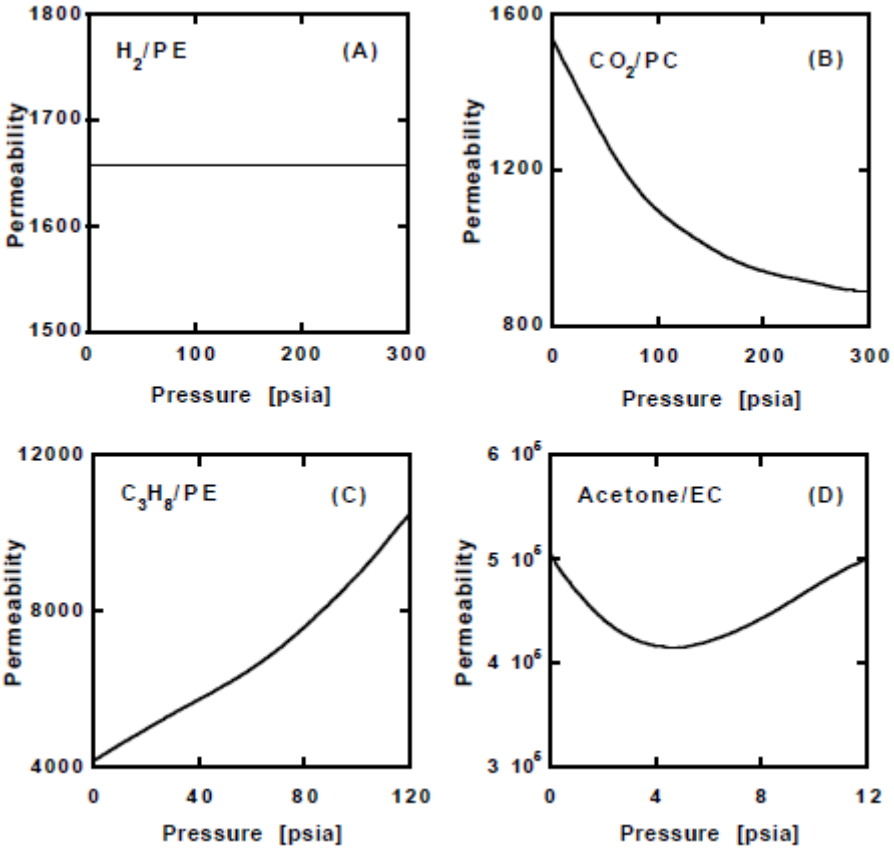

Figure 1.7. *Typical dependence pressure-permeability in glassy and rubbery polymers. (A) hydrogen in the polyethylene (PE) at 30 ° C, (B) carbon dioxide in polycarbonate (PC) at 35 ° C, (C) propane in polyethylene at 20 ° C, (D) acetone in ethyl cellulose (EC) at 40 ° C. The permeability values have units of (cm^3 mil / (100 in^2 day atm)).*

1.3.6 Humidity

The water absorption may increase, decrease, or have no effect on the permeability of barrier polymers[5-6]. For example, increasing the relative humidity from 0 to 50%, increases by an order of magnitude the oxygen permeability of the cellophane (regenerated cellulose) and, the exposure to 90% relative humidity removes it from the class of materials with high barrier due to a further increase of the permeability of more than an order of magnitude. For the packaging of food products which require protection against the ingress of oxygen from the external environment, the cellophane is coated or laminated with barriers to water such as polyolefins. Other hydrophilic barrier polymers , with the exception of certain amorphous polyamides, lose their barrier properties with increasing relative humidity. This happens because of the high affinity of these polymers with water which acts as a plasticizer, increasing the free volume of the polymer. However, at low to moderate relative humidity values, amorphous polyamides and PET exhibit properties slightly better with the increase of the relative humidity. This behavior has been explained by stating that since the water molecules do not swell the polymer, but they occupy, instead, part of the sites of the free volume of the polymer, leading to a reduction in the permeability of other gases. The copolymers of vinylden chloride, copolymers of acrylonitrile and polyolefins, for example, do not show any effect of relative humidity on gas permeability.

Chapter 2

Raw materials

This chapter describes the physical-chemical properties of all the materials used for the preparation of membranes, object of the present study.

2.1 Polymer: Polyether block amide (PEBAX)

Polyether block amide (PEBA) resin is best known under the trademark PEBAX (Arkema), and it is a thermoplastic elastomer (TPE) which combines linear chains of rigid polyamide segments interspaced with flexible polyether segments [8]. The history of PEBA resin can be dated back to 1972 when Atochem initiated research for a "soft nylon" material. The actual PEBA polymer was commercialized in 1981. It is produced by polycondensation of a dicarboxylic polyamide and a polyether diol in the presence of heat, vacuum, and a catalyst. The structure of the PEBAX repeating unit is shown in Figure 2.1:

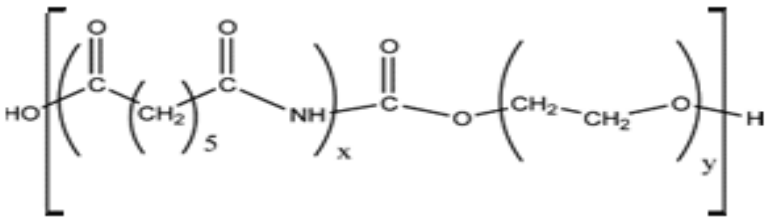

Figure 2.1. *Repeat unit of PEBAX structure.*

where PA is an aliphatic polyamide that constitutes the "hard segment" (i.e., Nylon-6 [PA6] or Nylon-12 [PA12]) and PEO is an amorphous polyether that constitutes the "soft segment" (i.e. Poly(ethylene oxide) or Poly(tetramethylene oxide)) of the polymer chain.

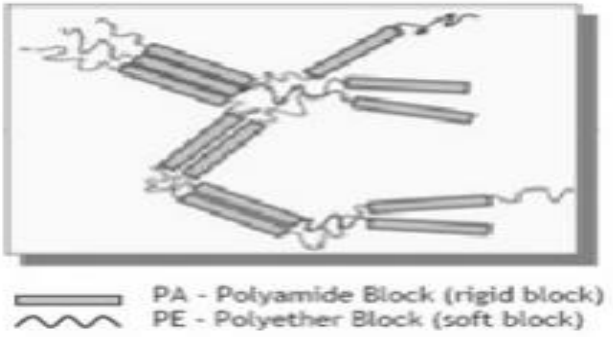

Figure 2.2. *Block structure of PEBAX.*

This crystalline/amorphous structure creates a blend of properties between thermoplastics and rubbers [9]. With reference to gas permeation, it was believed that the hard amide block provides the mechanical strength, whereas gas transport occurs primarily in the soft ether segments.

Currently, the main commercial applications of PEBA polymers range from sporting goods (shoe soles) and industrial equipment (conveyor belts) to functional films (breathable clothing, drying films) and various other materials. Only in recent years membranes based on PEBAX polymer have been investigated in separation processes.

PEBAX is a high performance thermoplastic elastomer [10]. It is used to replace common elastomers or thermoplastic polyurethanes, polyester elastomers, and silicones for the following characteristics: lower density among TPE, superior mechanical and dynamic properties (flexibility, high impact resistance, energy return, fatigue resistance) capability to retain these properties at low temperature (lower than -40 °C) and good resistance against a wide range of chemicals. It is sensitive to UV degradation, however.

Generally, depending on the particular composition that distinguishes it, PEBAX has a glass transition temperature ranging from -60 ° C to -40 ° C, and a melting temperature that varies from 140 °C to 170 °C [11]. As regards the properties of the material, it is possible to observe that from a rheological point of view, the area has a higher elasticity than that of conventional polyolefins. The physical properties depend on the molecular characteristics such as thickness of the crystallites, degree of crystallinity, size of spherulites, morphology and orientation of the chains.

The polymer used for the study is PEBAX 4533, its properties [11] are shown in Table 2.1:

Table 2.1. *Main physical-chemical properties of PEBAX 4533.*

Properties	Unit of measure	Value
Density	g/cm^3	1.01
Glass transition temperature	°C	-52
Melting temperature	°C	147
Tensile stress	MPa	9.1
Flexural Modulus	MPa	86
Water absorption	%	0.4-1.2

The mechanical properties, however, may vary from those of an amorphous polymer to those of a semi-crystalline polymer and are usually intermediate between those characteristics of the polyamide (rigid block) and that of the polyether (soft block).

In applications involving the removal of CO_2 from gas mixtures, PEBAX was found to have high selectivity for polar or quadrupolar/nonpolar systems [12]. Their sorption and permeation results suggested strong interactions between the polar gas CO_2 and the PE blocks in the

copolymers. It was found that PE composition and CO_2 permeability were directly correlated. Strong affinity of polar species to the PE block is attributed to the high permeability and perm-selectivity of polar gases through PEBAX copolymer. Even for H_2 can be found high permeability values, which are lower if respect to O_2 and N_2. This design has led to a ongoing search for methods to improve its barrier properties for gases such as air (O_2 and N_2), in order to separate gases such as CO_2 from a dirty air mixture.

2.2 Solvent: 1-Butanol (Bu-OH)

Butanol (also known as butyl alcohol) is a a four carbon atoms alcohol with a formula of C_4H_9OH[13]. There are four possible isomeric structures for butanol, ranging from a straight-chain primary alcohol (the one that is used as is shown in figure 2.3) to a branched-chain tertiary alcohol. It is primarily used as a solvent, as an intermediate in chemical synthesis, and as a fuel.

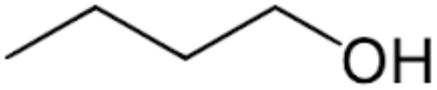

Figure 2.3. *Chemical structure of 1-Butanol.*

Since the 1950s, most butanol in the United States is produced commercially from fossil fuels. The most common process starts with propene (propylene), which is run through a hydroformylation reaction to form butyraldehyde, which is then reduced with hydrogen to 1-butanol and/or 2-butanol.
Next table shows the principal properties about 1-butanol:

Table 2.2. properties of 1-butanol.

Properties	Value
Molecular formula	$C_4H_{10}O$
Molar mass	4.12 $g \cdot mol^{-1}$
Appearance	Colourless, refractive liquid
Odor	banana-like, harsh, alcoholic and sweet
Density	0.81 g cm^{-3}
Melting point	−89.8 °C (−129.6 °F; 183.3 K)
Boiling point	117.7 °C (243.9 °F; 390.8 K)
Solubility in water	73 g L^{-1} at 25°C

2.3 Nanofiller (Graphene)

Polymer nanocomposites have existed for decades, as carbon black, pyrogenic silica and diatomite were used as additives in polymers [14]. Nevertheless, their characterizations and the effect of properties induced by the nanometric scale of these fillers was not fully understood at those times. The real starting point, corresponding to an understanding of the action of these fillers, is generally considered as corresponding to the first papers on a polyamide-6 filled with nanoclays [14]. Both these papers called it "hybrid" material. Rapidly the research increased and the first use of the term "nanocomposites" appeared in 1994. After these pioneers, a lot of researches started on various fillers. The demand for continual improvement in the performances of thermoplastic and thermoset polymer materials has led to the emergence of these new technologies. The number and typology of nanofillers has grown over the years (nanoclays, nano-oxides, carbon nanotubes, POSS , etc.), as well as the matrices in which they have been used. Nowadays, the development of polymer nanocomposites is one of the most active area of development of nanomaterials. The properties imparted by the nanoparticles are various and focus particularly on strengthening the electrical conduction and barrier properties to temperature, gases and liquids as well as the possible improvement of fire behavior. Being a method which consists of reinforcing polymer chains at the molecular scale in the same way that fibers do at a macroscopic scale, nanocomposites represent the new generation of two-phased materials, associating a basic matrix to nanofillers inserted between polymer chains. Nanofillers can significantly improve or adjust the different properties of the materials into which they are incorporated, such as optical, electrical, mechanical, thermal properties or fire-retardant properties, sometimes in synergy with conventional fillers. The properties of composite materials can be significantly impacted by the mixture ratio between the organic matrix and the nanofillers.

The study of graphene is one of the most exciting topics in materials science and condensed matter physics and graphene has good prospects for applications in a number of different fields. There has been a rapid rise of interest in the study of the structure and properties of graphene following the first report in 2004 of the preparation and isolation of single graphene layers in Manchester.

Graphene is a monoatomic layer of carbon atoms organized in a crystalline structure of hexagonal cells. This basic structure has a planar conformation and therefore the monoatomic layer is presented as a two-dimensional material. The graphene, whose carbon atoms are sp^2 hybridized, can be considered as the basic structure for the construction of all the other materials known as graphite fullerene (0D), carbon nanotubes (1D) and graphite (3D) [15]. Until the early 2000s, although it was recognized as an integral part of the materials graphite, graphene was studied as a "academic" material because everybody believed it was not

thermodynamically stable because of its tendency to bend and form structures such as fullerenes and nanotubes. In Figure 2.4 is a representation of the materials just mentioned.

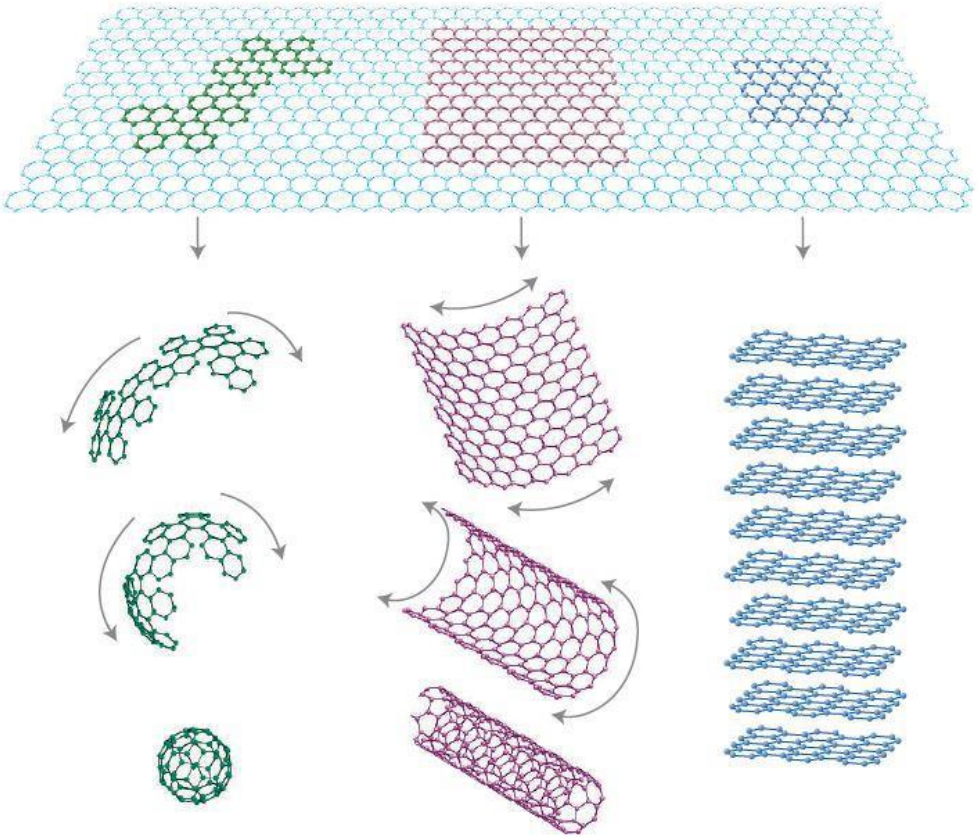

Figure 2.4. *Structure of graphitic materials. From left to right there is a representation of a fullerene (OD), of a nanotube (1D) and graphite (3D)*[15].

In 2004, Geim and Novoselov scientists were able to isolate a layer of graphene using the "scotch-tape" technique, which is based on the mechanical exfoliation of graphite attached along the surface of silicon wafer through a piece of tape [16].

2.3.1 The properties of graphene

The properties of graphene are necessarily linked to the 2D structure of the material and a complete physical and chemical characterization is ongoing because its discovery is relatively recent. Below an overview of the most important properties of the material is provided.

2.3.1.1. Electronic properties

One of the most important characteristics of graphene is that it is a semiconductor with zero *energy gap* (where electrons are the charge carriers) with a very high electrical conductivity [17-20]. Carbon atoms have a total of six electrons, two in the first valence shell and four in the

outermost shell. The latter, for each single carbon atom, have the ability to create chemical bonds in graphene but each atom is bonded to three others in the same x-y plane, leaving a free electron in the third dimension z.

Orbitals represented by these electrons, called "π electrons", are located above and below each sheet of graphene and they overlap and reinforce the carbon-carbon bonds.

It was shown that the point of Dirac of graphene (energy spectrum in the vicinity of the maximum of the valence band and the minimum of the conduction band) electrons and omissions have a zero mass. This is because the energy-related displacement is linear at low energies, in the vicinity of the vertices of the Brillouin zone; the electrons and the omissions are known as " Dirac Fermions" and six vertices of the Brillouin zone as "points of Dirac".

It can be noted that, since the density of points on the Dirac distribution, the electronic conductivity is very low, however, the Fermi level can be varied by doping the material (with electrons or holes) that has a better electrical conductivity at room temperature.

The energy bands of graphene are shown in Figure 2.5.

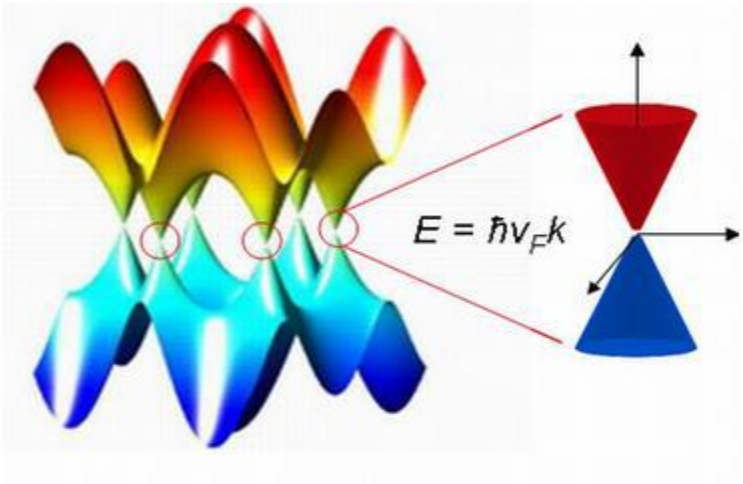

Figure 2.5. *The energy bands associated with sublattices intersect at zero, near the edge of the Brillouin zone, and give rise to conic sections of the energy spectrum with | E | <1 eV*[1].

Several tests have demonstrated the high mobility of the electron cloud of graphene, with results from 15 000 $cm^2 \cdot V^{-1} \cdot s^{-1}$ to 200 000 $cm^2 \cdot V^{-1} \cdot s^{-1}$ (limit due to acoustic scattering of photons).

The most limiting factors are, however, the quality of graphene and the substrate used; in the most frequent case, in which silicon dioxide is used, the electron mobility of up to 40000 $cm^2 \cdot V^{-1} \cdot s^{-1}$.

Equivalently, it can be started that graphene is the material known so far with the lowest resistivity, $1.0 \cdot 10^{-8}$ Ωm, also lower than that of silver ($1.59 \cdot 10^{-8}$ Ωm), which makes possible to obtain current densities even greater than 108 A/cm^2, or about six orders of magnitude larger than those that can flow in silver [17-21].

2.3.1.2. Mechanical properties.

Another fundamental characteristic of graphene is its mechanical strength. To now, it is considered the most resistant material in nature, due to tensile strength of 130 GPa, coupled to a very low density equal to 0.77 mg · m^{-3}, much higher than the modulus of the steel A36 (0.4 GPa) or that of Kevlar (0.38 GPa). Its elastic modulus is about 1 TPa, higher than that of materials such as diamond (0.82 TPa) or steel (0.2 TPa). These values may, however, vary greatly because of the difficulty of determining the precise geometry of the graphene sample, the voltage at the contact points of the membrane support, and for the intrinsic density of the defects of the material that has never a completely perfect structure [22-24].
Moreover, many studies, of both theoretical and experimental nature, have shown how it is possible to manipulate the elastic properties of the material by varying the temperature, sample size or density of the defects [25,26].

2.3.1.3. Optical properties.

The optical properties of graphene, like the electric ones, can be treated through the theory of partially-particle Dirac and the particular structure of the linear spectrum in the vicinity of the CNP (charge neutral points) points, characteristic that help to explain how a material thickness can be seen only with the light microscope. On this basis it is possible to calculate the transmittance of graphene using the Fresnel equation for thin films [27,28].

$$T = \left(1 + \frac{\pi\alpha}{2}\right)^{-2} \approx 1 - \pi\alpha \approx 0{,}977 \qquad (2.1)$$

This means that the absorption is given by:

$$A = \pi\alpha = 0.023 \qquad (2.2)$$

In other words, monoatomic graphene, while possessing the thickness of a single atom, is able to absorb a significant fraction of incident white light, equal to 2.3%. These percentages of absorption and transmittance depends on:

- wavelength of the incident radiation: usually uses the region of the spectrum between infrared (IR) and visible (VIS) where the contribution to absorption by the transitions within the bands is negligible, while at higher frequencies absorption may even exceed 10%.
- Number (n) of layers of graphene sheet: the relationship remains linear Fresnel until quantum n <5 (with 5 layers absorbance is about 12%) [29-32].

The figure shows a partially opening covered by a membrane made up of different layers of graphene so as to allow the crossing by the light radiation. It is noted that the right side of the membrane, where a sheet of bilayer graphene (BLG) is placed, is slightly darker, and this is confirmed by the increase to 4.6% of the absorbance.

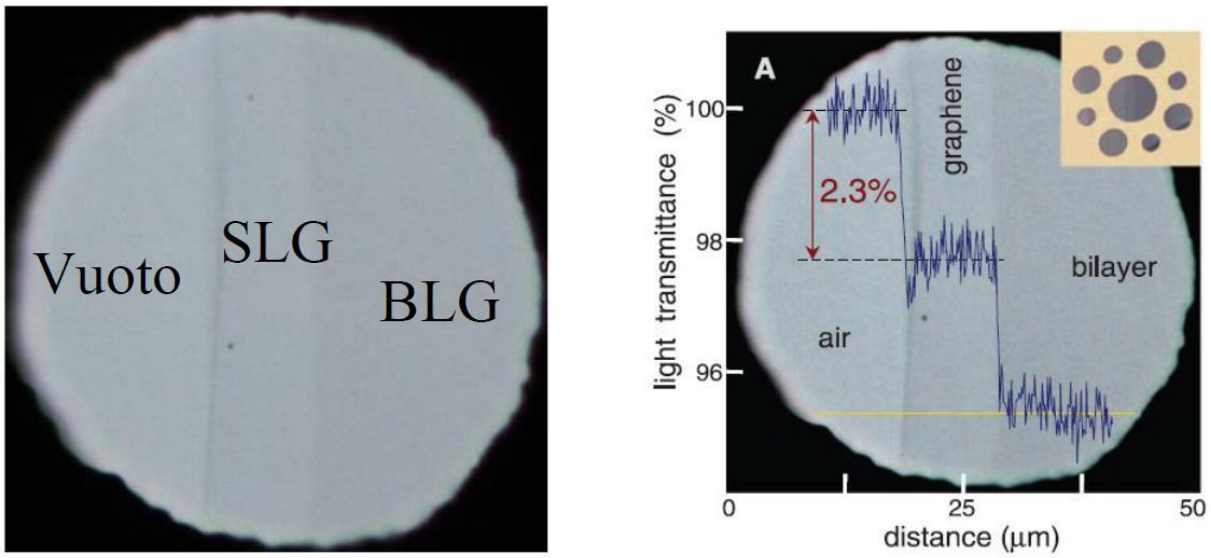

Figure 2.6. *Picture of different membranes of graphene (left), SLG = single layer graphene, BLG = bi-layer graphene; intensity of the light transmitted along the diameter of the membrane (right)* [28].

In consequence of this feature, it was observed that when the optical intensity reaches a certain threshold (known as "saturation flux"), the phenomenon of "Saturable absorbency" occurs, in which a very intense incident radiation causes a reduction of absorption of the material. This phenomenon means that in many electronic applications, graphene can be considered slightly influenced by the length of the incident radiation. In Figure 3.4 shows a comparison of transmittance between the graphene and the ITO (indium tin oxide, the most commonly used material for transparent conductive films) as a function of wavelength [26]. It is clear the difference in transmittance between the two materials; the first is a reduction at low wavelengths less than 10%, the second presents, however, an irregular trend.

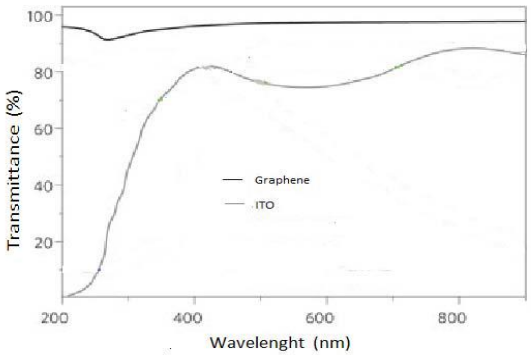

Figure 2.7. *Comparison of transmittance between the graphene and the ITO as a function of wavelength* [25].

2.3.1.4. Thermal properties.

Graphene is a perfect thermal conductor. Its thermal conductivity, around 5000 $Wm^{-1}K^{-1}$, was recently measured at room temperature and is much higher than all the values observed for the structures as carbonaceous nanotubes, graphite, diamond.

The monolayer deposited on a substrate of SiO_2, instead, shows a conductivity of 600 $Wm^{-1}K^{-1}$, exceeding that of metals such as copper (380 $Wm^{-1}K^{-1}$) and silver (430 $Wm^{-1}K^{-1}$).

It is assumed that the decrease of about one order of magnitude in the value of the conductivity of the monolayer of graphene deposited on the substrate compared to that in the free state is due to the scattering of phonons with the impurities at the interface of SiO_2 [31,32].

The ballistic thermal conductance of graphene is isotropic, it remains the same in all directions of rotation similarly to other material properties.

The study of the thermal conductivity has strong implications in possible new electronic devices continue to shrink in size compared to an increase in the density of the circuits. In this sense by providing a high thermal conductivity to such devices allows to dissipate heat efficiently while maintaining the internal circuits [33].

2.3.1.5. Chemical properties.

Similarly to graphite, graphene can absorb and desorb various weakly bound atoms or molecules that act as donors or acceptors and lead to a variation that change the gas flow, in this way the graphene remains highly conductive. Among the first ones, more usually used in the test are carbon monoxide (CO), ammonia and ethanol while the nitrogen dioxide (NO_2), water (H_2O) and the molecule of iodine (I_2) act as acceptors [33,34].

This characteristic is exploited in the field of sensors, particularly in environmental monitoring. Several experimental studies have confirmed the idea that the graphene, used in particular chemical sensors, is able to detect even a single molecule of gas. The ultimate goal of any detection method, in fact, is to achieve a level of sensitivity such as to discriminate the quantum of the measured quantity [36-38].

The main limitation to the resolution for these types of sensors is generally represented by intrinsic defects of the material of which they are made that result in high noise and, consequently, a low signal to noise ratio (SNR, Signal to noise ratio) [39].

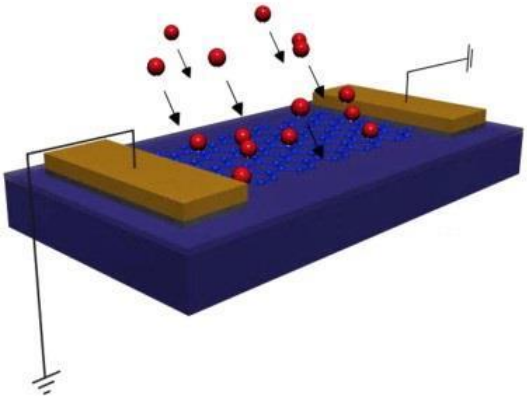

Figure 2.8. *Schematic diagram of a sensor with graphene* [40].

In addition to this type of adsorption, graphene can be functionalized by different chemical groups (such as -OH, -F) forming graphene oxide or fluorinated graphene. It was shown that a single layer of graphene is much more reactive than a sheet to 2-3 layers and the edges are even more reactive surfaces. However, it must be stated that, even if exposed to severe conditions of reaction, the graphene remains a material quite inert and does not react in a short time even if each atom is exposed to all the surrounding species[18].

2.3.2 Kind of graphene used

The kind of graphene used in the present study is Nano Graphene Platelets (NGP), also known as Graphene Nano Platelets (GNP): it is called N008-100-P-10 from the company (Angstron Materials) that produces it. There are several performance characteristics such as:

- Conductivity: NGPs have a very high thermal conductivity, up to 5,300 W/(mK), which is five times that of copper, while their density is four times lower than that of copper; the in-plane electrical conductivity of up to 20,000 S/cm is also excellent;
- Strength: NGPs are about 50 times stronger compared to steel; also they have a very high Young's modulus of about 1 TPa and extremely high intrinsic strength of approximately 130 GPa;
- Surface Area: NGPs have a specific surface area of up to 2,675 m^2/g, which is twice the surface area of CNTs;
- Density: NGPs have a density of about 2.25 g/cm^3;
- Dimensions: NGPs are available in a broad range of platelet lengths of 1 to 20 µm and thicknesses range of approximately 0.34 to 100 nm; also single layer graphene is very thin with a thickness of just 0.34 nm.

The figure below provides a graphical representation of the cost/performance benefits of NGPs compared to other competing material types.

Figure 2.9. Cost/performance benefits of NGPs compared to other competing material types.

2.4 Ionic Liquid (Bmim TFSI)

Ionic liquids (ILs) are widely recognized solvents due to their extended list of excellent physio-chemical properties such as wide liquid range, stability at high temperatures, no flammability and negligible vapor pressure; Their mainly success derives from their unique and fascinating characteristics such as being non-molecular solvents, having a negligible vapor pressure associated to a high thermal stability, tunable viscosity and miscibility with water and organic solvents [41]. These properties are the result of being molten salts that are liquid below 100 °C which generally consist of organic cation (e.g. imidazolium, pyrrolidinium, pyridinium, tetraalkyl ammonium or tetraalkyl phosphonium) and inorganic or organic anion (e.g. tetrafluoroborate, hexafluorophosphate, bromide). In addition, the high number of possible combination provides a long list of ILs with different polarity, hydrophobicity and viscosity, among others. For this reason ILs are known as "designer solvents".

ILs have been applied in the different fields of chemistry, such as organic and inorganic chemistry, electrochemistry and analytical chemistry. The growing interest towards ILs in analytical chemistry can be observed from the dramatic increase in the number of publications appeared during the last decade, and from the numerous reviews published during the years 2010 and 2011. The studies of ILs carried out in analytical chemistry have been mainly focused on extraction (i.e. liquid–liquid extraction, liquid-phase micro-extraction and solid-

phase micro-extraction), and separation (i.e. gas and liquid chromatography, and capillary electrophoresis).

Generally, a supported liquid membrane system used for gas separation, includes a feed solution, a solvent or solvent/carrier immobilized in the porous structure of a polymeric or ceramic membrane, and a receiving solution. The analyte dissolved in the feeding solution goes through the membrane and is enriched in the receiving solution. The organic solvent supported liquid membrane is not stable because of the loss of immobilized solvent via evaporation and its dissolution in the feed or the receiving solution. The unique properties of ILs such as negligible vapor pressure and immiscibility with water and some organic solvents can overcome these problems [42,43]. Moreover, mass transport is in general much faster in ionic liquids than in polymer materials, thus allowing higher fluxes through the membrane and more effective ‘‘faster’’ separation.

The Ionic liquid used for this project is:

1-Butyl-3-methylimidazoliumbis(trifluoromethanesulfonyl)imide known as bmim TFSI

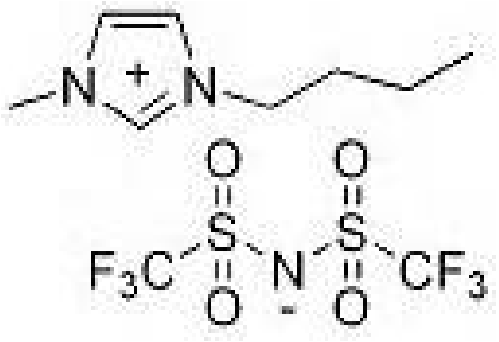

Figure 2.10. *Chemical structure of bmim TSFI.*

2.5 Detail of the raw materials

- Polymer: PEBAX 4533 (Arkema - France)
- Filler: Graphene nano platelets N008-100-P-10 (Angstron material – Ohio, USA)
- Solvent: 1-Butanol (Sigma Aldrich – USA)
- Filler: Ionic Liquid bmim-TFSI (Sigma Aldrich – USA)

Chapter 3

Technology processes and characterization methods

This chapter describes the processes and tools used for sample preparation, in the first part, and for the analysis of their properties, in the second.

3.1 Technology processes

In this study membranes were prepared by the solution-casting method [44]. The *polymer solution casting method* is a process where the polymer-filler solution (polymer + solvent + filler) is placed in a becker and, due to a combination of thermal and frictional properties, the polymer solution forms a thin film around the mold. The mold is then extracted from the becker in a precisely controlled manner, followed by a drying process.

3.1.1 Polymer Solution

The polymer solution was prepared by dissolving a weighed amount of polymer (PEBAX 4533) pellets inside the solvent (1-Butanol) [13]. The process of polymer dissolution in solvent has been made by mixing in a round bottom flask, keeping constant the temperature for a time sufficiently high to allow the polymer to dissolve, in order to form a homogeneous solution.
As shown in the figure 3.1, a typical configuration consists in a round bottom flask containing polymer and solvent, all inside of an oil bath which is heated, using a heating plate, at a temperature appropriate to obtain a solution. A condenser is connected to the round bottom flask to prevent solvent evaporation , given the high temperatures involved during the dissolution.

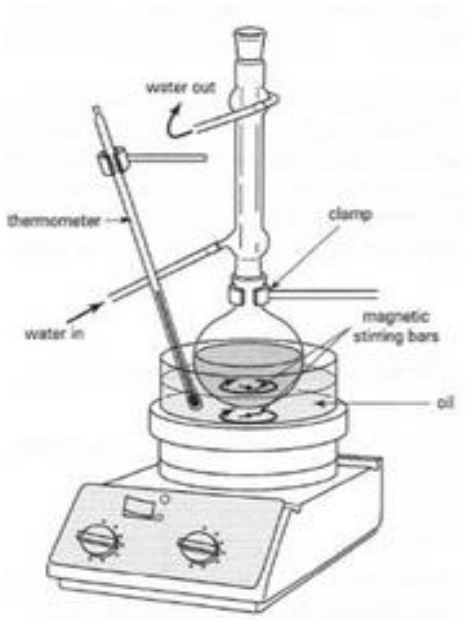

Figure 3.1. *Process of polymer dissolution.*

3.1.2 Filler Solution

Exfoliation in a solvent is a good way to produce a good filler solution, this technique is in fact used during this thesis work, and for this reason the focus is centered only on this method rather on other methods of production. The exfoliation techniques (also called top-down techniques), chemical and mechanical, unlike those related to the synthesis of substrates (also called bottom-up techniques), consist in the separation of the individual planes of graphite, because the ultimate objective is to be able to obtain on a large scale the single layer graphene.

The procedure of exfoliation in liquid phase, is composed of different operations, each of which can be changed in its operating variables (duration, power, concentration, temperature, pressure) making each procedure different from the others.

Generally, dispersions are obtained by treating, in an ultrasonic bath, the graphite powder dispersed in a solvent, so that the energy provided by the ultrasound favors the intercalation of solvent between the planes of the graphite and the separation between them. The power of the bath, however, has a fundamental role since, if too high, may result in the breaking of the graphene sheets [45]. After the sonication, the obtained dispersion presents a large number of macroscopic aggregates that can be separated by centrifugation.

The more intense research activity variables in this production method are [46-47]:

- The choice of a suitable solvent,
- The starting graphite material,
- The choice of the type of ultrasound procedure (bath or high-power sonication),
- The extent of the sonication and centrifugation processes.

As regards the choice of solvent, the most used are NMP (N-methyl-2-pyrrolidone) and DMF (N, N-dimethylformamide), among the organic solvents, and water with surfactants, between the inorganic solvents.

Generally, the organic solvents are more suitable for this method due to strong interactions that develop between solvent and carbonaceous surfaces favoring the exfoliation process.

From the thermodynamic point of view, the exfoliation occurs if the net energy cost is very small; this balance is expressed by the enthalpy of mixing ΔH_{mix} (per unit volume, V_{mix}) through the equation (3.1) from the Hildebrand-Scratchard model:

$$\frac{\Delta H_{mix}}{V_{mix}} = \frac{2}{T_{flake}} (\delta_G - \delta_{SOL})^2 \varphi \tag{3.1}$$

where $\delta_i = \sqrt{E_{sur}^i}$ is the square root of the surface tension of the stage, T_{flake} is the thickness of the graphene sheet and φ is the volume fraction of graphene, the subscripts G and SOL respectively refer to graphite and solvent.

The enthalpy of mixing, therefore, depends on the geometry of the nanomaterial and its surface tension, which for graphite is defined as the energy (per unit area) needed to overcome the Van der Waals forces for the two floors laminated exfoliation. From equation (3.1), it is expected that the best solvent for exfoliation are those with surface tension close to that of graphene.

This is analyzed by measuring the optical absorbance, A, after centrifugation with a spectrophotometer in a range of wavelength between 200-1000 nm (UV / Vis), because the value of A can be considered constant with good approximation. Subsequently, using the Lambert-Beer equation:

$$A = \alpha C_g L \tag{3.2}$$

where α is the coefficient of absorbance (specific for each solvent and function of the wavelength of the beam used) and L is the geometric path, C_g is the concentration of graphite/graphene remained in the tube.

As stated previously, the concentration of the dispersed phase shows a peak for solvents whose surface energy is close to that of graphite (which is around 70-80 $mJ*m^{-2}$); this implies that the enthalpy of mixing should be almost zero, and that interactions solvent-graphite should be of Van der Waals type rather than covalent character [47].

The equation 3.2 also indicates the range of 35-45 $mJ*m^{-2}$ for the surface tension of the most suitable solvents exfoliation, a value confirmed by various experimental trials [48-54]. As shown in Table 3.1 and other articles of literature, the organic solvents NMP and DMF are among those that have suitable surface tension, for which they are the most used for the exfoliation process in the liquid phase.

Table 3.1. *Surface tension and residual weight of graphite solutions in organic solvents* [55].

Solvent	Surface tension (mJ m^{-2})	Remaining after 4000 r.p.m. of centrifugation	
		Concentration (μg/ml)	wt% remaining
NMP	41	88.9	35.56
TMU	34.7	88.28	35.31
DMF	35.2	96.67	38.67
THF	26.4	76.03	30.41
Acetone	23.7	66.6	26.64
Ethanol	22.27	10.32	4.128
Formamide	58.35	3.67	1.468

These types of solvents, however, have some drawbacks among which:

- high boiling points (153°C for DMF, 202°C for NMP at atmospheric pressure) and therefore high energy cost of drying to recover the dispersed phase .
- difficulties for the realization of some reactions that require non-polar solvents, or which require an environment free of water (NMP and DMF are polar and hygroscopic solvents)
- they are flammable and toxic [56].

For these reasons there are several studies in the literature that use other types of solvents, in particular the aqueous solution in the presence of surfactants. The latter are necessary to decrease the surface tension between the solvent and graphite and ensure the exfoliation of the material. The surfactants used are: SDS (sodium dodecyl sulfate), COL (sodium cholate), TCNQ (tetracyanoquinodimethane), CTAB (hexadecyltrimethylammonium bromide) [57-60].
These solutions do not present problems of toxicity/flammability, have lower boiling points (and therefore they are easier to remove) but produces a degree of exfoliation sensibly lower [55].
To characterize the quality of the dispersed phase at the end of the process three parameters of the graphite sheets are evaluated: <N>, the number of layers; <L>, characteristic length; <W>, width feature.
Figure 3.2 shows the trend of these parameters as a function of the centrifugation speed and sonication time. It is noted that a greater speed of rotation decreases the concentration of the solution. This is because the dispersion is no longer homogeneous, but separates into a heavy and a lighter phase; in particular, both the thickness and the characteristic size of the supernatant decreased with increasing rotation speed. The above mentioned parameters have a similar trend by increasing the sonication time: this means that if on one side of the graphite particles are reduced at the typical thickness of a few layers graphene, to the other side the dimensions in the plane are reduced considerably and are almost always under the order of µm [50].

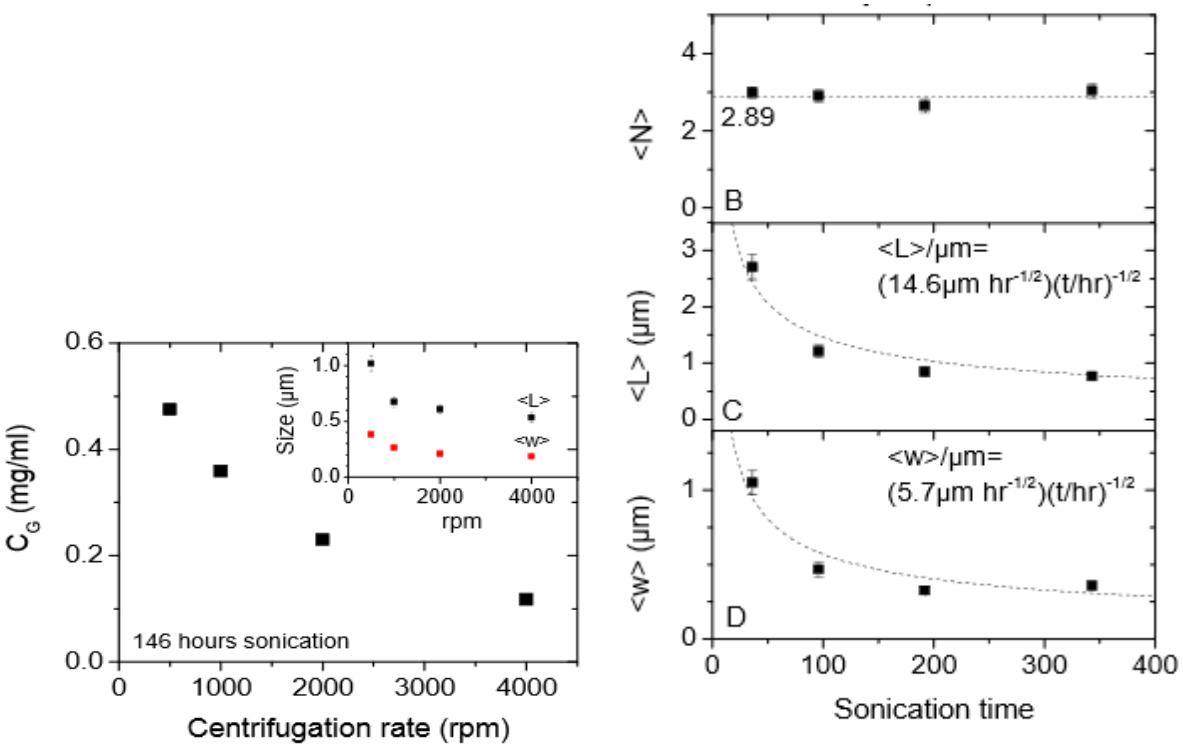

Figure 3.2. *(a) Variation of the concentration of graphene and size characteristics (in the box) as a function of the speed of centrifugation; (b) Variation of the dimensions and characteristics of the thickness of graphene as a function of sonication time* [50].

On the basis of these conclusions the filler solution was prepared by dissolving a weighed amount of nanofiller (graphene) inside the solvent (1-Butanol). The reason to use this solvent is that the solvents NMP and DMF are not capable to provide a good solubilization of the polymer (PEBAX 4533);while , as shown in literature, is 1-Butanol has proven to be a good solvent for both the polymer and the filler.

This process is divided in several steps:

- at the beginning, after weighing the graphene and adding to the solvent, the dispersion has been stirred to allow graphene layers to distribute well inside the solution, as shown in the figure 3.3.

Figure 3.3. *Stirring of graphene solution.*

- subsequently, the solution is placed in a *ultrasonic water bath* (figure 3.4) for a time sufficient to allow the layer of graphene to separate and then reach a solution better dispersed.

Figure 3.4. *Ultrasonic water bath sonicator.*

The working principle of ultrasonic water bath sonicator is the conversion of high frequency electrical energy into ultrasound waves by means of ultrasonic transducers, which are bonded to the base of a stainless steel water tank. These high frequency sound waves created in the liquid countless, microscopic vacuum bubbles, which rapidly expand and collapse. This phenomenon is called cavitation and this is the phenomenon behind the better dispersion that will be reached by the graphene: these bubbles act like miniature high speed brushes, driving the liquid into all the minute openings and recesses of the solid immersed in the liquid.

- Finally an *ultra shear homogenizer probe* (figure 3.5) is employed for a time sufficient to allow the layer of graphene to slip in order to reach a better solution dispersed.

Figura 3.5. *Ultra shear homogenizer probe.*

The *ultra shear homogenizer probe* uses a mechanical-rotation force to impart impact and shear forces to the dispersion , generating shear rates in the stream and decreasing the size of chains and allowing the layer of graphene to slip between themselves.

3.1.3 Polymer + Filler Solution

Final solution was prepared by placing the filler solution in the round bottom flask, where there is the polymer solution. Subsequently two steps are required:

- The first is to continue the mixing, as was done with the polymer solution (3.1.1), for a time sufficient to homogenize together both the solutions,
- The second is to use the *ultra shear homogenizer probe* in order to create intercalation between the filler and the polymer, always both inside the solvent.

3.1.4 Casting and drying

This is the last step, where the solution of polymer + filler + solvent is casted in a clean, dry, plate covered with Teflon. The Teflon plate is placed and leveled inside the oven, at a temperature that allow the solvent to evaporate, without degrading the polymer. After the time necessary to obtain almost the complete evaporation, the membrane is obtained and subsequently is placed in a vacuum oven in order to remove the last residues of solvent.
At the end, the final membrane is conserved into a plastic container, ready for future analysis.

Figure 3.6. *Final membrane.*

3.2 Graphene in polymers

The superior characteristics of graphene compared to other materials also determines an improvement their polymeric composites, in terms of mechanical, thermal, barrier, electrical properties and fire resistance.

In most applications, nanocomposites with graphene have mechanical and electrical properties better than those with graphite.

The physio-chemical characteristics depend on the distribution of the graphene layers in the polymeric matrix and bonds to the surface [36,61].

The natural graphite is not compatible with organic polymers and do not form homogeneous composites; on the contrary the graphene oxide (GO) is much more compatible and is used in place of graphene when the product should have properties of electrical insulator [62,63].

Numerous experimental investigations are still ongoing in order to overcome the limitations associated with the synthesis of these nanocomposites and they are particularly focused on:

- functionalization of graphene sheets;
- improvement of the homogenization of the dispersion as possible exfoliation;
- effective mixing of graphene and graphene oxide in the polymer;
- compatibilization of the properties and the interface of the two different phases;
- control of distension (folding), curling (crumpling) and flexion (bending) of the graphene sheets [64].

3.2.1 Properties of graphene-based polymer nanocomposites

Much of the nanocomposites produced with graphene are developed with very low loading (less than 3%) and only in a few cases by using high concentrations (but not more than 15%); this is justified by the fact that graphene is rather expensive to produce but increases the performance of the nanocomposite already in small percentages. The improvements mainly found in the nanocomposite polymer-graphene concern several properties ranging from the mechanical to the barrier ones.

3.2.1.1 Mechanical properties

Graphene significantly increases the tensile strength of polymeric materials thanks to the relationship between the shape (aspect ratio) and the tensile modulus of the filler. In Table 3.2 is presented a list of nanocomposites with graphite filler and the respective changes of the mechanical properties, in particular with regard to the elastic modulus (E), tensile (TS) and flexural strength.

Table 3.2. *Electrical properties of polymer nanocomposites with graphitic materials* [65].

Matrix	Filler type	Filler loading (wt.%[a], vol.%[b])	Process	% Increase E	% Increase TS	% Increase flexural strength
Epoxy	EG	1[a]	Sonication	8	−20	
	EG	1[a]	Shear	11	−7	
	EG	1[a]	Sonication and shear	15	−6	
	EG	0.1[a]	Solution			87
PMMA	EG	21[a]	Solution	21		
	GNP	5[a]	Solution	133		
PP	EG	3[b]	Melt			8
	xGnP-1	3[b]	Melt			26
	xGnP-15	3[b]	Melt			8
	Graphite	2.5[b]	SSSP		60	
LLDPE	xGnP	15[a]	Solution		200	
	Parrafin coated xGnP	30	Solution		22	
HDPE	EG	3[a]	Melt	100	4	
	UG	3[a]	Melt	33		
PPS	EG	4[a]	Melt			−20
	S-EG	4[a]	Melt			−33
PVA	GO	0.7[c]	Solution		76	
	Graphene	1.8[b]	Solution		150	
TPU	Graphene	5.1[b]	Solution	200		
	Sulfonated Graphene	1[a]	Solution		75	
PETI	EG	5[a]	*In situ*	39		
		10[a]	*In situ*	42		

3.2.1.2 Thermal properties

Stability and thermal conductivity of graphene (see § 2.3.1.4) have a positive impact on the thermal stability of the nanocomposites obtained; the geometry of the filler imparts an anisotropic character to the thermal conductivity of the material in the plane parallel to the particles, which can be 10 times higher than that in the perpendicular direction.

The most studied polymer, in this sense, are the epoxy resins in which a charge of 5% of GO leads to a thermal conductivity of about 1 W/ mK, four times greater than that of the pure resin. With a 20% of charge the conductivity can reach a value of 6.44 W/mK. As regards the thermal stability it has been possible to produce nanocomposites with a starting decomposition (onset) temperature of 100°C higher than those of pure polymer [64,65].

3.2.1.3. Electrical properties

The increase of the electrical conductivity is due to the formation of a conductive network made up only of graphene sheets in the polymer matrix.

In Table 3.3 are shown the significant variations of this property of the material as a function of the polymer, the method of production and the type of the carbonaceous filler. Correlations between these factors are difficult to determine, however it is important to note that the highest value of conductivity was obtained using very low concentrations of graphene , in comparison to other types of fillers.

Table 3.3. *Electrical properties of polymer nanocomposites with graphitic materials* [65].

Matrix	Filler	Filler loading (wt.%[a], vol.%[b])	Process	σ (S m^{-1}) of matrix	σ (S m^{-1}) of composite
Epoxy	EG	3.00[a]	Sonication	1E−13	1E−4
	EG	2.50[b]	Solution	1E−15	1E−2
	Graphene	0.52[b]	Solution	1E−10	1E−2
PMMA	NanoG	0.68[b]	*In situ*	1E−13	1E−3
	EG	1.00[a]	Solution	1E−15	1E−3
	EG	10[a]	*In situ*	–	77.65
PS	NanoG	1.00[a]	*In situ*	1E−14	1E−4
	Graphene	0.10[b]	Solution	1E−16	1E−5
	GNS^{CAF}	0.40[b]	Solution	1E−14	1E−5
	GNS^{CAF}	0.10[b]	Solution	1E−14	4
	GNS^{BB}	0.20[b]	Solution	1E−14	1E−5
	GNS^{SD}	0.30[b]	Solution	1E−14	1E−5
	Graphene	–	Solution	1E−16	24
	Graphene	2.0[a]	*In situ*	1E−10	1E−2
	EG	1.50[b]	*In situ*	1E−16	1E−4
	K-GIC	8.20[a]	Solution	NA	–
Nylon-6	EG	1.50[b]	*In situ*	1E−15	0.1
	FG	0.75[b]	*In situ*	1E−15	1E−5
PP	xGnP-1	3.00[b]	Coating	1E−12	0.1
	xGnP-1	3.00[b]	Solution	1E−12	1E−2
	xGnP-15	7.00[b]	Melt	1E−12	1E−3
	xGnP-15	5.00[b]	Coating	1E−12	0.1
	EG	0.67[b]	Solution	1E−16	0.1
HDPE	EG	3.00[a]	Melt	1E−16	1E−8
	UG	5.00[a]	Melt	1E−16	1E−10
PPS	EG	4.0[a]	Melt	1E−12	1E−3
	S-EG	4.0[a]	Melt	1E−12	1E−2
PANI	Graphite	1.5[a]	*In situ*	5.0	3300.3
	GO	–	*In situ*	2.0	1000
PVDF	FGS	2.0[a]	Solution	1E−11	1E−2
	EG	5.0[a]	Solution	1E−11	1E−3
PVA-S	NanoG	0.2[a]	Solution	1E−13	1E−3
PET	Graphene	0.47[b]	Melt	1E−14	7.4E−2
Polycarbonate	FGS	2.0[a]	Melt	1E−14	1E−9
	Graphite	12	Melt	1E−14	6.6E−11

3.2.1.4 Barrier properties.

The introduction of graphene sheets or GO can significantly reduce the gas permeability through the polymer matrix, due to the formation of a percolating network that produces a tortuous path which slows the diffusion of gas molecules. A schematic representation of this phenomenon is represented by Figure 3.7.

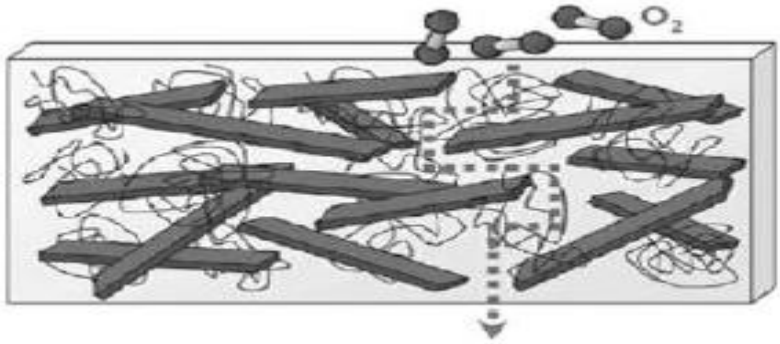

Figure 3.7. *Illustration of the formation of a "tortuous path" from the carbonaceous filler in the polymer* [66].

The most important factors to take into consideration in order to obtain an accentuated barrier effect are the concentration of graphene, the preferential orientation of the particles and the aspect ratio.

Practical case study about this phenomenon are:

- PP-graphene nanocomposites at 6.5% with a 20% reduction in the oxygen permeability [36,61-64],
- Polycarbonate nanocomposites-GO 3.5% with a reduction of almost 40% to the permeability of nitrogen [36,61-64],
- GO-polyurethane nanocomposites (thermoplastic): in this case it was observed a greater barrier effect for the GO functionalized compared to thermally reduced [36,61-64].

3.3 Characterization methods

3.3.1 Measurements of gas barrier: permeabilimeter

One of the properties of interest for the investigation conducted on the materials available is the permeability, since it allows to identify the barrier ability of the films examined in relation to the passage of gas through the surface. This property is particularly important for the industrial sector, where the ability to limit the passage of carbon dioxide or the leakage of oxygen and nitrogen allows to better separate the gaseous streams.

The measurements were conducted using films of about 50 cm^2 of area, obtained by solution casting, under constant and controlled conditions of temperature and relative humidity. The

instrument employed consists of two cells separated by the polymer film to be analyzed, between which a pressure difference is established in order to assess the passage of the gas from one end to other of the sample. The top cell is constituted by a cylinder fixed by the pressure of a metal screw, the seat of the film where a rubber o-ring allows to isolate the system from the infiltration of the outer atmosphere and, through the formation of vacuum in the lower cell, create the pressure difference that allows the flow of gas through the film.

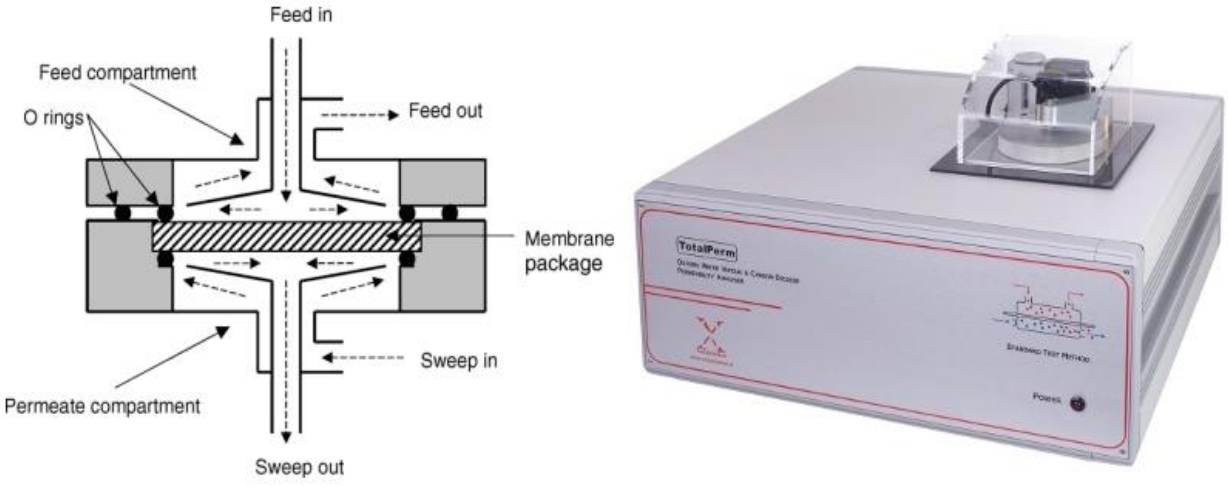

Figure 3.8. *Detail of the measuring cell (left) and permeabilimeter (TotalPerm, Extrasolution) for measuring permeability to O_2, CO_2 and water vapor.*

In the early stages of the operation there is a conditioning phase during which the machine sends a stream of anhydrous nitrogen electronically controlled, both in the top cell and the bottom where there is the detection of the effective permeability of the film. This step is necessary in order to remove traces of residual gas which are present during the loading procedure of the instrument and in the sample. When the concentration of the gas reaches a minimum value, the nitrogen flow in the lower half cell (carrier) is reduced to the operating value. It follows an increase of gas concentration up to a stationary value. The value of stationary reached is the starting reference point to make a differential measurement, which is realized by flowing a stream of the gas under analysis (O_2, CO_2 or water vapor) in the upper cell so to allow its permeation through the polymeric film. Once that by permeation the gas reaches the bottom cell it is collected from the carrier and detected by the downstream sensor. When the transmission speed of the gas reaches a constant value the instrument records the value as the output of the measurement. All the above described operations are performed while maintaining the cell at a constant temperature set by the user with a long term stability of better than ± 0.1°C. Is also executed a control/monitoring of the relative humidity, flows and of all the variables that may alter the permeation of the object under examination such as, for example, atmospheric pressure. The output of the machine is the degree of gas transmission, Q, expressed as:

$$Q = \frac{V}{A}\frac{273}{273+T}\frac{1}{\Delta P}\frac{1}{dt} \tag{3.1}$$

where V [cm^3] is the volume of the cell at low pressure, A [m^2] is the area of the transmission section, T [°C] is the temperature of the cell at low pressure, ΔP [bar] is the pressure between the two faces of the film, t [s] is the time of diffusion and dt is the slope of the pressure vs. measurement time determined in the stationary state. The gas permeability is therefore characterized by the permeability coefficient, P, the product of the diffusion coefficient for the solubility and measured in [cc·cm/(m^2·24h·bar)]:

$$\mathrm{P} = \frac{\mathrm{l}}{\Delta \mathrm{PAt}}\mathrm{Q} \tag{3.2}$$

where *l* is the thickness of the film in cm.

3.2.2 Mechanical characterization: dynamometer

Each time a force is applied to a solid, this will deform in response to the stress. Considering only small deformations, if after removing the force applied to the material, it returns to its original configuration, the deformation is called elastic. In this type of deformation all the work that is done to deform the material is stored in the form of elastic energy that is released once the stress stops. For this reason it is possible to compare samples of different forms: by dividing the applied force, F, for the cross-section area, A, by the stress, σ, is obtained and dividing the change in length, ΔL, for the original length, L_0 , you get the deformation, ε. The relationship between stress and strain allows the calculation of the elastic modulus:

$$\frac{F}{A} = \sigma = E\varepsilon \tag{3.3}$$

Measurable as the slope of the stress-strain curve in the elastic conditions. The behavior of a real material is generally different from that ideally elastic: the presence of large deformations leads to a plastic type response . In these conditions, the energy spent to deform the material is not recovered at all, as well as part of the deformation itself. In the complete σ-ε curve particular points that are useful in the determination of the mechanical properties can be highlighted:

- *Proportional limit*: is the point where the curve σ-ε begins to deviate from linearity. The value of the module is obtained from the curve points that are within this limit,

- *Enervation limit*: is the point where the material begins to deform plastically, over these values the material is unable to recover all of the deformation,
- *Break limit*: is the point on the curve where there is the breaking of the sample of material.

An explanation of the elastic-plastic behavior can be given by analyzing the structure and organization of the macromolecules of the polymer. In the elastic range the deformation takes place by effect of a recoverable movement of the chains, represented by the unentanglement of the macromolecules of the amorphous phase that are oriented along the stress direction, with a low deformation of the crystalline part of the structure. Exceeded the yielding point, the deformations become permanent, the movements of the chains leads to the breakdown of the entanglements between the molecules, which slide along the crystalline planes leading to the formation of cracks and cavities. The engineering curve σ-ε presents a maximum given by the yield strength, which is followed by a decrease as the applied stress, the necking effect, which reduces the resistant effective cross-section of the specimen. After the complete necking of the specimen, the applied stress remains more or less constant until the onset of the hardening phenomena, which correspond to the increase of the stress applied to maintain a given constant strain rate ; at this stage it gradually changes to the rupture of the secondary bonds and unentanglement of macromolecules, the real break of the main chain. To quantify the effect of the introduction of some additives on the mechanical properties of PEBAX mechanical tests were carried out by means of the dynamometer in order to determine:

- Tensile modulus,
- Bending modulus of elasticity,
- Percentage elongation at break,
- Load at yield.

Figure 3.9. *Dynamometer Sum 2500.*

3.2.2.1 Tensile tests dynamometer

The specimens used for the execution of the pull test have the typical shape of a dog bone. This samples were obtained from the films, produced by solution casting, by using a die cutter. The specimens have geometrical parameters in agreement with a system of internal reference, reported in Table 3.4, so as to allow the comparison between them. The specimens shall be free from twist, the edges without incisions, defects, surface pitting and burrs. In order to obtain greater accuracy in the values of strain a strain gauge is used: only the crosshead movement as a reference for the recording of the data is in fact often imprecise and less reliable.

Table 3.4. *Geometric characteristics of the specimens for the tensile test.*

Geometric characteristic	Size [mm]
Total length	100
Length of the useful part	35
Width at the ends	25
Width of the useful part	6
Thickness	0.1 - 0.15

For a correct measurement of the specimen deformation it is necessary that the strain gauge is essentially free of inertia and capable to measuring the variations in the length with a good accuracy : this corresponds to an accuracy of 1 micron for the measurement of the module, based on a measuring length of 50 mm. It 'also necessary that there is no damage to the specimen by knives or slipping between the extensometer and the specimen. After the tests, it

was decided to calculate the tensile modulus graphically as the slope of a secant line in the first section of the elastic deformation of the specimen.

3.2.2.2 Bending tests dynamometer

The method is used generally for the analysis of the specimen behavior to bending for the determination of the relevant module, of its resistance and for the study of other aspects relating to the stress-strain relationship.

Table 3.5. *Geometric characteristics of the specimens for the bending test*.

Geometric characteristic	Size [mm]
length	80
width	10
thickness	4

The test was performed on specimens that had the dimensions shown in Table 3.5 and is applicable to a simple beam, supported freely and with load applied on the center line (three-point test). With these load conditions, the Young's bending modulus is calculated according to the following equation:

$$E_f = \frac{L^3}{4be}\left[\frac{\Delta F}{\Delta y}\right] \tag{3.4}$$

where L is the distance between the supports, b is the length of the specimen, and e is the thickness of the tube, Δf is the increase of the force which is subject to the material between two points of the initial portion of the stress-strain curve, Δy is the difference of the arrows corresponding to Δf.

3.2.3 Resilience IZOD

In order to determine the influence of the charge on the impact resistance of the material resilience IZOD tests were carried. The test consists of measuring the energy required to break a specimen appropriately notched: the specimen is impacted by a pendulum which is allowed to swing from a known height. The initial potential energy of the pendulum is 1 Joule and after the impact of the tool directly returns the value of the absorbed energy, which must be the energy lost to friction. The value of IZOD is obtained by the formula:

$$IZOD = \frac{Energy}{Thickness} \tag{3.5}$$

where the energy is absorbed and the thickness is expressed in meters.

3.2.4 DMA (Dynamic Mechanical Analysis)

The dynamic-mechanical analysis consists in imposing a small cyclic deformation of a sample and measuring the resulting stress response, or equivalently, to impose a stress cycle on the sample and measuring the resulting response of deformation. The DMA is used both for the study of relaxation processes in polymers and for the determination of the mechanical properties (e.g., modulus and damping) and inherent flow, as a function of time and temperature. With these results an analysis of structure-properties of the polymer can be carried out by finding:

- glass transition temperature,
- secondary transitions,
- crystallinity,
- molecular mass / crosslinking,
- phase separations,
- aging,
- effect of additives.

To understand the behavior of the sample, let's consider what happens when a sinusoidal deformation is applied to a linear elastic solid:

$$\varepsilon(t) = \varepsilon_0 \sin(\omega t) \tag{3.6}$$

At each point in time, the effort will be proportional to the deformation in accordance with Hooke's law:

$$\sigma(t) = E \cdot \varepsilon(t) = E \cdot \varepsilon_0 \cdot \sin(\omega t) \tag{3.7}$$

So, for an ideal solid, the effort will be a sinusoidal function in phase with the deformation and the ratio of the effort and the deformation is the modulus of the material:

$$E = \frac{\sigma_0}{\varepsilon_0} \tag{3.8}$$

Now if we consider what happens if a sinusoidal shear deformation is applied to an ideal liquid:

$$\gamma = \gamma_0 \cdot \sin(\omega t) \tag{3.9}$$

At each point in time the stress will be proportional to the rate of deformation in accordance with Newton's law for viscosity:

$$\tau(t) = \eta\dot{\gamma}(t) = \eta\frac{d\gamma(t)}{dt} = \eta\gamma_0\cos(\omega t) = \eta\gamma_0\sin\left(\omega t + \frac{\pi}{2}\right) \qquad (3.10)$$

So for an ideal liquid the effort will be a sinusoidal function out of phase by 90° with respect to deformation. This phase difference of 90° between the sinusoidal stress and deformation in liquids is the key to use the DMA as a tool for the characterization of viscoelastic materials such as polymers.

Since a viscoelastic material has properties intermediate between an ideal solid and an ideal liquid, it shows a phase delay of between 0° (solid ideal) and 90° (ideal liquid). This delay between stress and strain corresponds to the time necessary to obtain molecular rearrangements. The data obtained by this type of analysis are commonly expressed using an amount which is defined as a complex module. This quantity is derived from a discussion of the variables of the complex sinusoidal deformation and can be defined as the ratio between the stress applied and the resulting sinusoidal deformation. The complex modulus is a characteristic property of the material which changes only when the material changes. It is exclusively a function of time, since the DMA experiments are made in conditions of very small deformations.

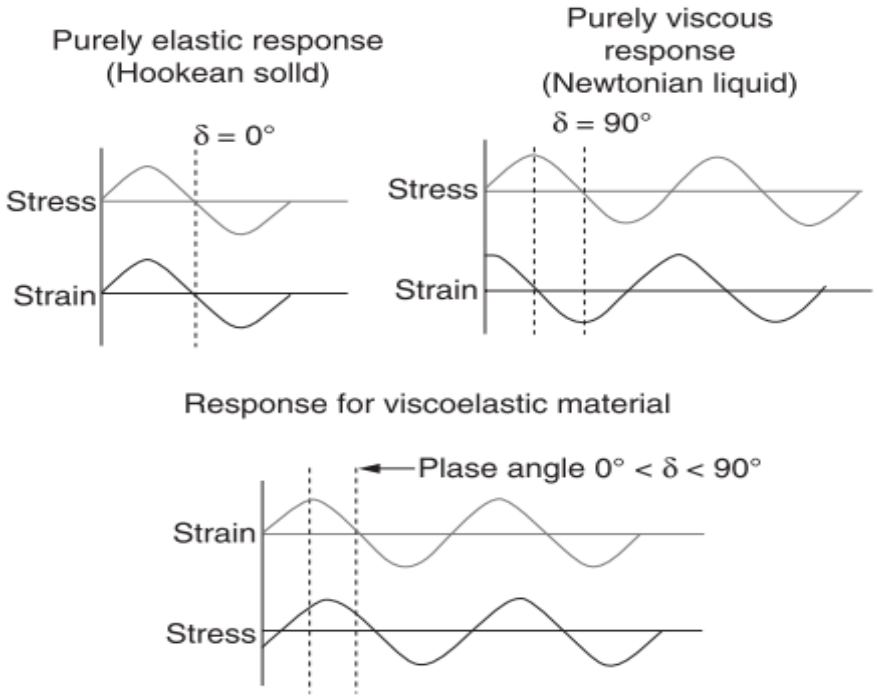

Figure 3.10. *Graphs for comparison of the response of an elastic material with respect to a viscous and a viscoelastic one in relation to the application of a stress of sinusoidal type.*

Under these conditions, the response of the material is in the range of linear viscoelastic. This means that the magnitude of stress and strain are linearly related to each other and the deformation behavior is completely specified by the function of the complex modulus. The complex modulus can be divided into two components: a real and an imaginary part:

$$E^* = E' + iE'' \tag{3.11}$$

where:

$$E' = \frac{\sigma_0}{\varepsilon_0}\cos(\delta) \tag{3.12}$$

$$E'' = \frac{\sigma_0}{\varepsilon_0}\sin(\delta) \tag{3.13}$$

E' is known as the *storage modulus* and it is a measure of the pseudo elastic solid character or nature of the material; E" is known as the *loss modulus* and is a measure of the pseudo liquid or viscous character of the material. When E' is higher than E", more energy is required to deform the sample in an elastically reversible manner. When E" is higher than E', higher is the strain energy which is dissipated viscously as heat. From a physical point of view, the *storage modulus* is related to the stiffness of the material and the *loss modulus* reflects the damping capacity of the material. There is, then, a third quantity can be defined by taking into consideration the ratio between the *loss modulus* and *storage modulus*:

$$\frac{E'}{E''} = \frac{\sin(\delta)}{\cos(\delta)} = \tan(\delta) \tag{3.14}$$

This amount is known as the loss factor of the material or commonly "*tan δ*". The *tan δ* varies from zero for an ideal elastic solid up to infinity for an ideal liquid and represents the ratio between the energy dissipated and energy stored per cycle of deformation. The performance of these three quantities enables to identify the variations in the phase and structure of the polymer. The performance of these quantities are, in fact, associated to the effects of resonance between the frequency of the stress imposed and certain molecular motions that become spontaneously active at certain temperatures. From a structural point of view, in fact, the polymer chain during heating is subject to a series of movements that take the name of thermal transitions. The most important of these is the glass transition temperature (Tg) which is the minimum temperature at which cooperative movements of large segments of the chain are possible. From the macroscopic point of view this transition can be detected in terms of change in the properties of the material that passes from a hard-brittle, glassy state, to a rubbery and easily deformed one. The techniques for determining the value of the Tg are

numerous: in this work was obtained at the peak of the *loss modulus*, i.e. the range where the *storage modulus* decreased sharply.

3.2.5 DMA – HDT

The heat distortion temperature (HDT) or deflection temperature under load (DTUL) is the maximum temperature to which a thermoplastic polymer can be used as a rigid material. The test is performed on rectangular specimens, with specific dimensions, in a 3-Point Bending device, applying them to the center of a fixed load (3.23 N) and by heating the samples with a constant rate (1°C/min) within a fixed temperature range. Is obtained from the analysis the trend of the deformation (displacement) of the specimen as a function of temperature, from which one can derive the value of HDT as it is the temperature which corresponds to a deformation of 0.121%, equal to about 11 microns whereas the geometry of the specimens used (4 x 10 mm - thickness x width) and a distance between the supports of 15 mm.

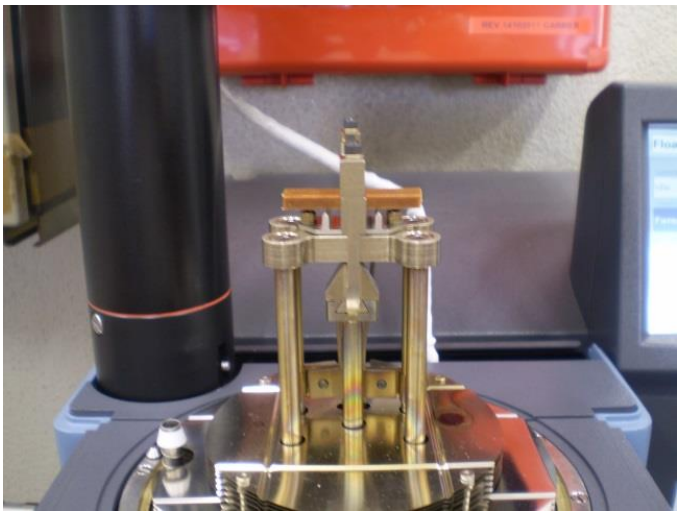

Figure 3.11. *Tool to calculate the HDT*

3.2.6 DSC (Differential Scanning Calorimetry)

The DSC[4] (Differential Scanning Calorimetry) is a thermo-analytical technique that measures the heat flow associated to the thermal transitions of a sample with respect to a reference (inert), when these are subjected to scanning temperature in a controlled atmosphere. In agreement with the classification of thermodynamic phase transitions of a material can be distinguished:

- *First-order transitions:* when you have a discontinuity in the first derivative of the Gibbs free energy with respect to a thermodynamic variable (i.e. temperature,

[4] In accordance with ASTM Standard E 473, the DSC is a technique where the difference in the speed of the heat flow of a substance compared to a sample is measured as a function of temperature, while the sample is subjected to a controlled temperature program.

pressure). Since these derivatives correspond to variables such as volume, entropy and enthalpy, processes such as melting, evaporation, crystallization, sublimation and condensation are first order transitions,

- *Second-order transitions*: when you have continuity of the first derivative, but discontinuity in the second derivative of the Gibbs free energy. Examples of these phenomena are the magnetic transition at the Curie point, the transition superfluid liquid helium, the glass transition and the transitions secondary in the case of amorphous polymers and semi-crystalline.

In the case of polymers, such technique is particularly useful in order to determine information such as:

- melting temperature,
- heat of fusion,
- percentage of crystallinity,
- glass transition temperature,
- crystallisation,
- presence of recycled / regrind,
- plasticizers,
- presence, composition and compatibility of polymer blends.

The technique is based on measurement of the energy required to cancel the temperature difference between the test substance and the reference that consists of an inert, while both are subject to the same temperature regimes in a heated or cooled at a controlled rate. There are two types of commonly used systems DSC:

- *A power compensation DSC*: where the analysis cell consists of two separate furnaces that are controlled independently, according to a heating program defined. If an endothermic or exothermic phenomenon leads to a variation in temperature compared to the reference, the machine provides or removes energy from the furnace of the sample in order to compensate for this variation. The energy required to do this is a measure of the enthalpy of the sample relative to the reference,
- DSC heat flow: in this case the sample and the reference are connected by a low-resistance metal disk and the system is enclosed in a single furnace. In this way the temperature of the cell is varied according to a preset program, while the instrument provides to measure the temperature difference between sample and reference, as a function of temperature. This difference is directly proportional to heat flow.

3.2.6.1 DSC heat flow

This equipment typically consists of a reference cell and a sample port separated by a bridge which acts as a heat sink, surrounded by a block constituted by a body at a constant temperature. The block is the housing that contains the heating system, the sensors and media. The latter are raised platforms on which the vessels of the reference and the sample are placed. The loss of heat facilitates a rapid transfer of heat and allow a reasonable time to reach the steady state. The differential behavior of the sample and the reference is recorded and is subsequently used to determine the thermal properties of the sample.

A temperature sensor is positioned at the base of each platform. Associated with the cell there is a furnace and a sensor. The furnace is designed to provide a heating with linear speed. However, not only the rate of heating should be linear, but also the cooling. This can be achieved by cooling the housing up to low temperatures.

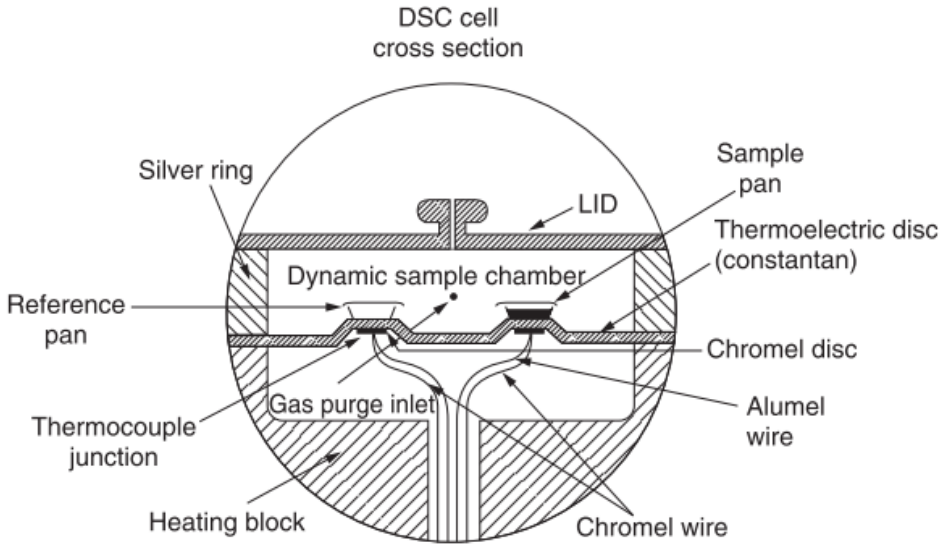

Figure 3.12. *Schematic representation of a DSC cell.*

Finally, the inert gas, typically nitrogen, flows within the cell. The operation of the heat flow of the DSC is based on the equivalent thermal Ohm's law. Ohm's law states that the current is the ratio of the voltage and resistance, so, if in the same heat, we have:

$$\dot{Q} = \frac{\Delta T}{R} \tag{3.15}$$

where $\dot{Q}$ is the rate of heat flow, ΔT is the temperature difference between the sensors of the sample and the reference, and R is the thermal resistance of the heat sink disc.

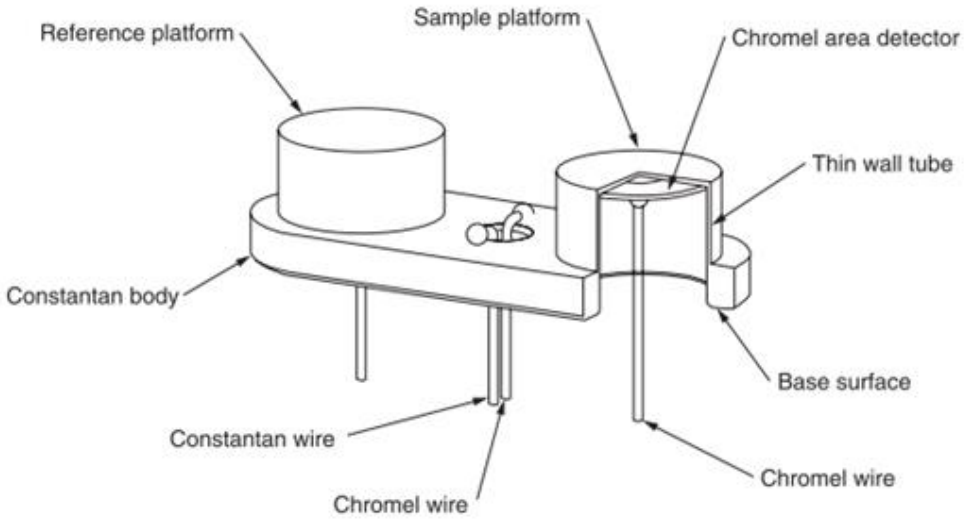

Figure 3.13. *Representation of the support of a DSC cell.*

3.2.7 TGA (Thermo Gravimetric Analysis)

The thermogravimetric analysis is a technique where the variation of the mass of a sample is measured as a function of the temperature and / or time and the sample is subjected to a heating program at a constant speed in a controlled atmosphere. This technique is commonly applied in research and analysis of polymers as it provides useful information about thermal stability, oxidative stability, amount of moisture absorbed and of volatiles present, quantities of organic and inorganic components (i.r. offices) present in the material.

The data is recorded on a thermogram showing decomposition of the sample by the decrease of its mass with increasing temperature. The essence of the instrument consists of a thermobalance, enclosed inside a cylindrical furnace, which measures the changes in weight of the sample with respect to a reference as a function of temperature on the basis of the heating program adopted. A change in mass of the sample produces a deflection yoke that goes to interpose a shutter between the lamp and one of the two photodiodes. The consequent variation of the current of the photodiode is amplified and sent to a coil located between the poles of a permanent magnet. The magnetic field generated by the current in the coil shows the yoke in its original position.

The current is amplified by the photodiodes is measured and translated into a mass or mass loss through the processing system. In the case of polymers, heat causes chemical modifications with cleavage of the bonds that usually lead to the formation of volatile species. For this reason, the data of the TGA analysis provide characteristic curves for a given polymer as each polymer possesses a unique pattern of reactions to specific temperatures.

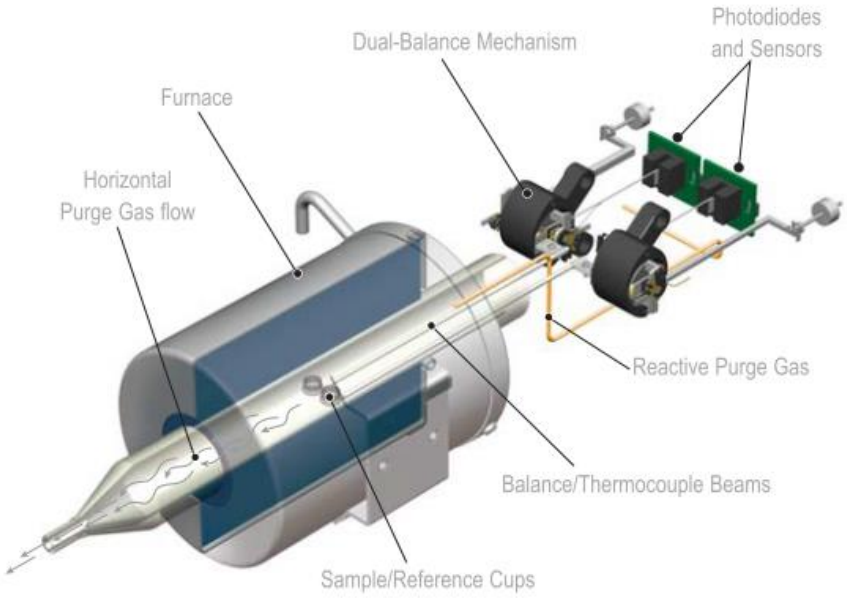

Figure 3.14. *Schematic representation of a TGA thermobalance*

The choice of the atmosphere can have a significant effect on the results of an analysis TGA. Use nitrogen or another type of inert as opposed to oxygen or air delays the start of decomposition and can change the shape of the interior thermogram.

3.2.8 SEM (Scanning Electron Microscopy)

In the scanning electron microscope (SEM), an electron source is focused, under vacuum atmosphere, in a thin beam which is collimated on the surface of the sample. The electron beam emitted by the thermionic effect is accelerated in a direction to the application of a potential difference. Thereafter, the beam passes through a system of electromagnetic lenses which have the task of focusing the beam reducing the size up to the order of nm. Then there are electrostatic deflectors deflecting the trajectories of the electrons allow the scanning of the beam on the sample surface. As the electrons penetrate the surface, occur a number of interactions that determine the emission of electrons or photons from or through the surface.
A reasonable fraction of the emitted electrons can be collected from appropriate *detectors*, and the *output* can be used to modulate the brightness of a cathode ray tube[5] whose inputs x and y are driven in synchronism with the voltages of *xy rastering* the electron beam. In this way produces an image in the cathode ray tube; each point that the beam strikes the sample is directly mapped on a point of the screen.

[5] A cathode ray tube is a tube, where there is vacuum, that produces images when its phosphorescent surface is struck by the electron beams. These tubes can be monochrome (using a single electron gun) or colored (typically using three electron guns to produce images of red, green and blue, which when combined form a multi-color image).

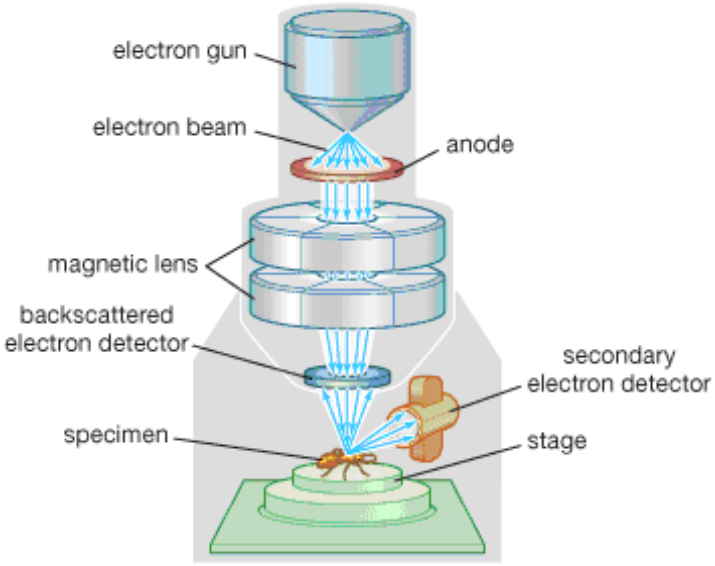

Figure 3.15. *Sketch of a SEM.*

3.2.9 TEM (Transmission Electron Microscopy)

The transmission electron microscopy (TEM) is a further electron microscopy technique based on the passage and the interaction of a beam of electrons with a given sample. The electrons are emitted from a source and are focused and accelerated by a system of magnetic lenses. The beam of electrons confined by two condenser lenses, which also control the brightness of the beam, passes through the aperture of the condenser and hits the surface of the sample. The electrons, that are elastically scattered, consist of transmitted rays, which pass through the objective lens. The objective lenses forming the displayed image, while the successive openings, the goal and the opening of the selected area is used to choose the elastically scattered electrons that form the microscope image. Finally, the beam reaches the magnification system that consists of three lenses, the first and the second lens control the magnification of the image and the last is the projector lens. The formed image is displayed on a fluorescent screen or on a monitor, or both.

The samples to be analyzed by TEM should be very thin to allow the penetration of the electrons. For this reason, we resort to using an ultramicrotome with a diamond tipped cutting at cryogenic temperatures in order to obtain very thin samples.

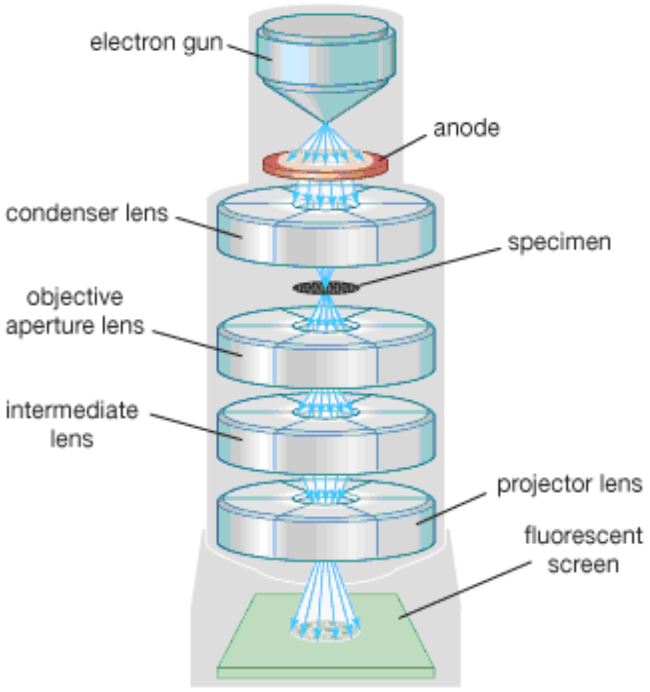

Figure 3.16. *Sketch of a TEM.*

3.2.10 Image analysis

The image analysis allows to evaluate the size of the dispersed phase structures present in the mixture, in order to make a qualitative and quantitative comparison between mixtures that differ in the type and concentration of additive. This work was performed using software (ImageJ) through which, after setting the scale known equivalence between pixels and maeker photos, were measured the length and width of the structures under consideration. It was then calculated, as a product, the area between the two measured parameters and was obtained the equivalent diameter (*deq*) with the formula:

$$deq = \sqrt{\frac{4A}{\pi}} \tag{3.16}$$

Due to the irregular shape of the structures considered, the equivalent diameter allows to represent them as the hypothetical circumferences and simplify the comparison between the different blends. Obviously the *deq* will be more reliable as more as the shape of the structures under consideration will be approximated to a perfect sphere, otherwise it will have a certain approximation error.

3.2.11 Raman Spectroscopy

Spectroscopy is the main experimental method to determinate the vibration frequencies of a molecule. It is based on the radiation interaction, which can lead to several effects, among which the absorption and spread by the molecules. In the first case one obtains a spectrum of infrared absorption, in the second a spectrum of Raman scattering.

In Raman spectroscopy the radiation emitted by a laser beam interacts with the roto-vibrational motion of the molecules, with the subsequent re-emission of different wavelengths from that of the incident. The spectrum that is obtained, said Raman spectrum, provides a sort of fingerprint of the molecule studied, allowing the identification.

When monochromatic radiation affects a substance may result in the following effects:

1) most of the radiation pass through the sample;
2) elastic scattering, a small part of the radiation, in all directions without energy loss, that is, at the same frequency of the incident radiation (elastic scattering or Rayleigh); such diffusion is believed to have caused by elastic collisions between molecules and quantum;
3) inelastic scattering of an even smaller part, yielding (Stokes Raman scattering) or acquired (anti-Stokes Raman scattering) energy interacting with the molecule, vibrating at frequencies that differ in vibrational energy quantum.

The intensity of the scattered radiation (less than the intensity of the incident radiation) depends both from the contribution given by the elastic scattering that by inelastic scattering. These, in turn, depend on the chemical structure of the molecules responsible for the spread. A typical spectrum of the scattered light is generally given by intensity against shift as frequence of the radiation exciter ($\Delta\nu$ = defined as the difference between the scattered radiation emitted by the sample and that emitted by the source, a parameter therefore independent of the wavelength of the laser). For Raman spectrum, in fact, it generally means the part of the spectrum containing the Stokes lines. They, as already mentioned, correspond to frequencies that differ for those vibrational energy (inelastic scattering, or Raman effect). The phenomenon described is shown in Figure 3.17.

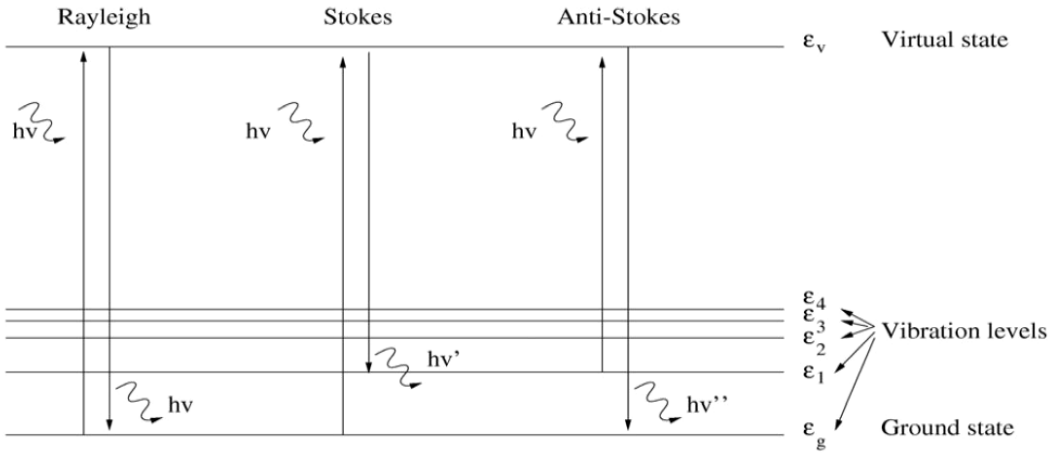

Figure 3.17. *Differences of vibrational quantum between various components of Raman spectrum.*

These differences correspond to the separation of two vibrational levels and are the characteristic frequencies molecules emission impacted by the incident light. The set of these differences generates the Raman spectrum of compound. It derives its origin from absorption and re-emission related to vibrational excitation or relaxation. This scattered radiation can be spectrally resolved and recorded.

In Raman spectroscopy, the energy levels of the molecule are explored by analyzing the frequencies present in the scattered radiation from the molecule. In a typical Raman experiment, a beam of monochromatic light is made to affect the sample in order to detect the radiation scattered at an orthogonal angle to the direction of the incident beam. When the incident photons collide the molecule, they may lose or gain energy. If the molecule absorbs part of the photonic energy to switch to an excited state, the photon will reemerge with an energy (frequency) less than that of incidence, going to form the so-called Stokes lines of the Raman spectrum. If the molecule is already in an excited state (the thermal energy at room temperature excites some states rotational) may assign to the incident photon energy that will emerge by the impact with more energy, going to form the anti-Stokes lines. The component of the scattered radiation in the same direction of origin without any change in frequency is called Rayleigh radiation.

Then, the Raman lines are the result of the inelastic scattering of incident radiation by the sample: the rows shifted to lower frequencies are produced by molecules that lose energy to photons, passing from the ground state to the first excited (Stokes lines); those at higher frequencies, are produced from molecules in an excited vibrational state that absorb energy from photons (anti-Stokes lines). Stokes lines are more intense than anti-Stokes one and are used for analytical purposes. The row with the same frequency of the source, resulting from the Rayleigh scattering of the incident radiation, is the component most intense of the Raman spectrum and must be removed. A system for Raman spectroscopy (Figure 3.18) is briefly composed of a laser source, a sampling system to send the laser beam on the sample and

collect the Raman signal, a system for separating the Raman signal from the diffused light component in an elastic way (the so-called Rayleigh scattering), an interferometer and a detection system.

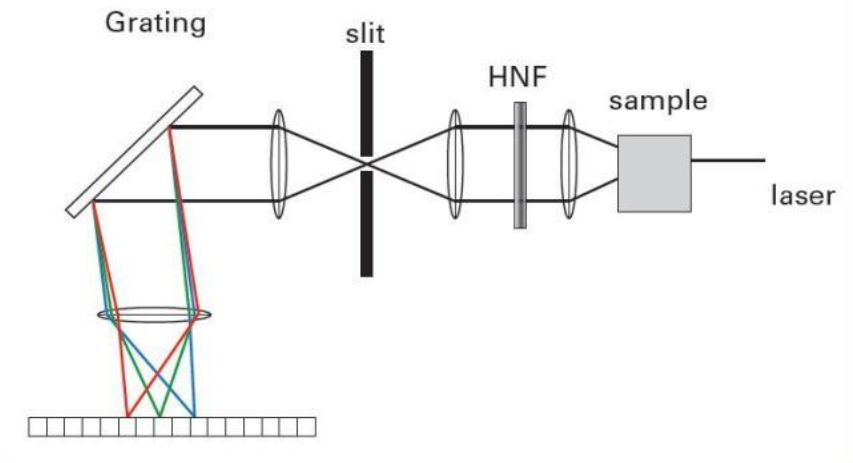

Figure 3.18. *Raman spectrometer scheme.*

3.2.12 X-ray diffractometry (XRD)

X-rays are produced when an electrically charged particle with sufficient kinetic energy, is rapidly decelerated. The X-radiation is generated in an X-ray tube containing an electron source and two metal electrodes at high potential difference. The electrons hit the anode with high impact energy and produce X-rays which are radiated in all directions. Not all the electrons are decelerated in the same way: some lose their energy only with the impact, giving X-rays with a minimum wavelength λ. The relationship between λ with d.d.p. applied is of the type:

$$\lambda\text{min} = \frac{h \cdot c}{e \cdot V} \tag{3.17}$$

with c the speed of light, V the potential difference, h Planck's constant and e the electron charge. X-rays can interact with ordered structures (e.g. polymer crystals or lamellar structures silicate) undergoing phenomena of reflection and diffraction from the crystal planes. In the specific application of the characterization of polymer nanocomposites (but more generally the crystal structures) one of the possible techniques of investigation by means of X-rays is based on the theory of Bragg, briefly summarized by the reaction:

$$\text{n} \cdot \lambda = 2 \cdot \text{d} \cdot \sin\theta \tag{3.18}$$

where n is the order of reflection, λ the wavelength, θ the angle between the diffracted light and the crystal plane, d is the interplanar distance. Thanks to the Bragg relation is possible to trace precisely the interplanar distances, varying the wavelength or the angle of detection. The diffraction fact is mainly due to the existence of interactions between multiple phase waves: if for any reason, such as the presence of lattice planes or lamellar structures, differences arise in the paths trodden by the various rays, can exist strengthened or attenuation of intensity of radiation. If this difference is an integer multiple of λ we will have a mutual reinforcement in the direction θ. The XRD analysis is widely used in the study of polymer composites based lamellar silicates in order to determine precisely the enlargement of the lamellar clay floors due to interleaving of the polymer. In the ideal case of complete exfoliation, the disappearance of short-range ordered structures (with spacings between the crystallographic planes of the nanometer order) makes it impossible diffraction.

Chapter 4

Experimental tests results on PEBAX membranes

The purpose of the following analysis is to characterize some types of membranes, all prepared with the intention of improve the properties of the PEBAX, in order to have a complete description which allows to identify the best solutions, for a possible practical use.
In addition to the permeability measuring, which is the main test, have been performed also other tests to measure the morphological properties, thermal and physical properties of various samples, for example the elastic modulus, the glass transition temperature (Tg) and melting temperature (Tm) etc. The samples analyzed differ in the type and the concentration of the added charge to the matrix of PEBAX via solution casting process.

4.1 Raw material

PEBAX 4533 is made available from Arkema, polymer composed of polyether block amide obtained from oil, its exact composition is not disclosed by the manufacturer. As regards the nanofiller, the Angstron Material provides the Graphene nano platelets N008-100-P-10. Finally, the Sigma Aldrich, provides both the solvent and the ionic liquid used, respectively, the 1-butanol and bmim-TFSI

4.2 Samples preparation

The sample preparation, make by solution casting method, starts from the pure polymer film (blank), after that an increasing amounts of graphene is gradually added. Final step is the addition of the ionic liquid inside polymer + graphene membrane. Table 4.1 at next page shows all the best samples prepared during the internship work.

Table 4.1. *Prepared samples.*

N°	Sample name	Graphene %	Ionic Liquid %
1	PEBAX 4533 pure (blank)	0	0
2	PEBAX 4533 + 1.5% graphene	1,5	0
3	PEBAX 4533 + 3% graphene	3	0
4	PEBAX 4533 + 5% graphene	5	0
5	PEBAX 4533 + 5% ionic liquid	0	5
6	PEBAX 4533 + 1.5% graphene + 5% ionic liquid	1,5	5
7	PEBAX 4533 + 3% graphene + 5% ionic liquid	3	5
8	PEBAX 4533 + 5% graphene + 5% ionic liquid	5	5

The procedure for the preparation is: (follow the number on table 4.1)

1) PEBAX 4533 solution was prepared by dissolving PEBAX 4533 (2 gr) in 1-Butanol (30 ml) under slow continuous stirring for 2 hours at 90 °C until the polymer dissolved. Then, PEBAX 4533 films were cast on a clean, dry, level teflon plate. Finally membranes were dried in an oven at 30 °C about 5 hours to remove the remained solvent from the initial solution and in a vacuum oven at 25 °C about 6 hours in order to be sure that the solvent is totally away.

2) First N008-100-P-10 nanopowder (0.03 gr) was dispersed in 1-Butanol (25 ml) under continuous stirring for 1 hour and by bath sonication for 2 hours to break up any aggregation and improve the dispersion quality following by shear mixer (power 2) for 1 hour. Then polymer solution prepared in the same way as for pure[6] was gradually added (T=90 °C) and the shear mixing (power 2) was continued for 2 hours to achieve a homogenous solution. After that, membranes were cast and dry in the same way as for pure PEBAX membranes.

3) First N008-100-P-10 nanopowder (0.06 gr) was dispersed in 1-Butanol (35 ml) under continuous stirring for 1 hour and by bath sonication for 2 hours to break up any aggregation and improve the dispersion quality following by shear mixer (power 3) for 1 hour. Then polymer solution prepared in the same way as for pure was gradually added (T=90 °C) and the shear mixing (power 3) was continued for 2 hours to achieve a homogenous solution. After that, membranes were cast and dry in the same way as for pure PEBAX membranes.

[6] Prepared in the same way as for pure means same quantity of polymer and solvent and same conditions as the preparation of pure polymer membranes.

4) First N008-100-P-10 nanopowder (0.1 gr) was dispersed in 1-Butanol (50 ml) under continuous stirring for 1 hour and by bath sonication for 2 hours to break up any aggregation and improve the dispersion quality following by shear mixer (power 4) for 1 hour. Then polymer solution prepared in the same way as for pure was gradually added (T=90 °C) and the shear mixing (power 4) was continued for 2 hours to achieve a homogenous solution. After that, membranes were cast and dry in the same way as for pure PEBAX membranes.

5) Polymer solution was prepared in the same way as for pure. After that the IL (0.075 gr) mixed with 1-Butanol (10 ml) was added on the solution (T=80 °C) and stirred for 15 mins. In the end membranes were cast and dry in the same way as for pure PEBAX membranes.

6) First N008-100-P-10 nanopowder (0.03 gr) was dispersed in 1-Butanol (25 ml) under continuous stirring for 1 hour and by bath sonication for 2 hours to break up any aggregation and improve the dispersion quality following by shear mixer (power 2) for 1 hour. Then polymer solution prepared in the same way as for pure was gradually added (T=90 °C) and the shear mixing (power 2) was continued for 2 hours to achieve a homogenous solution. After that the IL (0.075 gr) mixed with 1-Butanol (10 ml) was added on the solution (T=80 °C) and stirred for 15 mins. In the end membranes were cast and dry in the same way as for pure PEBAX membranes.

7) First N008-100-P-10 nanopowder (0.06 gr) was dispersed in 1-Butanol (35 ml) under continuous stirring for 1 hour and by bath sonication for 2 hours to break up any aggregation and improve the dispersion quality following by shear mixer (power 3) for 1 hour. Then polymer solution prepared in the same way as for pure was gradually added (T=90 °C) and the shear mixing (power 3) was continued for 2 hours to achieve a homogenous solution. After that the IL (0.075 gr) mixed with 1-Butanol (10 ml) was added on the solution (T=80 °C) and stirred for 15 mins. In the end membranes were cast and dry in the same way as for pure PEBAX membranes.

8) First N008-100-P-10 nanopowder (0.1 gr) was dispersed in 1-Butanol (50 ml) under continuous stirring for 1 hour and by bath sonication for 2 hours to break up any aggregation and improve the dispersion quality following by shear mixer (power 4) for 1 hour. Then polymer solution prepared in the same way as for pure was gradually added (T=90 °C) and the shear mixing (power 4) was continued for 2 hours to achieve a homogenous solution. After that the IL (0.075 gr) mixed with 1-Butanol (10 ml) was

added on the solution (T=80 °C) and stirred for 15 mins. In the end membranes were cast and dry in the same way as for pure PEBAX membranes.

The goal for each membrane is to get a film with about 100 µm of thickness.

4.3 Permeability measurements

The oxygen permeability and the transmission speed of the water vapor are the diffusional properties more frequently measured, because the exchange of oxygen and water vapor present in the air give a good initial information about the permeability. In fact the air permeability should always be taken into account within a chemical plant. At the end of this work it will be found most relevant purposes to which these membranes are suitable.
The permeability tests, O_2 and water vapor, have been realized by employing a permeabilimeter (Extrasolution, TotalPerm model) and use some circular samples of 8 cm diameter, obtained from films previously manufactured by solution casting.
On some of the blend was also tested the CO_2 permeability, in order to have a more complete description of the phenomenon, such analysis is not negligible since the purpose of such membranes is precisely to separate the CO_2 from other gaseous steam.

4.3.1 Oxygen permeability

The measurements were made on samples about 50 cm^2 of surface, setting the required parameters with specific values (Table 4.2). For each type of blend were tested two or more samples, being careful not to perform more tests on the same sample because has been verified that, tests subsequent to the first, depart from an initial situation with the concentration of the permeating gas is not nothing, thus altering the measure.

Table 4.2. *Set parameters for oxygen test permeability.*

T Set Point [°C]	**Relative Umidity [%]**	**Barometric compensation [mbar]**	**Conditioning**
25	0	automatic	high

Then, with the obtained values was calculated the constant permeability P using the following relationship:

$$P = \frac{J*l}{\Delta P} \qquad (5.1)$$

Where J represents the net flow of the permeating through the film, l its thickness (found as the average of thickness values on the four sides of the film) and ΔP and the difference of partial pressure of the gas on the two surfaces of the membrane.

The commercial interest of PEBAX in the gaseous separation application is due to its easy way of processing, also that is a polymer discovered recently and excellent strength properties, flexibility and gas permeability-selectivity studied recently. Table 4.3 shows the values of the oxygen's constant permeability, obtained from the average of the results from all samples analyzed for a certain blend. Is shown also the standard deviation and the percentage change compared to the value of the constant of PEBAX. As can be seen, the addition of the charge to the matrix of PEBAX determines a reduction of the permeability constant, also reaching high values for high graphene percentage. For this reason, it can be said that graphene has a discreet barrier effect.

In Figure 4.1 you can see a typical trend of the curve of permeability.

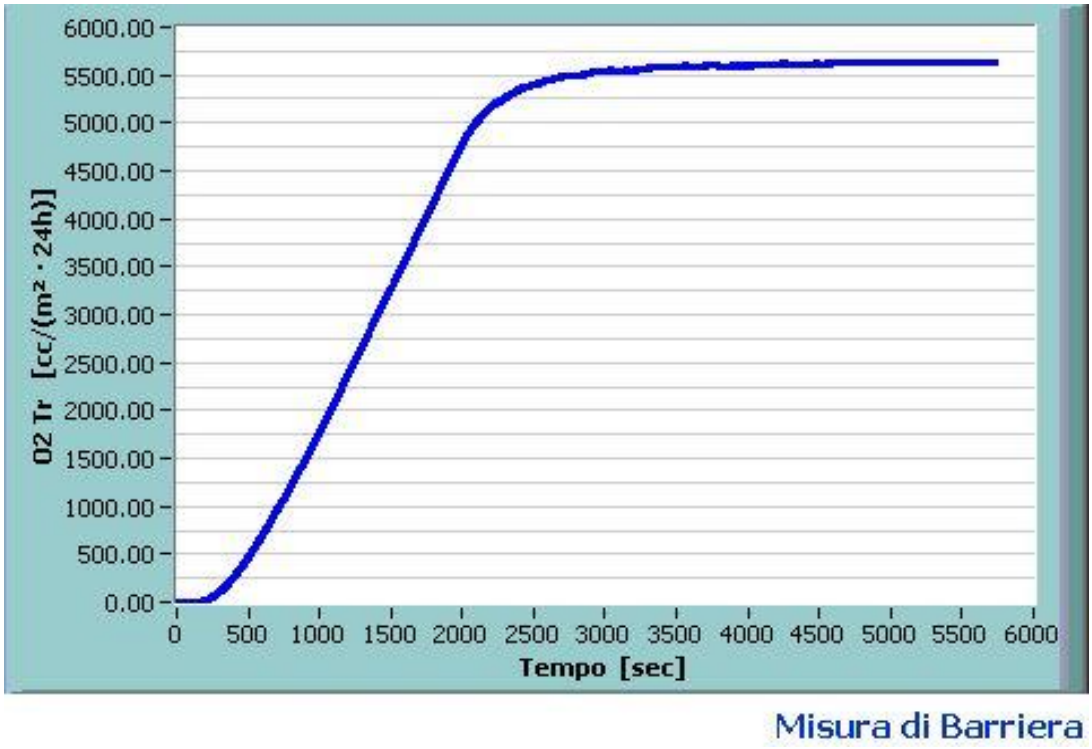

Figure 4.1. *Example of oxygen permeability curve for PEBAX.*

As for the blend prepared using the ionic liquid, there is an increase of permeability with the result that its addition increases the flow of oxygen through the membrane.

For deepen the analysis of this trend, were determined the diffusion coefficient (D) and solubility (S), Table 4.3, using the *time-lag method.*

Table4.3. *Measurement results of oxygen permeability for PEBAX and its compounds.*

Sample	Permeability costant [(cc·mm)/(m^2·24h·bar)]	Standard deviation	Variation %
PEBAX pure	588.02	3.5	-
PEBAX + 1.5% G	552.44	8.3	-6.4
PEBAX + 3% G	509.89	6.0	-15.3
PEBAX + 5% G	455.06	5.3	-29.2
PEBAX + 3% G + 5% IL	586.05	2.8	-0.3

Table 4.4. *Model solution-diffusion coefficients for oxygen permeability measurements.*

Sample	Diffusion coefficient [mm^2/s]	Solubility coefficient [cm^3/(cm^3·bar]
PEBAX pure	3.14*E-06 ± 4.52*E-07	2.17 ± 8.42*E-02
PEBAX + 1.5% G	2.88*E-06 ± 3.01*E-08	2.15 ± 7.24*E-02
PEBAX + 3% G	2.77*E-06 ± 1.52*E-08	2.13 ± 3.87*E-02
PEBAX + 5% G	2.73*E-06 ± 2.06*E-07	2.04 ± 8.32*E-02
PEBAX + 3% G + 5% IL	2.82*E-06 ± 1.24*E-07	2.57 ± 6.12*E-02

The diffusion coefficient D varies with the concentration of charge and this leads to think that, the reduction of permeability, is closely linked to physical phenomena, also considering the small size of the molecule of oxygen. Instead, less influential is the solubility coefficient S, which remains constant and does not influence the adsorption of molecules on the membrane. Otherwise it should be noted with the addition of the ionic liquid: the diffusion coefficient is practically the same with respect to the charged membrane to 3% without the ionic liquid. The big difference is the solubility coefficient, it increase a lot compared to the pure polymer, it comes to fill the failure of given permeability barrier effect of graphene.

4.3.2 Water vapor permeability

The samples were obtained in the same way as for the tests of oxygen permeability. The tests were carried out at a temperature of 25 ° C and relative humidity of 50%. The permeability constant was calculated by normalizing the value obtained for the test with the thickness of the film.

In Figure 4.2 you can see a typical trend of the curve of permeability.

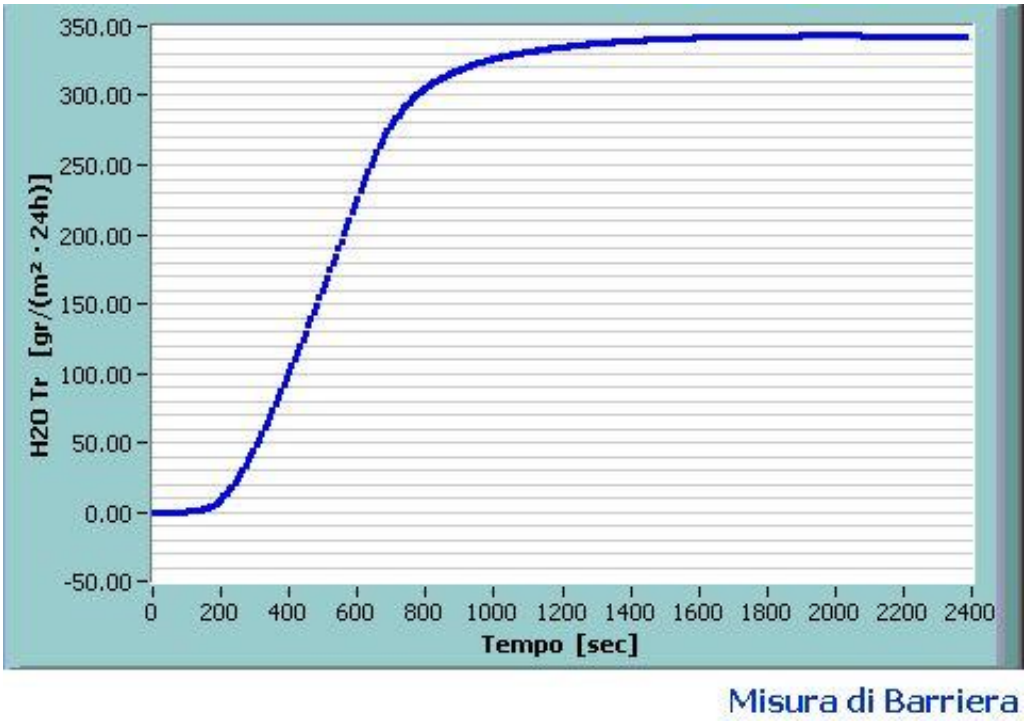

Figure 4.2. *Example of vapor water permeability curve for PEBAX.*

Also for the water vapor permeability, the results show a moderate barrier effect of graphene, this is because there is a reduction of the permeability constant as can be seen from Table 4.5. This decrease is due to the lowering of the diffusion coefficient as it increases the percentage of graphene, while the coefficient of solubility remains practically unchanged (Table 4.6).

Table 4.5. *Measurement results of vapor water permeability for PEBAX and its compounds.*

Sample	**Permeability constant [(cc·mm)/(m^2·24h·bar)]**	**Standard deviation**	**Variation %**
PEBAX pure	20.77	0.32	-
PEBAX + 1.5% G	17.92	0.28	-15.9
PEBAX + 3% G	17.26	0.13	-20.3
PEBAX + 5% G	16.53	0.31	-25.6
PEBAX + 3% G + 5% IL	27.39	0.22	+31.9

Table 4.6. *Model solution-diffusion coefficients for vapor water permeability measurements.*

Sample	Diffusion coefficient [mm^2/s]	Solubility coefficient [$cm^3/(cm^3 \cdot bar$]
PEBAX pure	5.15*E-06 ± 1.32*E-08	0.047 ± 8.03*E-03
PEBAX + 1.5% G	4.84*E-06 ± 8.41*E-07	0.043 ± 7.75*E-03
PEBAX + 3% G	4.50*E-06 ± 1.94*E-08	0.044 ± 1.99 *E-04
PEBAX + 5% G	3.90*E-06 ± 7.52*E-07	0.049 ± 7.22*E-03
PEBAX + 3% G + 5% IL	4.36*E-06 ± 2.30*E-08	0.073 ± 3.02*E-04

A large variation of the solubility coefficient can be seen in the compound with the ionic liquid, where this value is doubled if compared to the other composites: there is an increase of about 32% of the permeability constant by comparing the membrane in pure polymer with the one formed also from the liquid ionic.
Also in this case, as for the oxygen, the ionic liquid goes to improve the permeation properties of the membrane, improving the solubility coefficient.

4.3.3 Carbon dioxide permeability

This test was performed to complete the study of gas permeability in the films obtained with PEBAX, since the CO_2 permeability is a very important test to evaluate the use of such membranes in the plant. The test was carried out by setting the same conditions used for the test with oxygen and has been performed only on some of the blends, for a qualitative assessment of the parameter performance, varying the components used as a filler.

Table 4.7. *Measurement results of carbon dioxide permeability for PEBAX and its compounds.*

Sample	Permeability constant [$(cc \cdot mm)/(m^2 \cdot 24h \cdot bar)$]	Standard deviation	Variation %
PEBAX pure	6234.04	0.32	-
PEBAX + 3% G	5552.94	0.13	-12.3
PEBAX + 3% G + 5% IL	6856.70	0.22	+ 9.9

Table 4.8. *Model solution-diffusion coefficients for carbon dioxide permeability measurements.*

Sample	Diffusion coefficient [mm^2/s]	Solubility coefficient [$cm^3/(cm^3 \cdot bar$]
PEBAX pure	5.52*E-05 ± 6.32*E-08	1.31 ± 3.51*E-02
PEBAX + 3% G	4.98*E-05 ± 1.58*E-07	1.29 ± 2.24*E-02
PEBAX + 3% G + 5% IL	5.04*E-05 ± 3.22*E-08	1.58 ± 2.60*E-02

The CO_2 permeability, such as water vapor and oxygen, decreases as the percentage concentration of graphene, again because of the charge that makes the gas path more tortuous, decreasing the diffusion coefficient. On the other hand, the same effects of the ionic liquid seen in the two previous analyzes, are also visible in the latter, with the conclusion that its addition improve significantly the passage of carbon dioxide.
In Figure 4.3 you can see a typical trend of the curve of permeability.

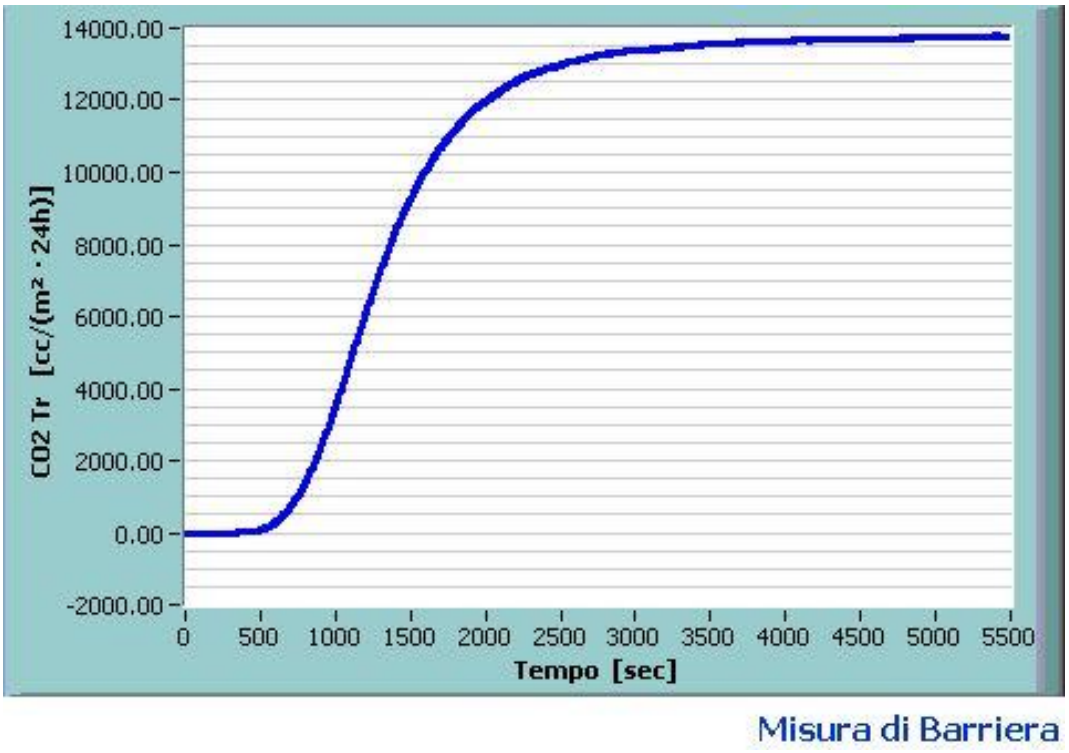

Figure 4.3. *Example of carbon dioxide permeability curve for PEBAX.*

4.4 Scanning electron microscopy (SEM)

From the SEM images, both the surface and the cross-section, it can be noted that there is not the presence of holes, in fact the surfaces are very homogeneous and compact. This is shown on figure 4.4. Also, there is not the presence of macro and micro porosity.

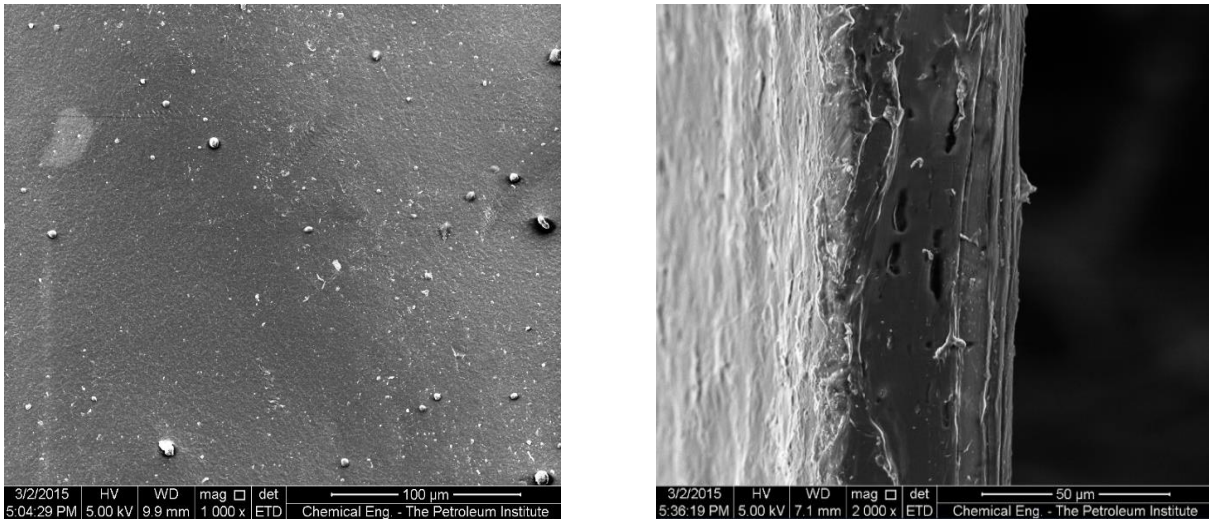

Figure 4.4. *SEM images about surface and cross-section of PEBAX 4533 + graphene.*

When the *ionic liquid* is added, as seen in 4.5, there is not difference in the membrane complex. The only thing to see is the rough surface but is not so important because the reason is probably not the presence of the ionic liquid.

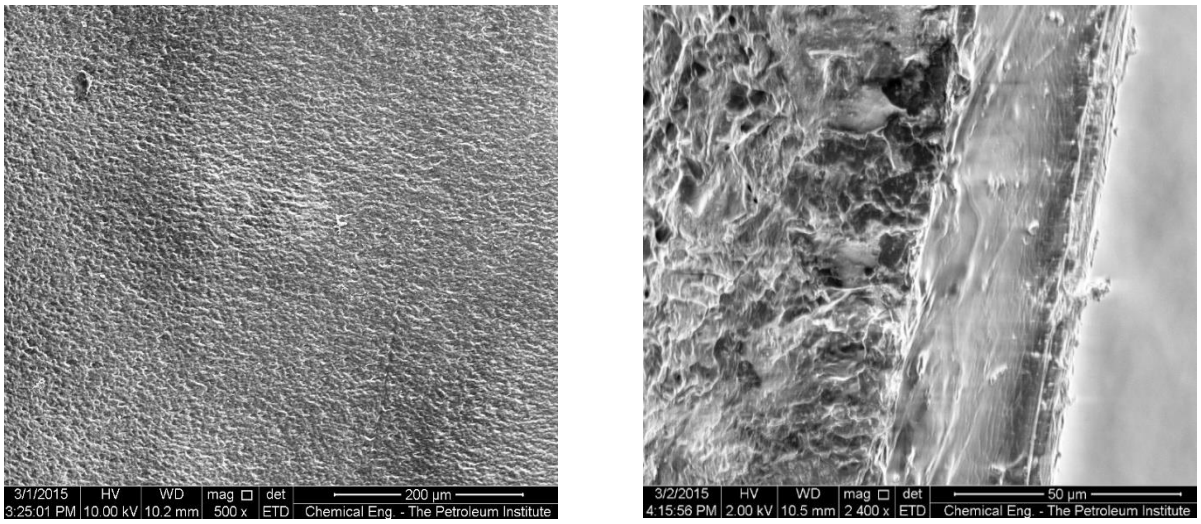

Figure 4.5. *SEM images about surface and cross-section of PEBAX 4533 + graphene + ionic liquid.*

In the end, the SEM is not so good to understand the dispersion of the filler inside the polymer, there is the need to proceed with the TEM analysis in order to better study the membranes.

Finally, an additional SEM analysis (figure 4.6) was performed on the *pure graphene*: it appears to many layers, therefore, to separate it, you need to use very high shear forces and lasted for a long time. This is not easily accomplished because there is the risk of breaking the graphene well as to separate it into layers, but with the breakage is changed to much the aspect ratio and the charge is deprived of its initial characteristics.

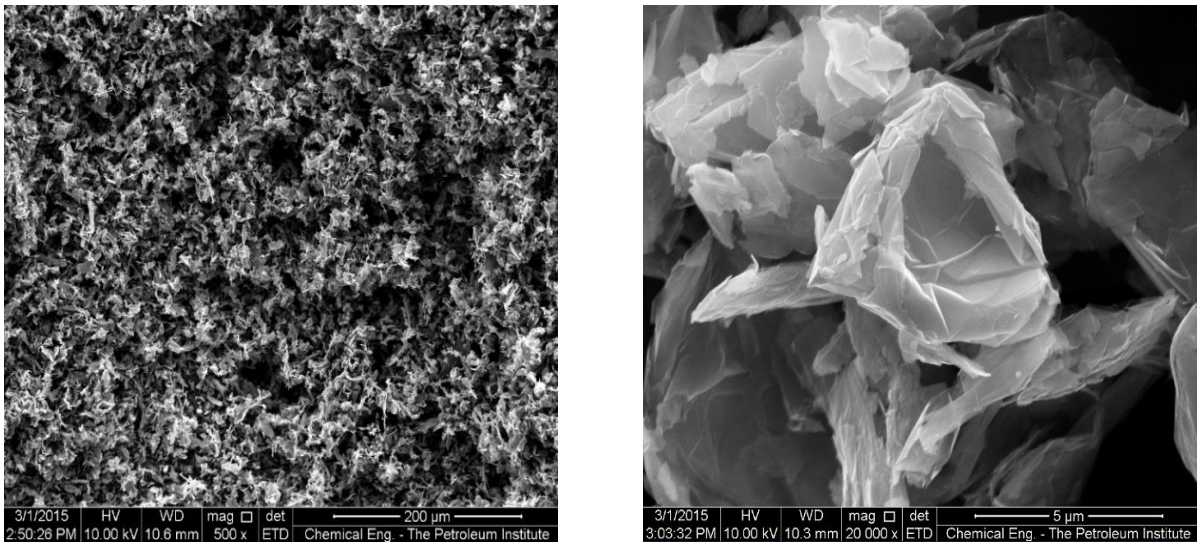

Figure 4.6. *SEM images of pure graphene.*

Another feature of the SEM is the ability to make a simple elemental analysis of the sample, for this purpose is shown an elemental analysis of pure graphene (figure 4.7).

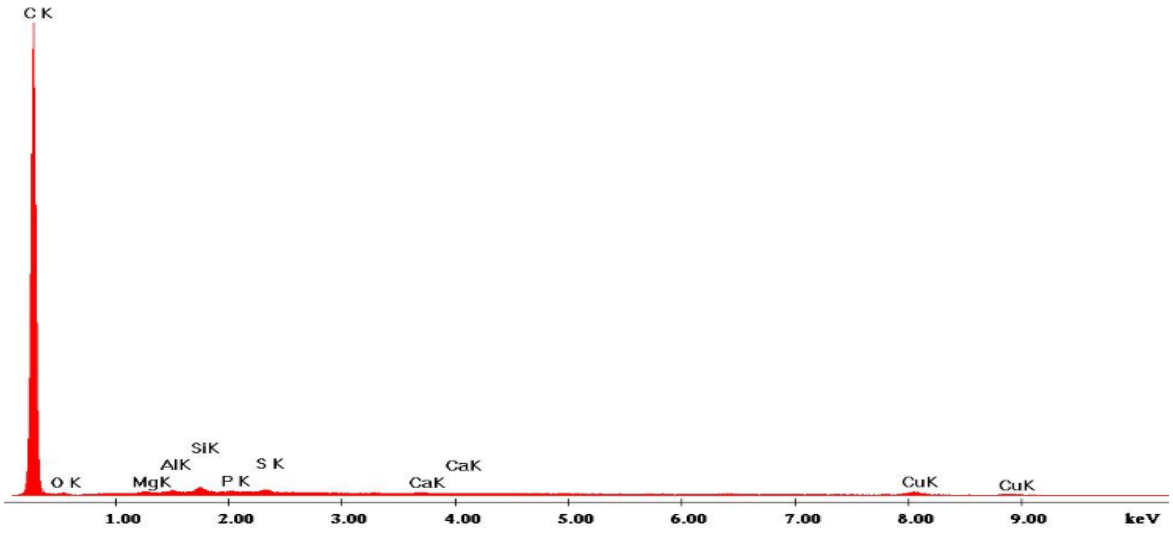

Figure 4.7. *SEM elemental analysis images of pure graphene.*

This analysis shows that the graphene is pure, there are only small quantities of impurities because of the industrial production process of the filler.
Looking also elementary analysis of the polymer + graphene and polymer + graphene + ionic liquid, there are not significant differences, the only one is the presence of the ionic liquid that results in a peak corresponding to oxygen.

4.5 Transmission electron microscopy (TEM)

From the TEM images is easier to understand the dispersion of the graphene. It is shown in figure 4.8 for polymer + graphene.

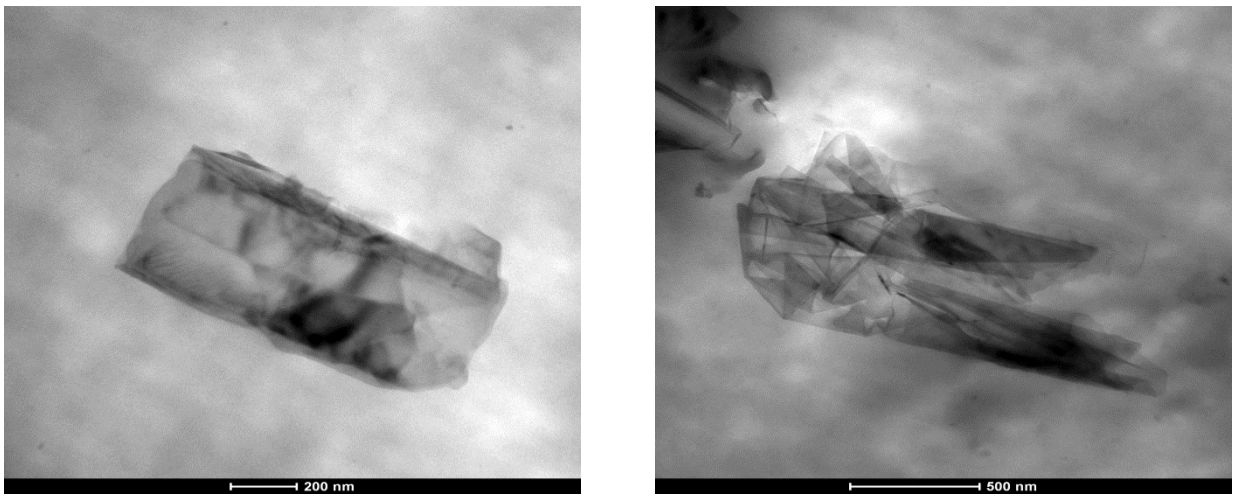

Figure 4.8. *TEM images about surface of PEBAX 4533 + graphene.*

As is shown from the figure, the first cluster (left image) of graphene is not well separated and it is almost the same as pure graphene that can be seen in the SEM analysis. In the second cluster (right image), however, there is a certain distance, symptom that graphene is separated and the polymer is able to enter inside it, called intercalation.
It needs to try to improve the dispersion but, as already said, the risk is to break the graphene if subjected to too high shear forces.

The same considerations can be made also with the addition of ionic liquid, as can be seen from the Figure 4.9.

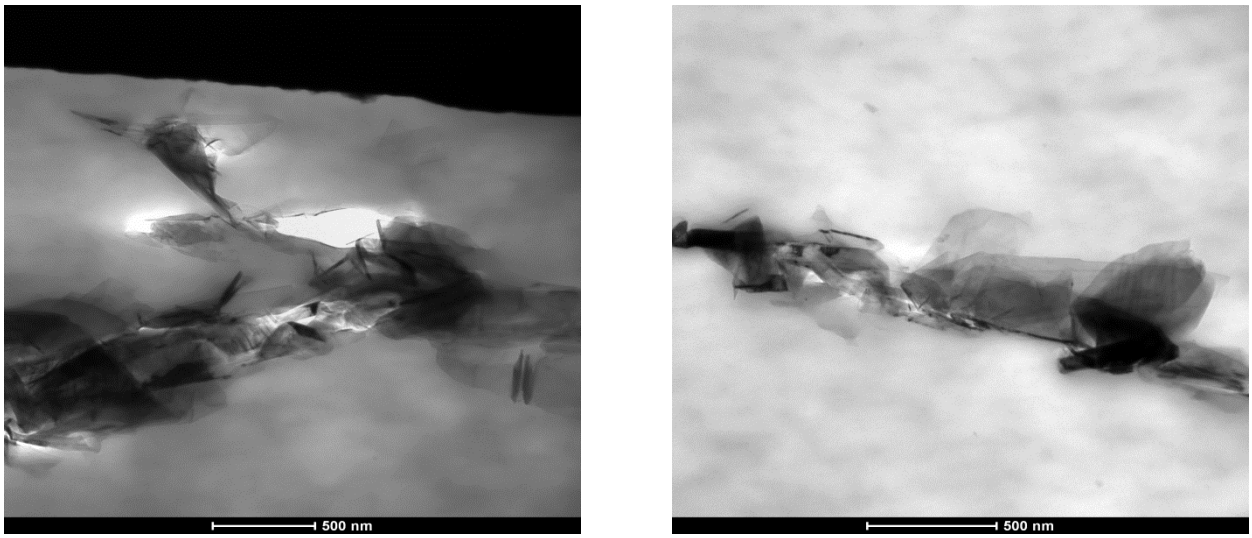

Figure 4.9. *TEM images about surface of PEBAX 4533 + graphene + ionic liquid.*

As shown, the ionic liquid has no interactions with graphene and not involve any change to the microscopic level. In the images you can see, as in the previous case, clusters well dispersed and other less, this tells that it is possible to improve the dispersion.

4.6 X-ray diffractometry (XRD)

The analysis of the diffraction peaks is one of the most popular methods to understand the degree of exfoliation of the lamellar nanofillers within a polymer matrix, following the mixing process. In fact, the comparison between the characteristic peaks of the nanofiller inside the polymer matrix and those characteristic of nanofiller alone, makes possible to evaluate the laminated plans expansion due to the polymer intercalation.

Polymer + Graphene

Figures 4.10, 4.11 and 4.12 show the XRD patterns of pure graphene (inside each of them with gray curve) and the compounds polymer + graphene with an increasing of charge percentage, respectively, each figure (black curve).

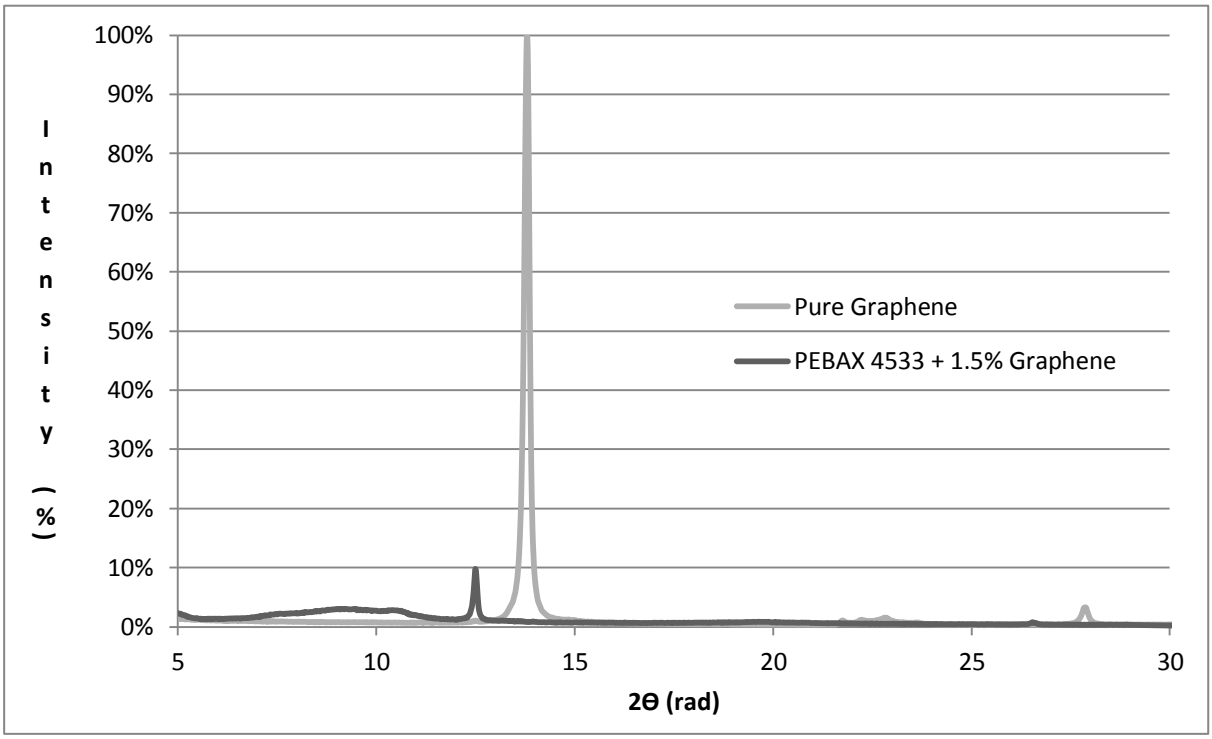

Figure 4.10. *XRD patterns of Pure Graphene (gray line) and PEBAX 4533 + 1.5% graphene (black line).*

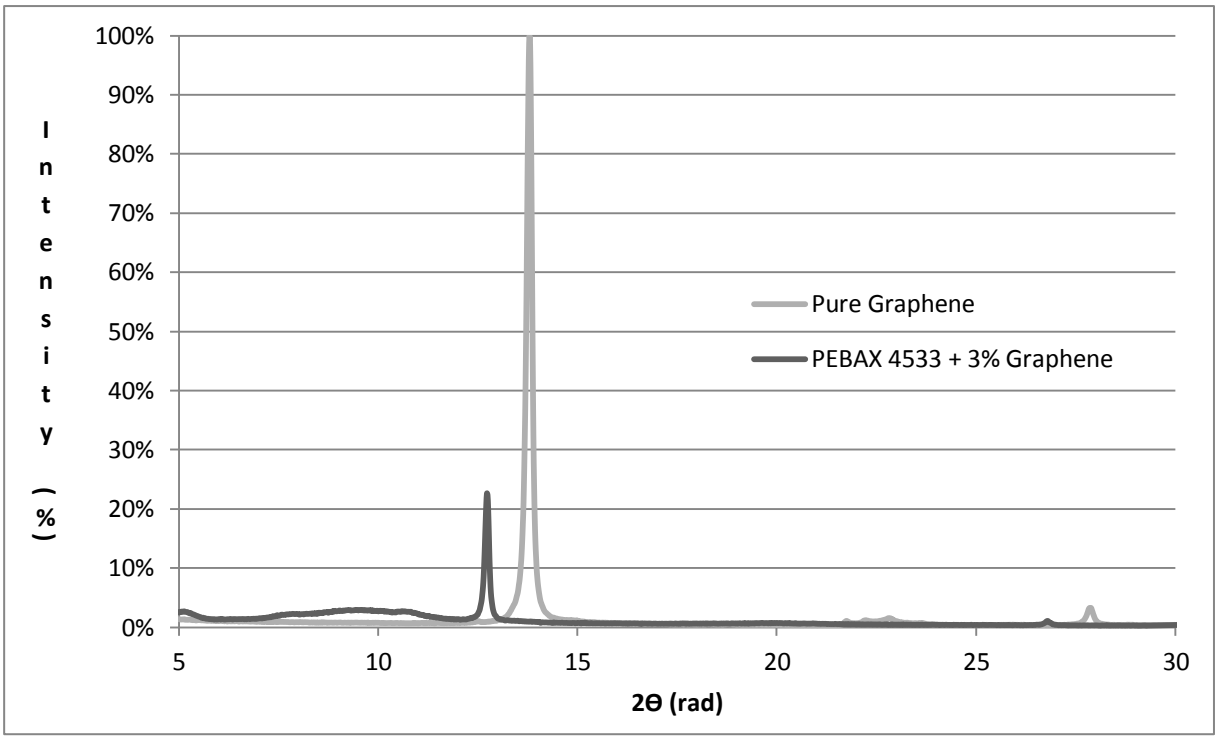

Figure 4.11. *XRD patterns of Pure Graphene (gray line) and PEBAX 4533 + 3% graphene (black line).*

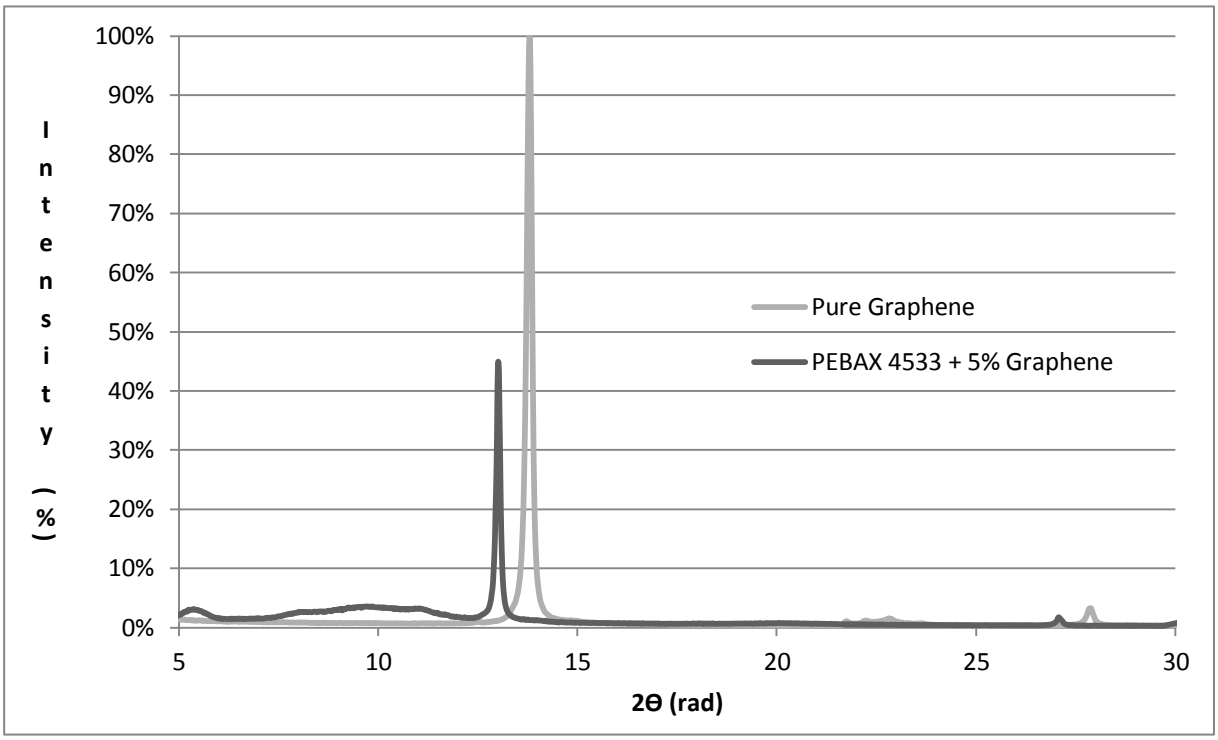

Figure 4.12. *XRD patterns of Pure Graphene (gray line) and PEBAX 4533 + 5% graphene (black line).*

The characteristic peak of nanofiller, situated at an angle of 13.80 degrees, in composites is instead be positioned at an angle of 12.50 degrees in 1.5% graphene, 12.73 degrees in 3% graphene and 13.01 degrees in 5% graphene. This means, following the Bragg theory, that the slats were spaced due to intercalation of the polymer, this because θ and *d* they are inversely proportional. There is also a second peak of graphene to 27.85 degrees, it has an intensity below the principal one but, when is compared in graphs, confirms the analysis just made.
The broad amorphous halo present at angles between 7 and 12 degrees is due to the presence of PEBAX, as well as a small peak that can be seen around 5 degrees.
The variations of the peaks intensity observable in the figures are not relevant to determining the successful exfoliation of the slats, as they are due primarily to the test conditions and the characteristics of the sample examined, as well as to the fact that the charge is "diluted" inside the polymer and therefore the intensity will be smaller if compared to the pure sample.
This analysis confirms the observations made on the TEM images, because you can see the intercalation of the polymer and then the exfoliation of the nanofiller.
It is reported in Table 4.9 the calculation of inter-lamellar spacing based on the Bragg's law.

Table 4.9. *Calculation of inter-lamellar spacing in graphene and in its composites.*

Sample	λ	θ_1 [rad]	θ_2 [rad]	d_1 [Å]	d_2 [Å]
Graphene	1.5418	0.120	0.243	6.418	3.203
PEBAX 4533 + 1.5% graphene	1.5418	0.109	0.232	7.084	3.359
PEBAX 4533 + 3% graphene	1.5418	0.111	0.234	6.954	3.328
PEBAX 4533 + 5% graphene	1.5418	0.114	0.236	6.803	3.294

Polymer + Graphene + Ionic Liquid

Table 4.10 shows the calculation of inter-lamellar spacings, while figure 4.13 presents the comparison between membrane with and without ionic liquid.

Table 4.10. *Calculation of interlamellar spacing in composites with ionic liquid.*

Sample	λ	θ_1 [rad]	θ_2 [rad]	d_1 [Å]	d_2 [Å]
Graphene	1.5418	0.120	0.243	6.418	3.203
PEBAX 4533 + 1.5% graphene + 5% ionic liquid	1.5418	0.108	0.231	7.152	3.367
PEBAX 4533 + 3% graphene + 5% ionic liquid	1.5418	0.111	0.234	6.954	3.328
PEBAX 4533 + 5% graphene + 5% ionic liquid	1.5418	0.115	0.237	6.718	3.283

In the ternary blend are obtained very similar trends about the characteristic peaks of the nanofiller, to those obtained for the binary blend. This means that the introduction of the ionic liquid is not able to increase the degree of exfoliation of the nanofiller.

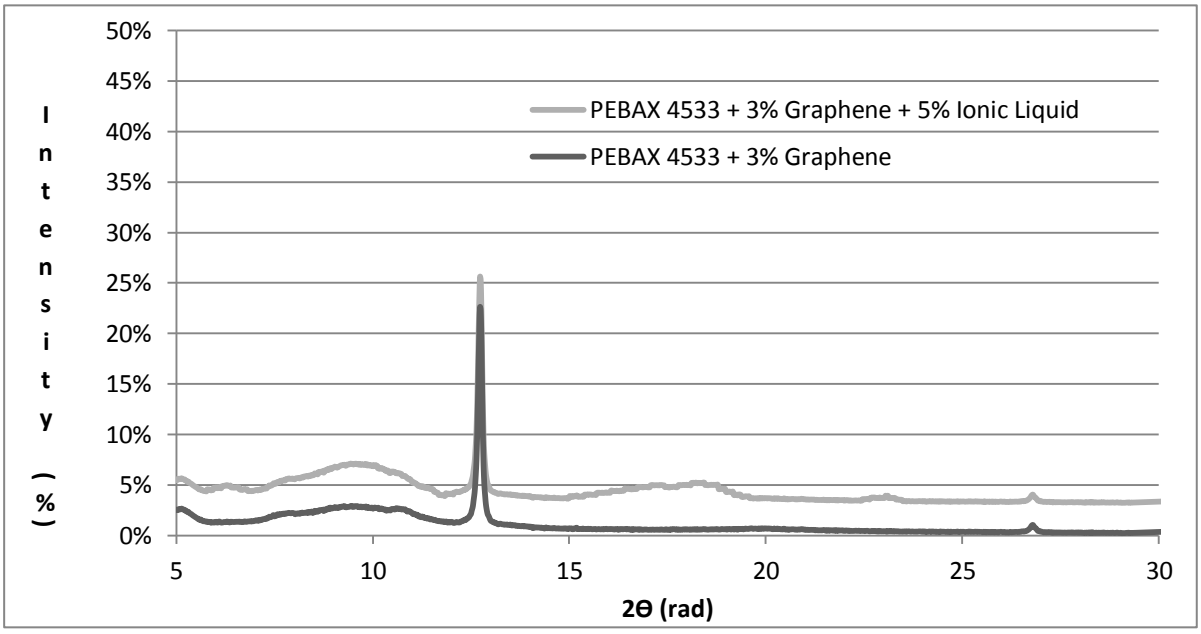

Figure 4.13. *XRD spectra of blend PEBAX 4533 + graphene (black line) and the blend PEBAX 4533 + graphene + ionic liquid (gray line).*

4.7 Mechanical tests

The knowledge of the mechanical properties about the materials is critical to choose which type of polymer is more suitable for a particular use. The tests were carried out using a tensile test operated by a dynamometer (Instron, model 5900) and obtaining samples from films by means of punching (Ceast). For each membrane, were tested a minimum of 5 samples in order to respect the reference standards.

The tests were conducted at once, in a way to calculate both the elastic modulus and the properties at break. They were carried out by setting a deformation speed of 10 mm/min, in agreement with the standard ASTM D 638 type V, and the rupture of the specimen as a condition of end cycle.

The elastic modulus of each sample analyzed was obtained from the stress-strain curve, then using the average of the values obtained for a certain blend was calculated the elastic modulus characteristic of the blend. The break test, whereas, give information about the elongation at break and the maximum stress applied to the specimen.

Using the test specimens of PEBAX has been verified that such material is elastic and ductile because the breakage of the sample occurs after a long yield strength.

4.7.1 Elastic modulus

The test results, indicated in Table 4.11 and Figure 4.14, show that an increasing of graphene percentage imply an increase of the tensile modulus, in the same way for both set of samples (with and without ionic liquid).

Table 4.11. *Results of traction mechanical tests conducted on PEBAX and its composites.*

Sample	Tensile modulus [MPa]
PEBAX 4533 pure	146.98 ± 11.32
PEBAX 4533 + 1.5% graphene	155.31 ± 4.38
PEBAX 4533 + 3% graphene	164.77 ± 7.22
PEBAX 4533 + 5% graphene	197.79 ± 3.44
PEBAX 4533 + 5% ionic liquid	140.62 ± 8.48
PEBAX 4533 + 1.5% graphene + 5% ionic liquid	149.09 ± 7.41
PEBAX 4533 + 3% graphene + 5% ionic liquid	159.47 ± 10.46
PEBAX 4533 + 5% graphene + 5% ionic liquid	172.11 ± 7.93

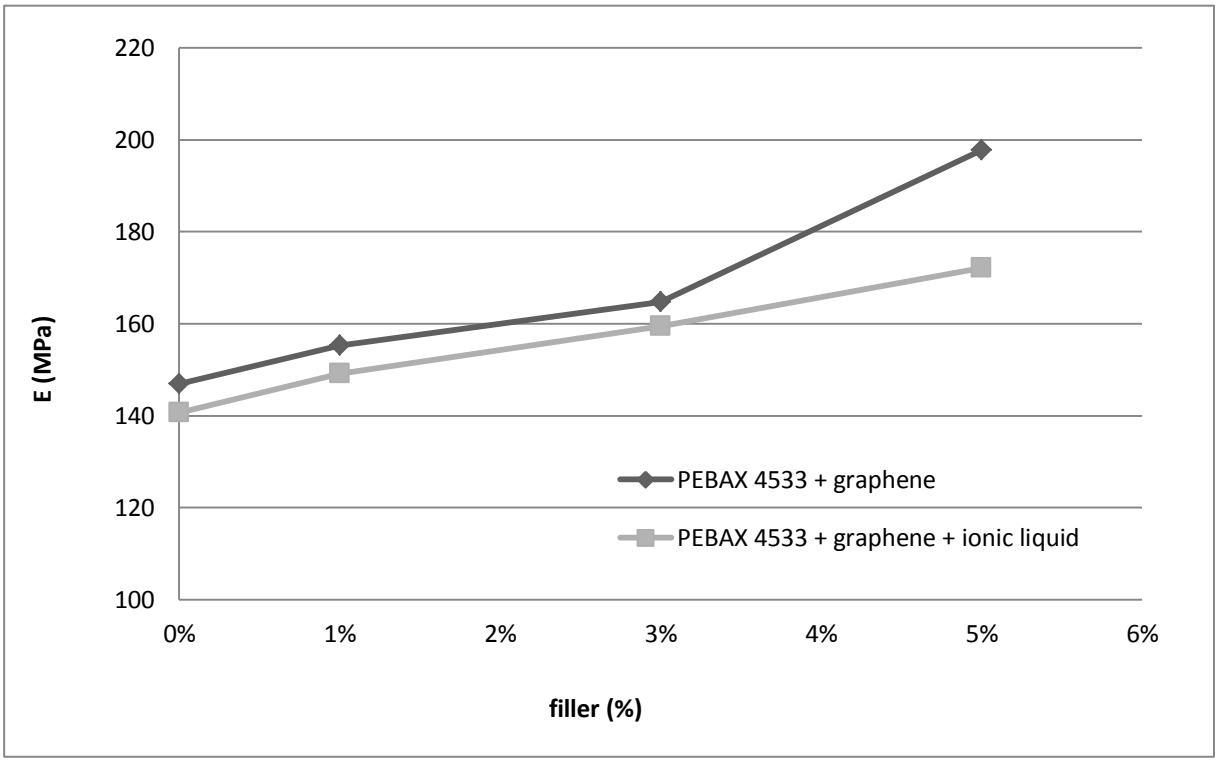

Figure 4.14 - *Performance of the tensile modulus as a function of percent concentration of graphene.*

In fact, in both cases, the capacity of the nanofiller to increase the tensile modulus depends essentially on the surface of contact between the charge and the matrix, then an exfoliated configuration allows a more sustained increase of the material stiffness, compared to that simply intercalated where interactions are minor. On the other hand, the addition of ionic liquid inside membranes goes to decrease, although not that much, the tensile modulus; this is normal because the polymer base is partially replaced with ionic liquid, which is less resistant to traction efforts, the polymer domain is not continuous as in the membranes polymer + graphene.

4.7.2 Break properties

The test results, indicated in Table 4.12, show that an increasing of the graphene content imply a decrease of the elongation at break, in the same way for both set of samples (with and without ionic liquid).

Table 4.12 - *Results of traction mechanical tests conducted on PEBAX and its composites.*

Sample	**Elongation at break [%]**	**Maximum stress [MPa]**
PEBAX 4533 pure	800.32 ± 47.96	20.95 ± 0.80
PEBAX 4533 + 1.5% graphene	706.49 ± 23.11	17.40 ± 0.56
PEBAX 4533 + 3% graphene	673.47 ± 58.95	17.17 ± 1.59
PEBAX 4533 + 5% graphene	607.11 ± 17.39	17.88 ± 1.31
PEBAX 4533 + 5% ionic liquid	736.12 ± 56.13	21.49 ± 1.40
PEBAX 4533 + 1.5% graphene + 5% ionic liquid	670.63 ± 18.70	20.42 ± 0.37
PEBAX 4533 + 3% graphene + 5% ionic liquid	683.97 ± 43.38	20.94 ± 0.81
PEBAX 4533 + 5% graphene + 5% ionic liquid	640.73 ± 57.37	20.26 ± 1.42

The addition of graphene to the PEBAX increases the fragility of the material, confirmed by the reduction percentage of elongation at break and maximum stress. This can be explained by the fact that, the slats dispersed in the matrix, limit the movement of the polymer chains, thus lowering the deformation capacity of the material and facilitating the initiation of cracks. Instead, the reduction of the maximum stress is probably due to the weak ties that develop between the matrix and the slats, which prevents the blades to distribute part of the effort applied.

Even the membranes with ionic liquids appear to be more fragile (a little more compared to composites with only graphene) due to the presence of the ionic liquid that interposes within the polymer domain. The maximum stress rather be higher, there is probably some sort of

interaction between graphene and the ionic liquid that can better distribute the effort applied on the slats.

In the two figures below, 4.15 (polymer + graphene) and 4.16 (polymer + graphene + ionic liquid), you can see the comparison between the different membranes prepared.

In particular, the elastic modulus is evaluated in the first part of the graphs, calculated as a straight line that starts from zero and tangent to the rising portion; while the total elongation expresses the elastic portion summed with the slightly growing line that starts from the initial point of enervation (after the end of elasticity curve) up to the breaking point of the specimen.

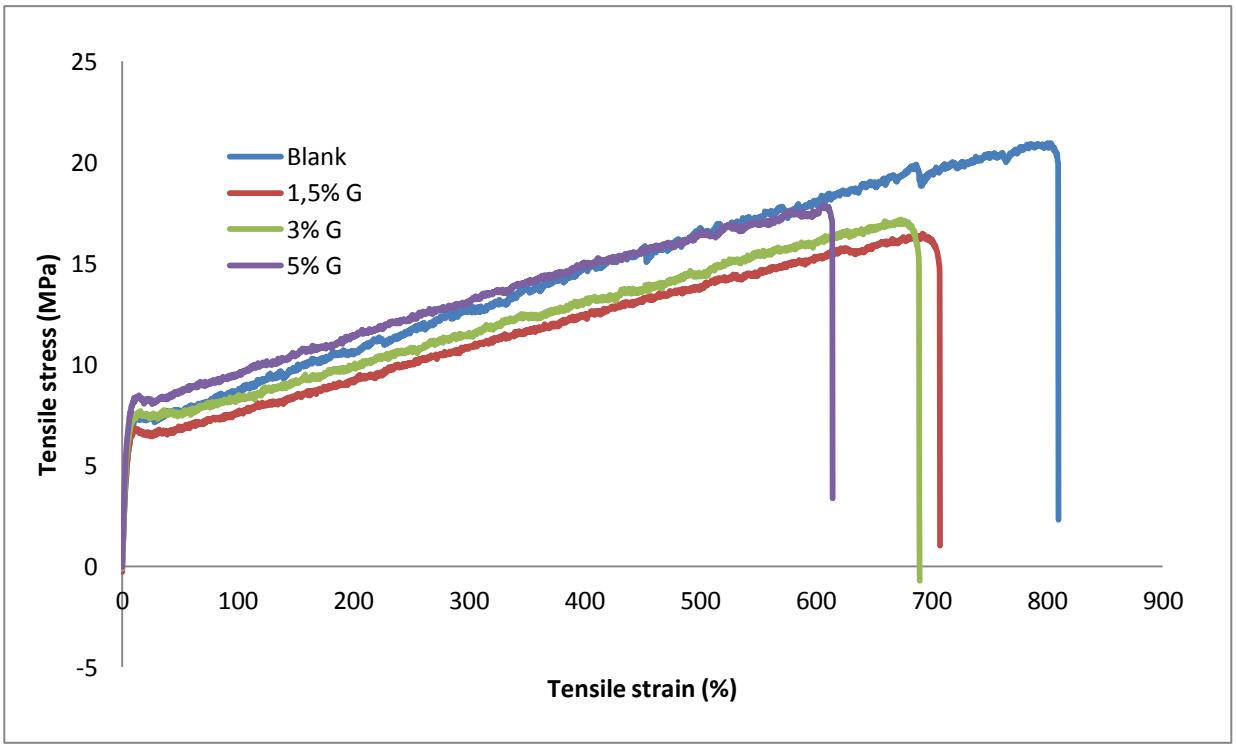

Figure 4.15. *Tensile curve of PEBAX as a function of percent concentration of graphene.*

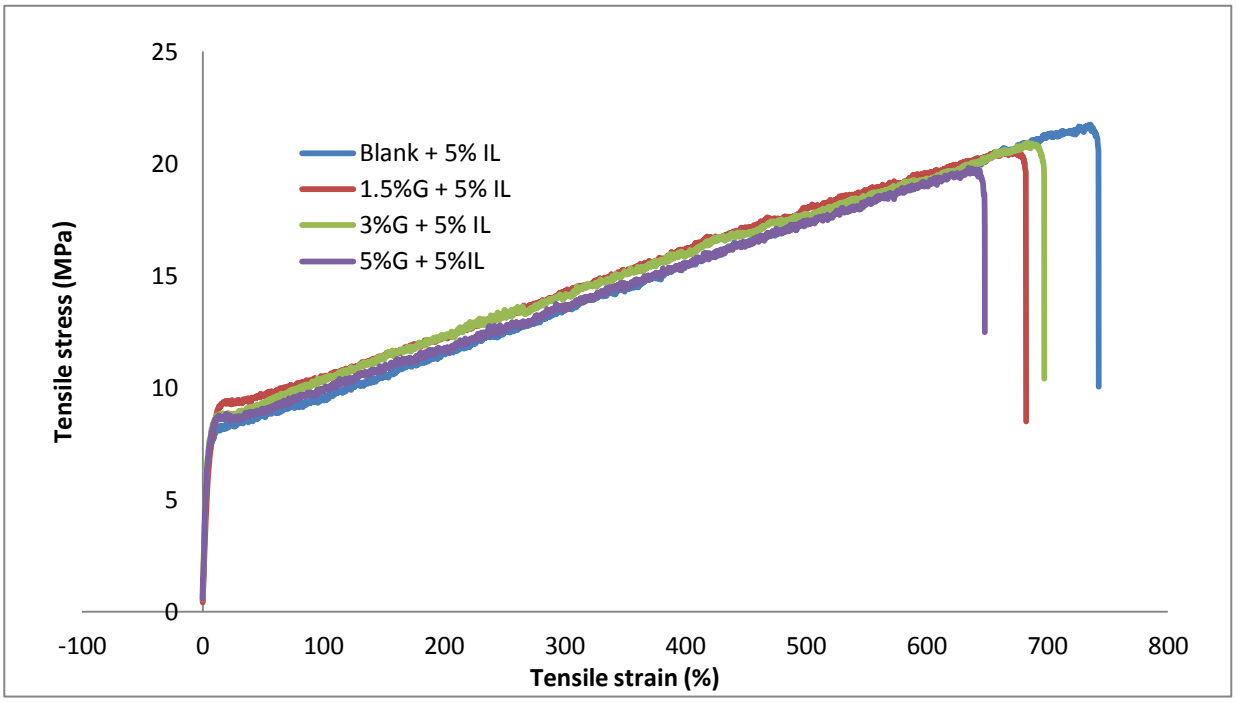

Figure 4.16. *Tensile curve of PEBAX + 5% IL as a function of percent concentration of graphene.*

4.8 Differential scanning calorimetry (DSC)

The analysis of differential scanning calorimetry were performed in order to assess the degree of crystallization and the value of the thermal properties of the analyzed blend. The test was performed with cycles of heating-cooling between the temperature of -60 ° C and 250 ° C, with ramps from 10 ° C / min and analyzing more than one sample per type of membrane.

Regarding the pure polymer it is noted that the PEBAX, thermoplastic and semi-crystalline elastomer, has two glass transition temperatures, one melting temperature and one crystallization temperature. The first glass transition temperature is related to PEO (polyether), but the instrument does not allow to see it because you cannot get to below -50°C, while the second is referred to the PA (polyamide) and is higher. Anyway, is better to see the glass transition temperature with the DMI analysis, shown in the end of this chapter.
Figures 4.17 and 4.18 show the comparison between the pure PEBAX and composites loaded with graphene, both in the heating and cooling portion.

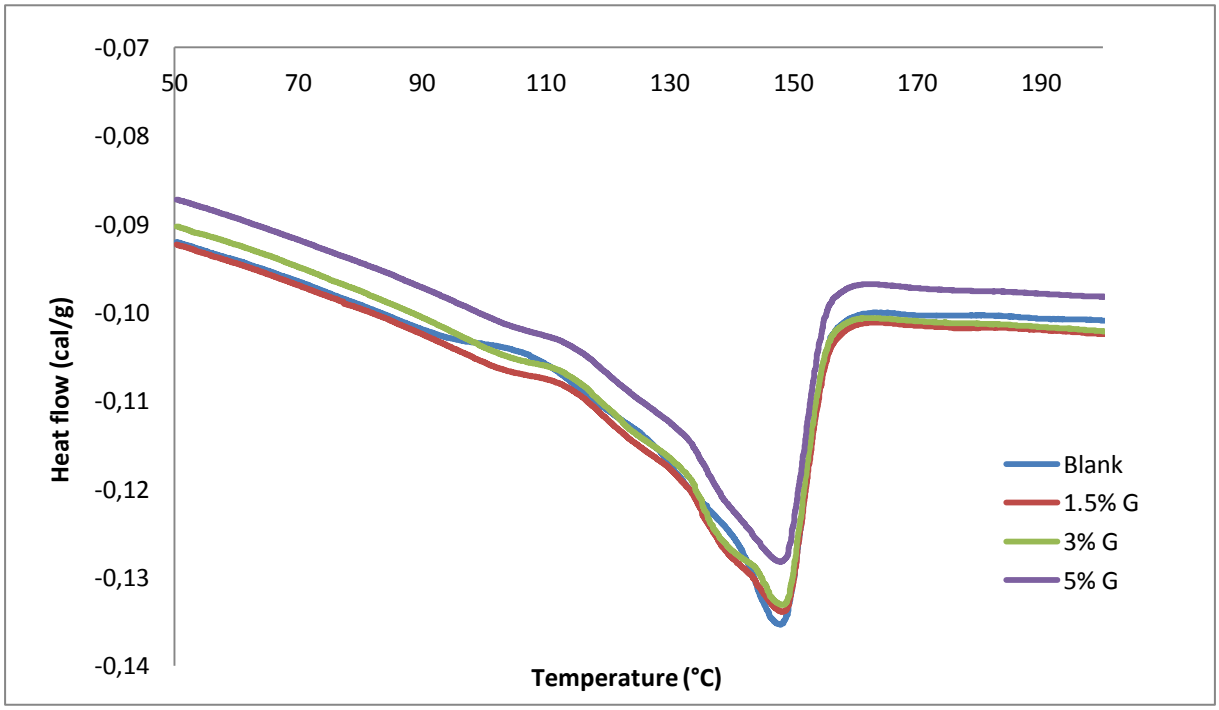

Figure 4.17. *DSC analysis of polymer + graphene: heating phase.*

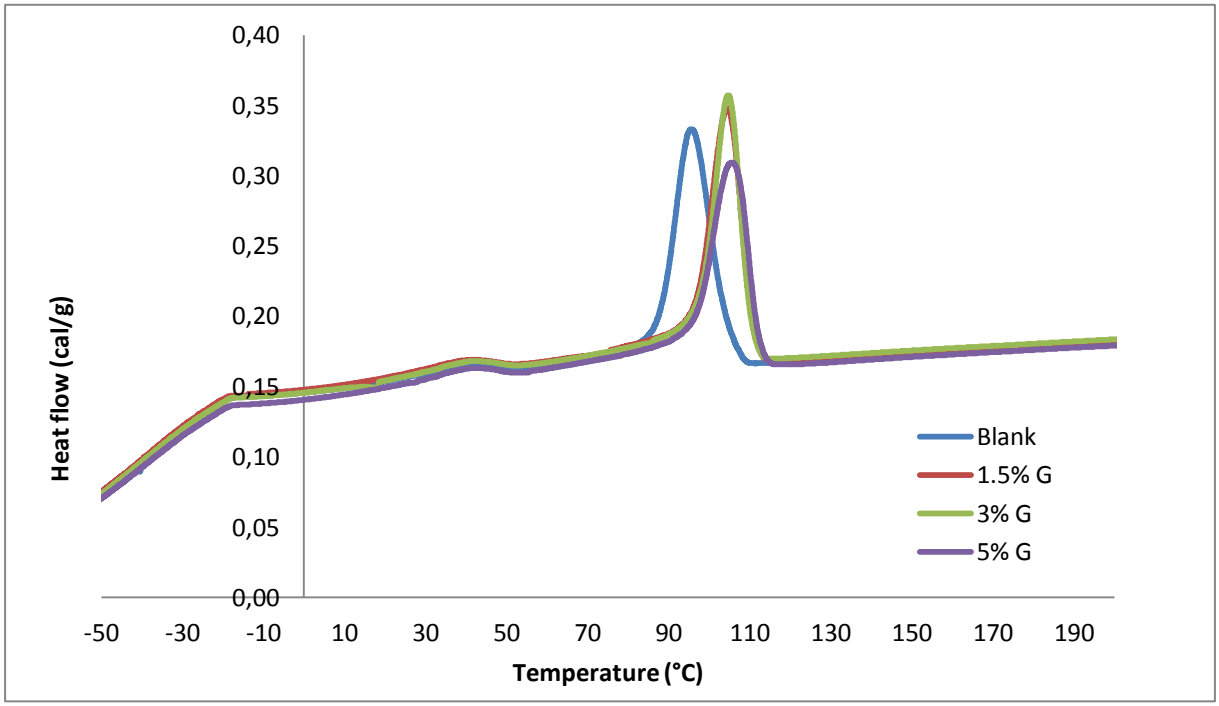

Figure 4.18. *DSC analysis of polymer + graphene: cooling phase.*

The addition of the charge to the matrix of PEBAX determines two main effects on the compound properties. The first is the increase of the melting temperature with increasing the percentage concentration of charge, this you can guess by the slight shift of peak as shown in Figure 4.17. This reduction is about few Celsius degrees, as can be seen from table 4.13.

Table 4.13. *DSC parameters of the polymers + graphene: crystallization temperature (Tc) and melting temperature (Tm).*

Sample	Tc [°C]	Tm [°C]
PEBAX 4533 blank	95.4	146.7
PEBAX 4533 +1.5% G	105.4	147.9
PEBAX 4533 + 3% G	105.5	148.2
PEBAX 4533 + 5% G	106.2	148.4

From the table can also see that there is a great difference in the crystallization temperature, analyzing the comparison between the pure polymer and the one with filler (second effect): PEBAX pure crystallizes at 10 ° C less than the polymer + graphene, the reason is that the well-dispersed graphene provides stable nucleation centers that make easier the formation of the crystallites to a lower degree of undercooling. This phenomenon already occurs with a small amounts of graphene therefore you do not see the difference by increasing from 1,5% to 5% the percentage of graphene.

Now, from table 4.14 it can be observed that, within the experimental error of measurement, is always valid the equation:

$$\Delta Hc, h + \Delta Hc, c = \Delta Hm \tag{5.1}$$

As the ΔHm does not consider the composition of the compound (PEBAX is never 100%), it is calculated the ΔHm_real. It is obtained by normalizing the heat of fusion measured with the actual percentage composition of PEBAX in the mixture and this allowed to compare the results with those of the pure PEBAX, in order to see if the addition of the charge determines a variation in the polymer crystallinity.

Table 4.14. *DSC parameters polymer + graphene: enthalpy (ΔH). The indices h and c indicate respectively the step of heating and cooling.*

Sample	ΔHc,h [cal/g]	ΔHc,c [cal/g]]	ΔHm [cal/g]	ΔHm_real [cal/g]
PEBAX 4533 blank	6.01	4.63	10.34	10.34
PEBAX 4533 +1.5% G	5.98	5.92	11.90	12.08
PEBAX 4533 + 3% G	5.95	5.95	11.90	12.27
PEBAX 4533 + 5% G	5.90	5.92	11.82	12.44

As can be seen, in the compounds prepared with graphene, the Δ*Hm_real* increases as the amount of charge present, indicating the presence of a nucleating effect due to the filler that improve a partial crystallization of PEBAX. On the other hand, there is not much difference between the Δ*Hm_real* of the filler compounds, the bigger exchange occurs between the pure PEBAX and all the others: as mentioned earlier, it is sufficient a small addition of graphene to improve nucleating effect, which does not linearly increase with the percentage increasing of the nanofiller.

It is now analyzed the addition of the ionic liquid: there is not much change if compared with the membranes already discussed. In Figures 4.19 and 4.20 you can see the DSC of heating and cooling portion.
In addition to the melting peak and the crystallization one, is known another small point, at the same temperature in both graphs (about 175 ° C), which is right of the ionic liquid. It does not appear in the DSC made in previous membranes because this is probably due to a state change of the ionic liquid.

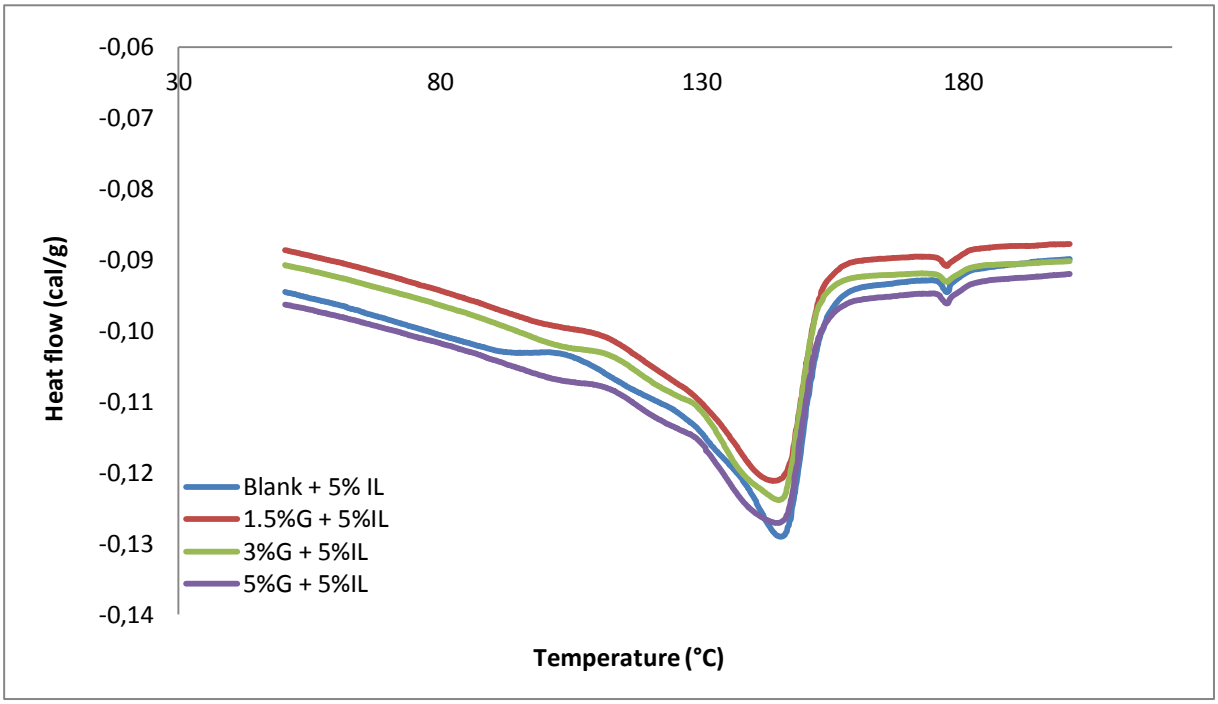

Figure 4.19. *DSC analysis of polymer + graphene + ionic liquid: heating phase.*

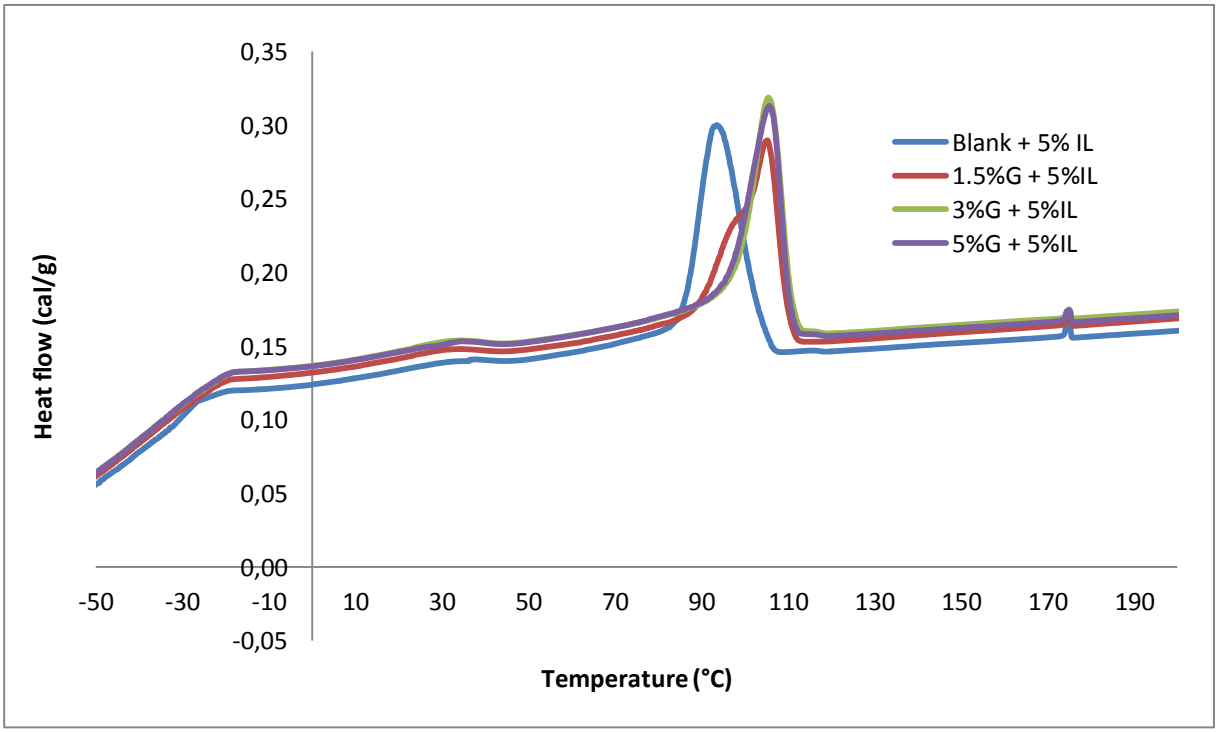

Figure 4.20. *DSC analysis of polymer + graphene + ionic liquid: cooling phase.*

As can be seen from the table below, the melting temperatures vary as those of compounds polymer + graphene. The difference is those temperatures are lower because the ionic liquid joined has a lower heat resistance than the one of the polymer, in that way it decreases the stability temperature characteristics.
What does not vary is the crystallization temperature, that remain unchanged, because the ionic liquid does not interfere.

Table 4.15. *DSC parameters of the polymers + graphene + ionic liquid: crystallization temperature (Tc) and melting temperature (Tm).*

Sample	Tc [°C]	Tm [°C]
PEBAX 4533 + 5% IL	93.6	142.8
PEBAX 4533 +1.5% G + 5% IL	105.2	143.9
PEBAX 4533 + 3% G + 5% IL	105.4	144.2
PEBAX 4533 + 5% G + 5% IL	105.7	144.6

Finally, Table 4.16 make the calculation of the ΔHm_real for the compounds with the ionic liquid. There is no difference between this one and the other discussed above: the ionic liquid is not going to interfere with the nucleating effect given by the addition of graphene.

Table 4.16. *DSC parameters polymer + graphene + ionic liquid: enthalpy (ΔH). The indices h and c indicate respectively the step of heating and cooling.*

Sample	ΔHc,h [cal/g]	ΔHc,c [cal/g]]	ΔHm [cal/g]	ΔHm_real [cal/g]
PEBAX 4533 + 5% IL	5.80	4.02	9.8	10.34
PEBAX 4533 +1.5% G + 5% IL	6.11	4.58	10.69	11.43
PEBAX 4533 + 3% G + 5% IL	6.05	4.62	10.67	11.59
PEBAX 4533 + 5% G + 5% IL	6.09	4.61	10.70	11.89

Now, is possible to calculate the percentage increase of the polyamide crystallinity with the addition of graphene. In reality, what should be done is to calculate the increase of crystallinity of the polymer mother (PEBAX 4533), but this is not possible because there are no data available in the literature and is not note either the composition of the block polymer, nor the percentage of polyamide crystallinity of the polymer base. For these reasons, we will only make the relationship between the heat involved (ΔHm_real) about polymer loaded and the pure, found by DSC analysis (Table 4.17).

Table 4.17. *Crystallinity increase for the PEBAX compounds.*

Sample	**ΔHm_real [cal/g]**	**Crystallinity increase [%]**
PEBAX 4533 blank	10.34	/
PEBAX 4533 +1.5% G	12.08	16.8
PEBAX 4533 + 3% G	12.27	18.7
PEBAX 4533 + 5% G	12.44	20.3
PEBAX 4533 + 5% IL	10.34	0
PEBAX 4533 +1.5% G + 5% IL	11.43	10.5
PEBAX 4533 + 3% G + 5% IL	11.59	12.1
PEBAX 4533 + 5% G + 5% IL	11.89	14.9

As can be seen from the table, there is a large increase of crystallinity even with a small addition of graphene. That's because just a few active centers are enough to enable its function as nucleating effect. The ionic liquid, however, does not involve any change to these results, even his presence in equal graphene proportion introduced make a decreasing of crystallinity.

4.9 Thermogravimetric Analysis (TGA)

The first analysis, conducted in a nitrogen atmosphere , gives information on the thermal degradation of the polymer.

Figure 4.21 shows the results of TGA for pure PEBAX and for composites prepared with graphene.

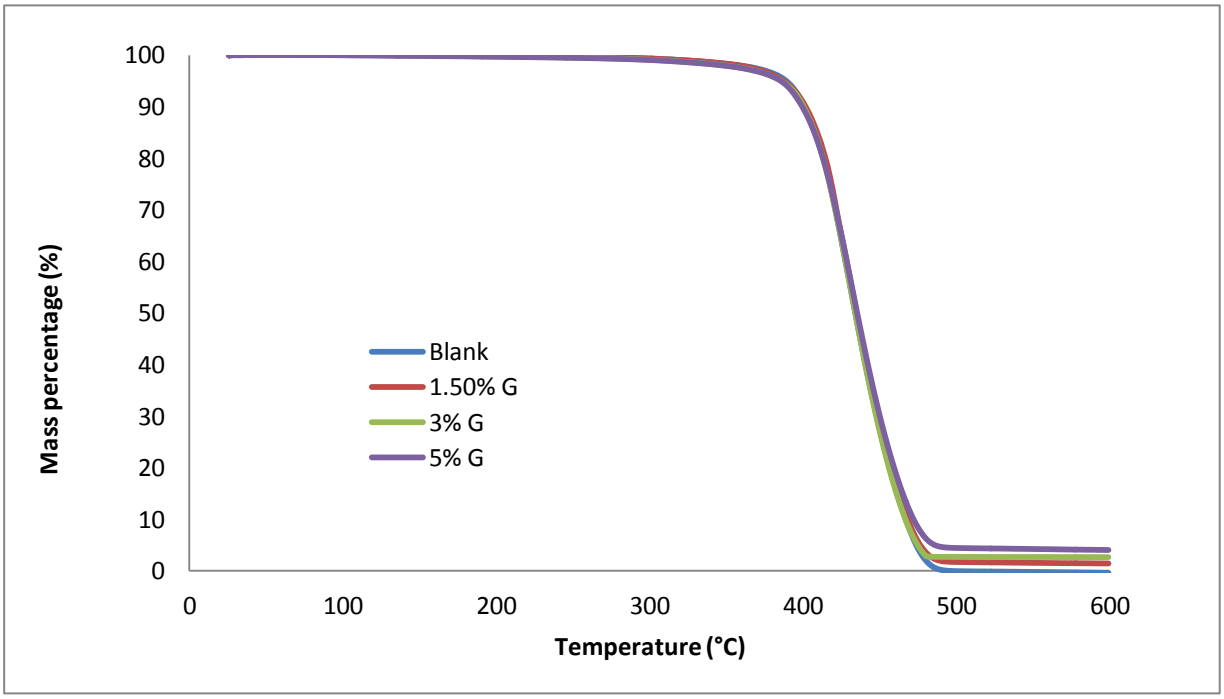

Figure 4.21. *Thermo-gravimetric analysis of the PEBAX and composites made with graphene*.

It may be noted, first, that all composites prepared with PEBAX have a very similar behavior. However, increasing the charge, it is noted a slight increase to the 95% mass temperature and the temperature to 50 % of mass, this means that graphene provides greater temperature stability compared to PEBAX such, the same conclusion explained for the DSC. In short, as you can see from the Table 4.18, it increases the thermoresistance of the polymer.

Table 4.18. *Values of $T_{50\%}$ of polymer + graphene compounds.*

Sample	$T_{95\%}$ [°C]	$T_{50\%}$ [°C]
PEBAX 4533 blank	375.2	434.1
PEBAX 4533 +1.5% G	376.1	435.2
PEBAX 4533 + 3% G	377.2	436.3
PEBAX 4533 + 5% G	378.8	438.0

This takes place thanks to the properties of graphene that, being a very good thermoconduct and resistant to high temperatures, provides to the polymer a higher resistance which results with an increase about the $T_{95\%}$ and $T_{50\%}$.

Figure 4.22 shows, instead, the results of TGA, in nitrogen atmosphere, for the composites prepared with ionic liquid.

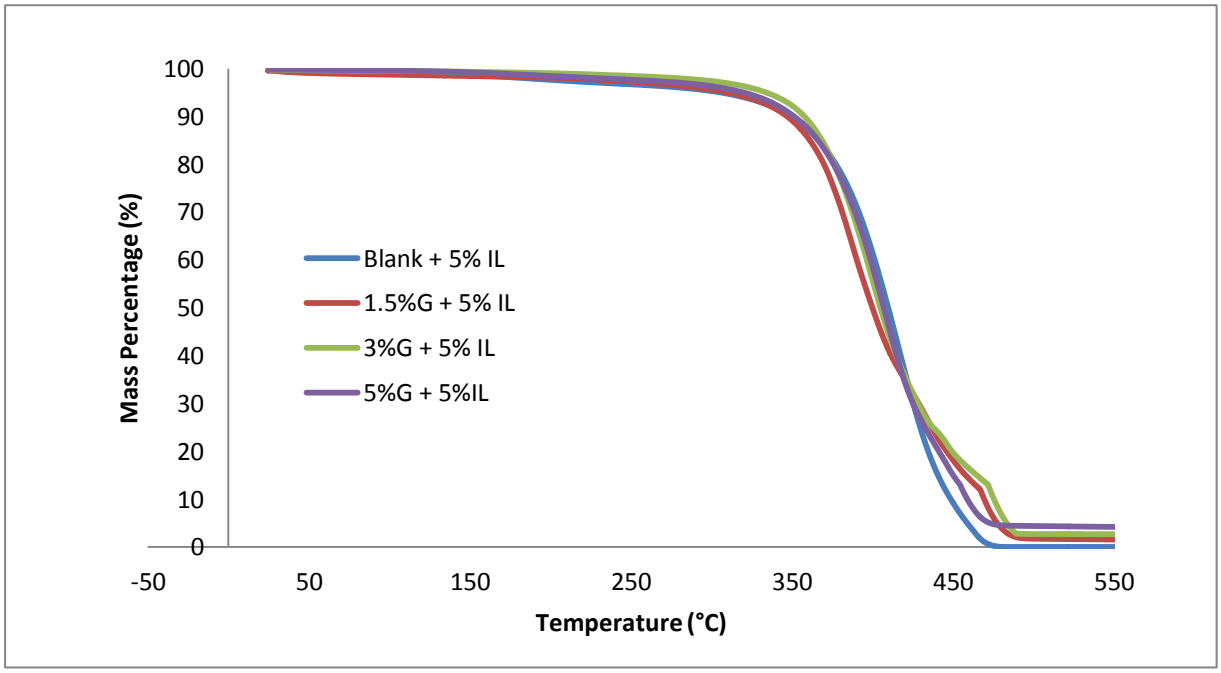

Figure 4.22. *Thermo-gravimetric analysis of the PEBAX and composites made with ionic liquid.*

Are also valid, in this case, the same considerations made previously: there is an increasing of resistance when increase the percentage of graphene, but both the $T_{95\%}$ and $T_{50\%}$ are found to be much lower after the addition of the ionic liquid, in particular there are 50 °C less for the $T_{95\%}$ and 25°C for the $T_{50\%}$ with the consequence that the ionic liquid changes a lot the stability of the polymer. This is because such liquid is not a thermos-resistant plasticizer as the polymer, in fact the polymer domain is not continuous as in the membranes polymer + graphene.

Table 4.19. *Values of $T_{50\%}$ of polymer + graphene + ionic liquid compounds.*

Sample	$T_{95\%}$ [°C]	$T_{50\%}$ [°C]
PEBAX 4533 blank + 5% IL	325.3	410.0
PEBAX 4533 +1.5% G + 5% IL	326.2	400.2
PEBAX 4533 + 3% G + 5% IL	329.3	403.6
PEBAX 4533 + 5% G + 5% IL	328.6	407.3

The second analysis is conducted in a air atmosphere then it gives information on the thermal oxidation of the polymer.

Figure 4.23 shows the results of TGA for pure PEBAX and for composites prepared with graphene.

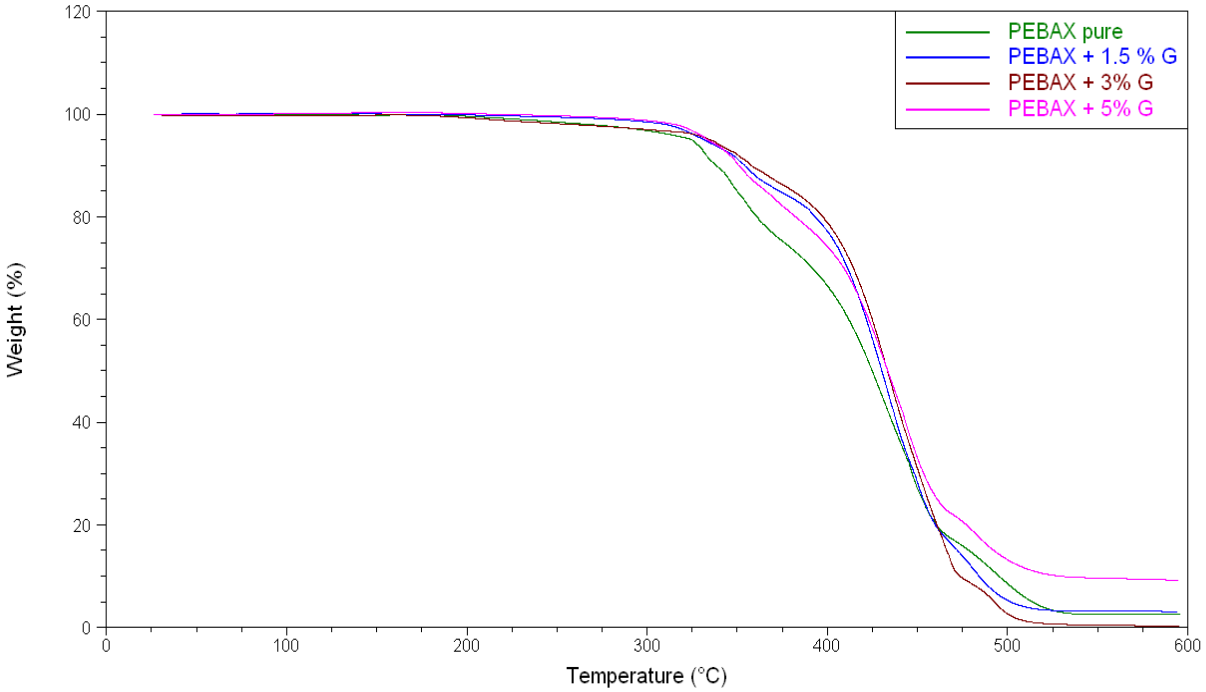

Figure 4.23. *Thermo-gravimetric analysis of the PEBAX and composites made with graphene*.

It may be noted, first, that all composites prepared with PEBAX have a very similar behavior. However, increasing the filler, it is noted a slight increase to the 95% mass temperature and the temperature to 50 % of mass, this means that graphene provides greater oxidation stability compared to PEBAX such. In short, as you can see from the table 4.20, it increases the thermos-resistance of the polymer mother.

Table 4.20. *Values of $T_{50\%}$ of polymer + graphene compounds.*

Sample	$T_{95\%}$ [°C]	$T_{50\%}$ [°C]
PEBAX 4533 blank	324.9	424.1
PEBAX 4533 +1.5% G	330.2	430.2
PEBAX 4533 + 3% G	332.3	433.5
PEBAX 4533 + 5% G	332.6	433.9

Comparing these results of oxidation with the previous in an inert environment, we are seen as the temperatures are lower comparing same mass percentage. This happens especially at $T_{95\%}$, for this reason we say that the polymer is affected by the temperature rise during the oxidation much earlier than either in a nitrogen environment.

Figure 4.24 shows the results of TGA for the composites prepared with ionic liquid.

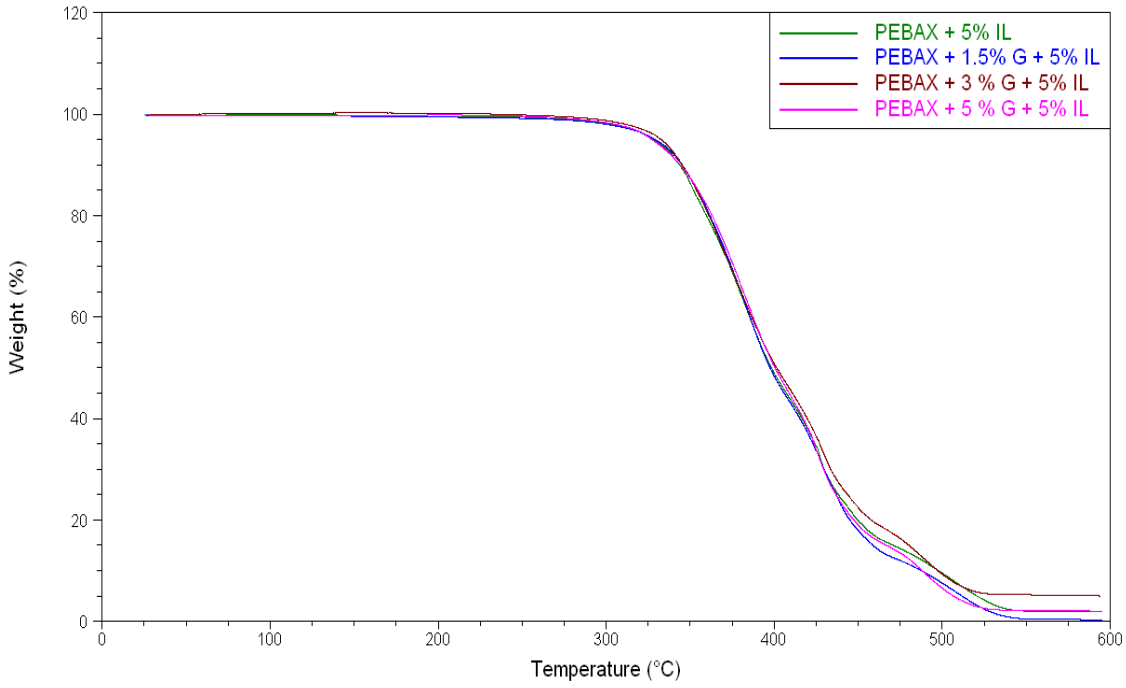

Figure 4.24. *Thermo-gravimetric analysis of the PEBAX and composites made with ionic liquid.*

Are also valid, in this case, the same considerations made previously: there is an increasing of resistance when increase the percentage of graphene. In particular, $T_{95\%}$ is almost the same but on the $T_{50\%}$ there is a difference of 30 °C with the consequence that the ionic liquid changes a lot the stability of the polymer but not from the beginning. Then, in this case, the difference can be noted only after the process of oxidation starts. This is because the ionic liquid is not thermoresistant as the polymer, in fact the polymer domain is not continuous as in the membranes polymer + graphene.

Table 4.21. *Values of $T_{50\%}$ of polymer + graphene + ionic liquid compounds.*

Sample	$T_{95\%}$ [°C]	$T_{50\%}$ [°C]
PEBAX 4533 blank + 5% IL	325.2	395.3
PEBAX 4533 +1.5% G + 5% IL	328.3	398.8
PEBAX 4533 + 3% G + 5% IL	329.2	399.1
PEBAX 4533 + 5% G + 5% IL	329.4	400.0

Finally, joining the ionic liquid, there is a decreasing of the polymer characteristics for both processes, inert one and oxidizing.

4.10 Dynamic Mechanical Analysis (DMA)

This test was performed to determine the characteristics of the blend with variable temperature and in the presence of mechanical stress-dynamics. The test was done only on 3 composites prepared with polymer, polymer + graphene and polymer + graphene + ionic liquid. For this purpose were used cut specimens from the film by the die cutter. As regards the conditions of analysis, it has been set a frequency of 1Hz and solicitation of a constant heating rate of 5 ° C per minute, from -110 ° C to 110 ° C.

From Figure 4.25 it can be seen that in general, at low temperatures, the storage modulus increases when you add the charge, but decreases when you go to add the ionic liquid. However, the effect of the increase that brings graphene is greater than the defect given by the ionic liquid. Furthermore it is observed that in the blend, the storage modulus decreases in the same way, as the temperature increases.

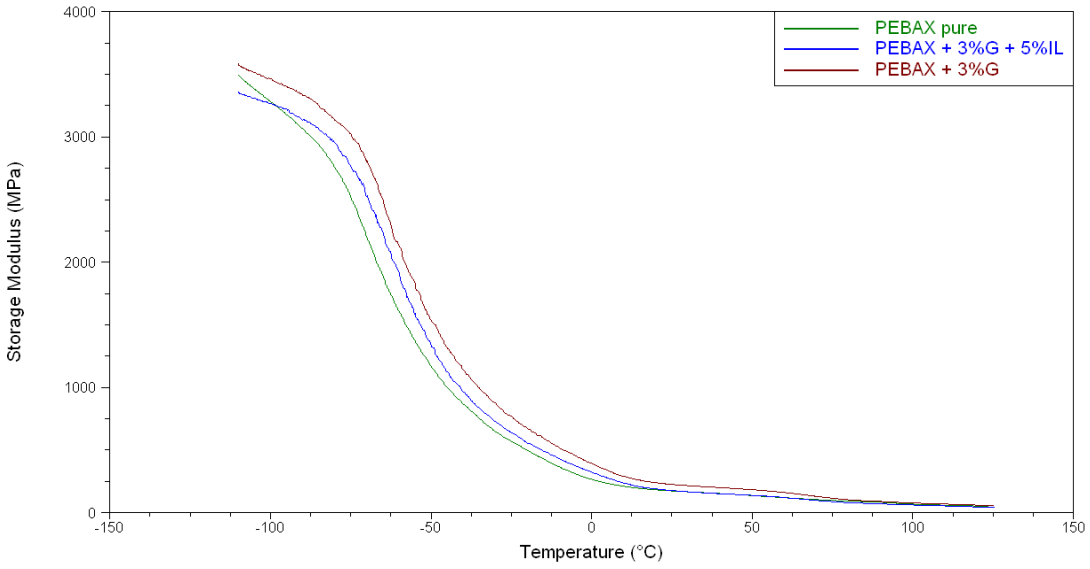

Figure 4.25. *Results of storage modulus versus temperature for the PEBAX and its composites.*

From Figure 4.26 it can be observed that the loss modulus forms a main peak (-60 ° C) at the first Tg of the blend, and that this peak tends to shift at temperatures slightly greater than that one characteristic of PEBAX, with increasing content of graphene. On the other hand, the ionic liquid does slightly decrease the Tg and therefore goes to confirm that, not being a plasticizer, must be to decrease the characteristics of the base polymer.
Also there is the presence of a second peak slightly marked, which is characteristic of the second Tg (70 °C). These observations are also confirmed by the values of Tg shown in table 4.22, derived from the peak of the loss modulus.

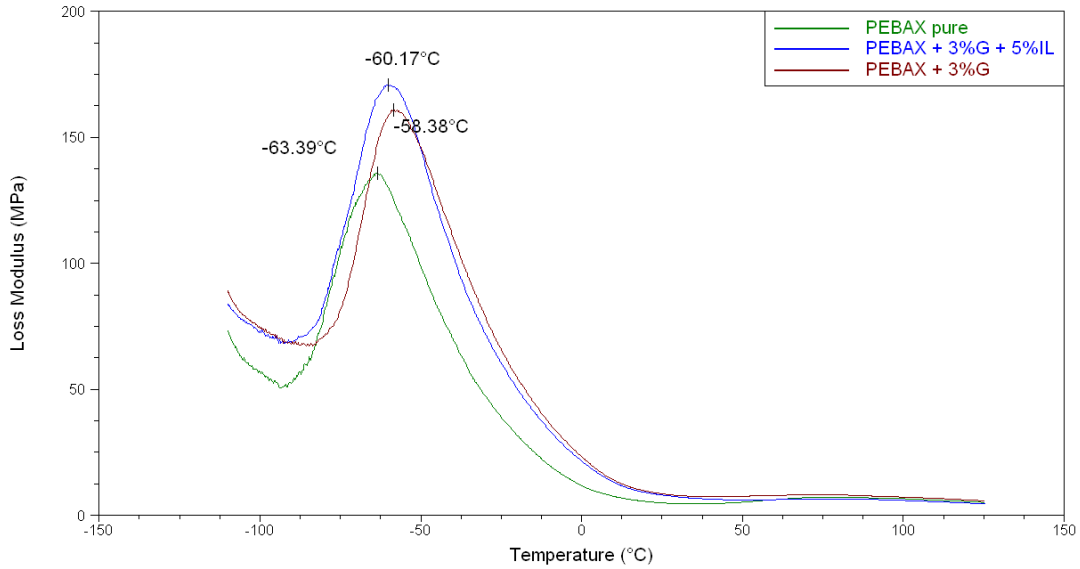

Figure 4.26. *Performance of the loss modulus as a function of temperature for the PEBAX and its composites*

Table 4.22. *Tg values of the PEBAX and its composites, derived from the curve of the loss modulus.*

Sample	**Tg 1 [°C]**
PEBAX pure	-63.39
PEBAX 4533 + 3% G	-60.17
PEBAX 4533 + 3% G + 5% IL	-58.38

4.11 Raman spectroscopy

The technique of Raman spectroscopy is immediate, non-invasive and is widely used to complement other analysis in the identification and quality evaluation of graphene.
The recognition of the monolayer graphene and the determination of the number of layers takes place through the combination of a number of properties of the Raman spectrum mainly concerning the 2D peak which represents the main feature of graphene. The spectra were acquired using a laser of wavelength equal to 532 nm, using a power of 0.5 mW, exposing the sample twice for 30 seconds, using a pinhole aperture of 25 micron and a 100x objective.
The samples characterized were prepared by dispersion in dimethylformamide with 1mg / mL of concentration, after sonication and drying until complete evaporation of the solvent.
Figure 4.27 shows a Raman spectrum of graphene.

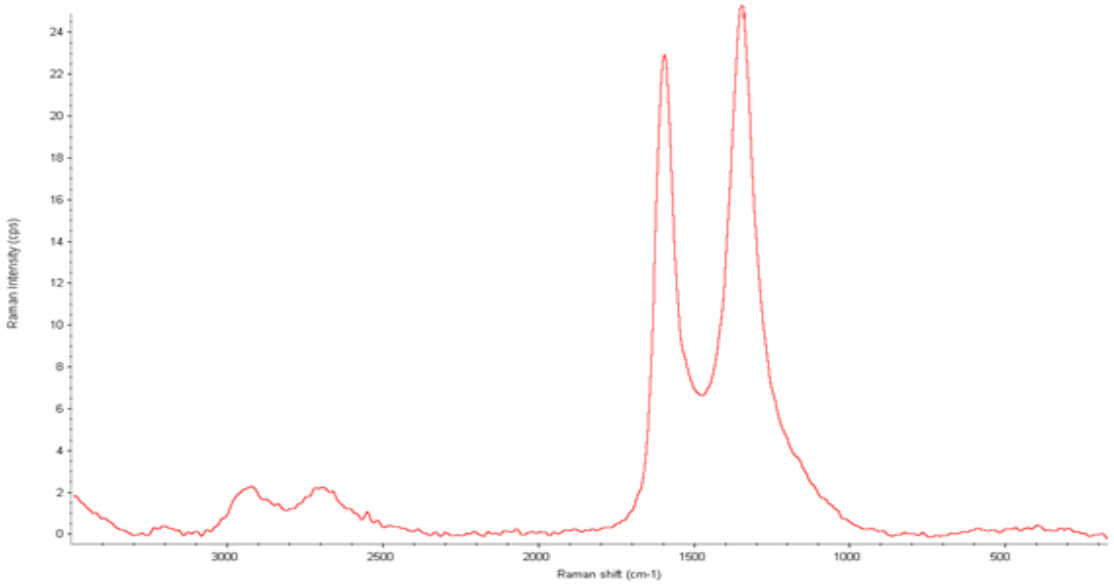

Figure 4.27. *Raman spectrum of Graphene.*

The three main bands of the spectrum are:

- G band: ~ 1582 cm^{-1}, represents the planar configuration sp^2 about carbon-carbon bonds which constitute the graphene. The location of the band is quite independent of the frequency of the incident laser, while it varies depending on the height of graphene analyzed: more are the layers, more the peak moves to lower levels of energy,
- D band: ~ 1350 cm^{-1}, it represents the modal vibration of the aromatic rings sp^2 of carbon, even if the rings have to be adjacent to the edges or to the defects to be active. The band is typically just accentuated by the high-quality graphene. When it is pronounced it means that the material contains a large number of defects is of

chemical type (presence of functional groups unrelated to the graphite structure) is of physical type (for example the edges crumpled),

- 2D band: ~ 2700 cm^{-1}, also called G', is due to the vibration process and to the consequent emission of two phonons, but differently to the D-band it is active only near the defects. The shape and position of this peak are the most distinguishing features for the detection of the number of layers of graphene. The higher is the number of layers of the material, the greater is the characteristic wavenumber. The peak assumes shoulder's shape, typical of the graphite, since the band is not constituted by a single layer of the material as in the ideal case of a monolayer.

The characteristic bands of the Raman spectrum of graphene shown in Figure 4.27, are:
- 2D band little pronounced (compared to the G band) with peak at around 2690 cm^{-1};
- D-band very pronounced;
- The presence of the band at around 2900 cm^{-1}.

These characteristics show that the graphene used consists of many layers, and that the structure is rich in structural defects, which may be physical and chemical.

Conclusions

The thesis realized has provided a survey of experimental type with the purpose of improving some characteristics of Polyether block amide, with the aim of improving the properties of the material for potential gas separation applications.

The study was divided into two main research: in the first, membrane based PEBA were prepared and analyzed with the addition of graphene, with the aim of improving the mechanical and thermal properties of the film. In the latter, with the aim to produce materials with an increase of permeant properties.

As regards the first line of research, the membranes were made by using different concentrations (1.5%, 3% and 5% by weight) of graphene as nanofiller. The samples obtained were characterized by permeability measurements (O_2, CO_2 and water vapor), mechanical tests (tensile tests) dynamic-mechanical (DMA), thermal (DSC and DMA), morphological (SEM and TEM) and X-ray (XRD) analysis.

The permeability measurements showed that the addition of the filler determines a reduction of the film permeability, which is provided by the barrier effect induced by the presence of graphene that, by increasing the path of the gas molecules through the membrane, leads to a decrease of the gas diffusion coefficient within the film without affecting the solubility coefficient. From the morphological point of view, the filler is disposed in the PEBAX matrix like platelets, increasing the tortuosity of the path that the gas molecules must follow during the permeation. In fact, for nanofillers, the barrier effect is related to their degree of exfoliation inside the polymer matrix and, since graphene is characterized by a good degree of exfoliation, the barrier effect is accomplished. However, this effect could be improved by increasing the time of the sonication process for the dispersion of the graphene into the solvent, or changing the sonication methodology by using more effective tools. The mechanical tests have revealed that the addition of filler determines an increase of the elastic modulus of the material and a reduction in ductility, justified by the decrease in elongation at break. As the percentage of graphene increases, there is a progressive increment in the effects just described. By the DSC analysis it was possible to establish the influence of the graphene inside the crystalline structure of PEBAX, in fact the presence of this charge results in a slight increase of the melting temperature. The presence of graphene also has a nucleating effect, even for small loadings, as it promotes the crystallization of the PEBAX and increases the degree of crystallinity of the final polymer seen through analysis of ΔHm_real. Also, by DMA it is possible to see how the graphene affects the thermo-mechanical behavior of the material, in particular the glass transition temperature is increased by a few degrees, as it happens for the melting temperature in DSC. From the two TGA analysis (inert and oxidative

atmosphere), it is possible to observe that the graphene slightly increases the stability of the PEBAX matrix. This effect is more pronounced under oxidative atmosphere, even if are noticed temperature lower than the TGA for an inert environment, by comparing the data for the same percentage of the degraded mass. The latest analysis, useful to fully understand the degree of exfoliation of graphene, were SEM, TEM and XRD. From SEM micrographs it was not possible to obtain particular morphologic information and it has been concluded that the films are very compact and homogeneous. Instead, from the other two, we see how the graphene has undergone a partial exfoliation: TEM images have shown the points where the dispersion is very good and others in which it is practically not present, while XRD diffractograms have shown that by increasing the percentage of graphene there is a lower degree of exfoliation in the matrix.

Instead, as regards the second line of research, the membranes were made by addition of a ionic liquid (Bmim-TSFI) to 5% by weight. The samples obtained were characterized by permeability measurements permeability (O_2, CO_2 and water vapor), mechanical analysis (test-drive the scale), dynamic-mechanical (DMA), thermal (DSC and DMA), morphological (SEM and TEM) and X-ray (XRD). The permeability measurements showed that the addition of the ionic liquid increases the permeability of the films, due to an increase in the solubility coefficient (S), and the diffusion coefficient (D) remaining unchanged if compared to the one of membranes already analyzed in the first line of research. Therefore, the ionic liquid is responsible for the increase of permeability because, since it has a chemical conformation which is affine to the passage of gas molecules, it allows the increase of the absorption about CO_2 and O_2 molecules. From the morphological point of view, the liquid is probably dispersed, in the matrix of PEBAX, on the form of small drops. The mechanical tests have revealed that the addition of ionic liquid results in a decrease of the elastic modulus of the material and a reduction in ductility, justified by the decrease in break elongation. These effects are all due because the ionic liquid is not a plasticizer such as polymers. By the DSC analysis it was possible to establish the influence of the ionic liquid on the membranes properties , in fact the presence of liquid causes a decrease of the melting temperature. Also, by DMA it has been seen how there is an effect on the glass transition temperature which decrease by a few degrees, as it happens for the melting temperature in the DSC. From the two TGA analysis, in inert and oxidative atmosphere, it has been shown that the ionic liquid decreases the stability of the PEBAX basis, always for the same reason mentioned before. This happens more in the oxidative atmosphere, by comparing the data for the same percentage of the mass loss. From the latest analysis, SEM, TEM and XRD, no particular conclusions can be drawn. SEM and TEM images do not clearly show the presence of the ionic liquid, which can be seen in the XRD diffractogram: there are no peaks associable to the presence the liquid, but it goes to vary the background inside the response to X-ray analysis.

Finally, it is possible to conclude that the effect of the ionic liquid is balanced by the effect of graphene: the first considerably increases the gas permeability, with the disadvantage that the mechanical-thermal properties of the base polymer will experience a decline. On the other hand graphene is useful to improve such properties, having a barrier effect almost negligible compared to the increase of permeability due from the ionic liquid. In summary, the addition of the nanofiller improves the structure and the resistance of the membrane while the ionic liquid decreases the properties, however, increasing the permeability.

Possible future developments might be to carry out an analysis of the membranes permeability to CH_4 and H_2S to understand what are the best applications for such membranes, as well as perform an analysis of selectivity to understand how separation takes place in a stream not pure. When these data will be available, it would be possible to verify the performance of such membranes and to understand possibility of the production of a small pilot plant.
Possible future applications, depending on the data in output, could be the purification of air and natural gas, on the basis of the comprehensive study realized for which these applications were defined as main targets of start for the development of the thesis project.

Nomenclature

P = permeability ($cm^3 \cdot mm/(m^2 \cdot day \cdot bar)$)

D = Fick diffusion coefficent (mm^2/s)

S = solubility coefficent ($cm^3/(cm^3 \cdot atm)$)

J = permeating gas flow ($cm^3/(m^2 \cdot day)$)

ΔP = pressure gradient (bar)

l = tickness (mm)

Q(t) = total amount (per unit area) of diffuse substance that has passed through the film over time t (cm^3/m^2); mathematically it is the integral over time of the magnitude gas TR

t = time (s)

d1,2,3 = interplanar distance (Å)

Greek letters:

θ = time-lag (s)

λ = wavelength (Å)

θ1,2,3 = angle between the diffracted light and the crystal plane (rad)

References

[1] S. M. Javaid Zaidi (2010). Removal of Acid gases from Natural Gas Streams by Membrane Technology, *Chemical Engineering Department and Centre of Excellence in Renewable Energy King Fahd University of Petroleum & Minerals, Dhahran-31261, Saudi Arabia.*

[2] Bernardo P., G. Clarizia (2013). 30 Years of Membrane Technology for Gas Separation, *Istituto di Ricerca per la Tecnologia delle Membrane, ITM-CNR, Italy.*

[3] Permeability Diffusivity And Solubility Of Gas And Solute Through Polymers, *chapter 4*.

[4] S.W. Rutherford and D.D. Do (1996). Review of Time Lag Permeation Technique as a Method for Characterization of Porous Media and Membranes, *Department of Chemical Engineering, The University of Queensland, Brisbane, Australia*.

[5] Rossini S. (2012). Acido Polilattico (PLA): miglioramento delle proprietà barriere e sviluppo di composti ecosostenibili, *Tesi di Laurea in Ingegneria Chimica e dei Processi Industriali, Università di Padova.*

[6] Duncan B., Urquhart J. and Roberts S (2005). Review of Measurement and Modelling of Permeation and Diffusion in Polymers, *National Physical Laboratory. Teddington. United Kingdom.*

[7] T. Ramanathan, A. A. Abdala, S. Stankovich, D. A. Dikin1, M. Herrera-Alonso, R. D. Piner1, D. H. Adamson, H. C. Schniepp, X. Chen1, R. S. Ruoff1, S. T. Nguyen, I. A. Aksay, R. K. Prud'Homme & L. C. Brinson (2008), Functionalized graphene sheets for polymer nanocomposites. Nature Nanotechnology **3**, 327 – 331

[8] JenniferChih-YiChen (2002), Evaluation of Polymeric Membranes for Gas Separation Processes: Poly(ether-b-amide) (PEBAX 4533) BlockCopolymer. *University of Waterloo,Ontario,Canada.*

[9] Vajiheh Nafisi, M.T. Guzman Gutierrez, May-Britt Hägg (2013), Development of novel nanocomposite membrane for CO_2 capture. *Norwegian University of Science and Technology.*

[10] Sabu Thomas,Visakh P.M. (2012), Handbook of Engineering and Specialty Thermoplastics, Nylons. *Salem, India.*

[11] Thierry Le Hénaff, Arkema company. *Colombes, France.*

[12] Jennifer C. Chen, Xianshe Feng and Alexander Penlidis (2010), Gas Permeation Through Poly(Ether-b-amide) (PEBAX 4533) Block Copolymer Membranes, Separation Science and Technology. *Department of chemical engineering, University of Waterloo, Ontario, Canada.*

[13] Ingo Blume, Ingo Pinnau (1990). Composite membrane, method of preparation and use. *Membrane Technology & Research, Inc.*

[14] Damien M. Marquis, Éric Guillaume and Carine Chivas-Joly (2005). Properties of Nanofillers in Polymer, *Laboratoire national de métrologie et d'essais (LNE) France.*

[15] Novoselov, K. S., A. K. Geim (2007). The rise of graphene. Nature Materials, **6**, 183 - 191.

[16] Novoselov, K. S., A. K. Geim, S. V. Morozov, D. Jiang, Y. Zhang, S. V. Dubonos, I. V (2004). Grigorieva, A. A. Firsov. Electric field effect in atomically thin carbon films. Science,**306**,666–669.

[17] Novoselov, K.S., D. Jiang, F. Schedin,T. J. Booth, V. V. Khotkevich, S. V. Morozov e A. K. Geim (2005). Two-dimensional atomic crystals. Proceedings of the National Academy of Sciences USA, **102**, 10451 (2005).

[18] Geim, A.K., (2009). Graphene: Status and Prospects. Science, **324**, 1530-1534.

[19] Novoselov, K. S., A. K. Geim, S.V. Morozov, D. Jiang, M.I. Katsnelson, I.V. Grigorieva, S. V. Dubonos e A. A. Firsov (2005). Two-dimensional gas of massless Dirac fermions in graphene. *Nature*, **438**, 197-200.

[20] Lee, C., X. Wei, L. Qunyang, R. Carpick, J. W. Kysar, J. Hone (2009). Elastic and frictional properties of graphene. *Physica Status Solidi*, **246**, 2562-2567.

[21] Faccio, R., L. Fernández-Werner, H. Pardo, C. Goyenola, P. A. Denis e Á. W. Mombrú (2011). Mechanical and Electronic Properties of Graphene Nanostructures, (InTech ed.), Montevideo (Uruguay).

[22] Lee, C., X. Wei, J. W. Kysar, J. Hone (2008). Measurement of the Elastic Properties and Intrinsic Strength of Monolayer Graphene. *Science,* **321**, 385 .

[23] Jiang, J.W., J.S. Wang e B. Li (2009). Young's modulus of graphene: A molecular dynamics study. *Physical Review B,* **80**, 113405.

[24] Ranjbartoreh, A.R., B. Wang, X. Shen e G. Wang. Advanced mechanical properties of graphene paper. *Journal of Applied Physics,* **109**, 014306.

[25] Kuzmenko, A.B., E. van Heumen, F. Carbone e D. van der Marel (2008). Universal Optical Conductance of Graphite. *Physical Review Letters,* **100**, 117401.

[26] Bonaccorso, F., Z. Sun, T. Hasan e A.C. Ferrari (2010). Graphene photonics and optoelectronics. Nature Photonics, **4**, 611.

[27] Bao, Q., H. Zhang,Y. Wang, Z. Ni, Y. Yan, Z.X. Shen, K.P. Loh e D.Y. Tang (2009). Atomic-Layer Graphene as a Saturable Absorber for Ultrafast Pulsed Lasers. *Advanced Functional Materials,* **19**, 3077.

[28] Nair, R.R., P. Blake, A. N. Grigorenko, K.S. Novoselov, T.J. Booth, T. Stauber, N.M.R. Peres e A.K. Geim (2008). Fine Structure Constant Defines Visual Transparency of Graphene. *Science,* **320,** 1308.

[29] Bruna, M. e S. Borini (2009). Optical constants of graphene layers in the visible range. *Applied Physics Letters,* **94**, 031901.

[30] K. S. Novoselov (2011). Nobel Lecture: Graphene: Materials in the Flatland. *Reviews of Modern Physics,* **83**, 838.

[31] Seol, J.H., I. Jo, A.L. Moore, L. Lindsay, Z.H. Aitken, M.T. Pettes, X. Li, Z. Yao, R. Huang, D. Broido, N. Mingo, R.S. Ruoff e L. Shi (2010). Two-Dimensional Phonon Transport in Supported Graphene. *Science,* **328**, 213.

[32] Zhu, Y., S. Murali, W. Cai, X. Li, J.W. Suk, J. R. Potts e R.S. Ruoff (2010). Graphene and Graphene Oxide: Synthesis, Properties, and Applications. *Advantage Materials,* **22**, 3906.

[33] Saito, K., J. Nakamura e A. Natori (2007). Ballistic thermal conductance of a graphene sheet. *Physical Review B,* **76**, 115409.

[34] Leenaerts, O., B. Partoens e F. M. Peeters (2008). Adsorption of H_2O, NH_3, CO, NO_2, and NO on graphene: A first-principles study. *Physical Review B,* **77**, 125416.

[35] Zhang, Y.H., Y.B. Chen, K.G. Zhou, C.H. Liu, J. Zeng, H.L. Zhang e Y. Peng (2009). Improving gas sensing properties of graphene by introducing dopants and defects: a first-principles study. *Nanotechnology,* **20**, 185504.

[36] Stankovich, S., D. A. Dikin, G.H. B. Dommett, K.M. Kohlhaas, E.J. Zimney, E.A. Stach, R.D. Piner, S.T. Nguyen e R. S. Ruoff (2006). Graphene-Based Composite Materials. *Nature,* **442**, 282.

[37] Schedin, F., A. K. Geim, S.V. Morozov, E.W. Hill, P. Blake, M.I. Katsnelson e K. S. Novoselov (2007). Detection of individual gas molecules adsorbed on graphene. *Natur,* **6**, 652.

[38] Ratinac, K.H., W. Yang, S.P. Ringer e F. Braet (2010). Toward Ubiquitous nvironmental Gas Sensors. *Environmental Science Technology,* **44**, 1167.

[39] Dutta, P. e P.M. Horn (1981). Low-frequency fluctuations in solids: 1/f noise. *Reviews of Modern Physics,* **53**, 497.

[40] Ko, G., H.Y. Kim, J. Ahn, Y.M. Park, K.Y. Lee e J. Kim (2010). Graphene- based nitrogene dioxide gas sensors. *Current Applied Physics,* **10**, 1002-1004.

[41] Lorena Vidala, b, Marja-Liisa Riekkolaa, Antonio Canalsb (2012). Ionic liquid-modified materials for solid-phase extraction and separation: A review. *Analytica Chimica Acta.*

[42] Branco, L. C.; Crespo, J. G.; Afonso, C. M. Highly selective transport of organic compounds by using supported liquid membranes based on ionic liquids. Angew. Chem., Int. Ed. 2002, **41**, 2771–2773.

[43] Branco, L. C.; Crespo, J. G.; Afonso, C. M. Studies on the selective transport of organic compounds by using ionic liquids as novel supported liquid membranes. Chem.—Eur. J. 2002, **8**, 3865–3871.

[44] V. Salles, L. Seveyrat, T. Fiorido, L. Hu, J. Galineau, C. Eid, B. Guiffard, A. Brioude1 and D. Guyomar (2012). Synthesis and Characterization of Advanced Carbon-Based Nanowires – Study of Composites Actuation Capabilities Containing These Nanowires as Fillers. *Nanotechnology and Nanomaterials, Nanowires - Recent Advances. Chapter 13.*

[45] Ling, C., Gabriel Setzler, M.W. Lin e K. Dhindsa (2011). Electrical transport properties of grapheme nanoribbons from sonicatin graphite in solution. Nanotechnology, **22**, 325-501

[46] Tung, V.C., M.J. Allen, Y. Yang e R.B. Kaner (2009). High-throughput solution processing of large-scale graphene. Nature Nanotechnology, **4**, 25-29.

[47] Hernandez,Y., V. Nicolosi, M. Lotya, F.M. Blighe,Z. Sun,S. De, I.T. McGovern, B. Holland, M.Byrne, Y.K.Gun'ko, J. J. Boland, P. Niraj, G. Duesberg, S. Krishnamurthy, R.Goodhue, J. Hutchison, V. Scardaci, A.C. Ferrari e J.N. Coleman (2008), High-Yield Production of Graphene by Liquid-Phase Exfoliation of Graphite. Nature Nanotechnology, **3**, 563–568.

[48] Blake, P., P.D. Brimicombe, R.R. Nair, T.J. Booth, D. Jiang, F. Schedin, L.A. Ponomarenko, S.V. Morozov, H. F. Gleeson, E.W. Hill, A.K. Geim e K.S. Novoselov, (2008). Graphene-based liquid crystal device. Nano Lett, **8**, 1704–1708. 46. Park, S., J. An, I. Jung, R.D. Piner, S.J. An, X.S. Li, A. Velamakanni e R.S. Ruoff (2009). Colloidal Suspensions of Highly Reduced Graphene Oxide in a Wide Variety of Organic Solvents. Nano Lett,**9**, 1593–1597.

[49] Khan, U., A. O'Neill, M. Lotya, S. De e J.N. Coleman, (2010). High-Concentration Solvent Exfoliation of Graphene. Small, **6**, 864–871.

[50] Hernandez, Y., M. Lotya, D. Rickard, S.D. Bergin e J.N. Coleman (2009). Measurement of multicomponent solubility parameters for graphene facilitates solvent discovery. ACS Nano, **26**, 3208–3213.

[51] Khan, U., H. Porwal, A. O'Neill, K. Nawaz, P. May e J. N. Coleman,(2011). Solvent-Exfoliated Graphene at Extremely High Concentration. Langmuir, **27**, 9077–9082.

[52] Hamilton, C.E., J.R. Lomeda, Z. Sun, J. M. Tour e A.R. Barron, (2009). High-Yield Organic Dispersions of Unfunctionalized Graphene, Nano Letters, **9**, 3460-3462.

[53] Coleman, J. N. (2012). Liquid Exfoliation of Defect-Free Graphene, Journal of American Chemical Society, **46**, 14-22.

[54] Zhao, W., F. Wu, H. Wu, e G. Chen (2010). Preparation of Colloidal Dispersions of Graphene Sheets in Organic Solvents by Using Ball Milling, Journal of Nanomaterials,

[55] Lotya, M., Y. Hernandez, P.J. King, R. J. Smith, V. Nicolosi, L.S. Karlsson, F.M. Blighe, S. De, Z. Wang, I. T. McGovern, Georg S. Duesberg e J.N. Coleman (2008). Liquid Phase Production of Graphene by Exfoliation of Graphite in Surfactant/Water Solutions, Journal of American Chemical Society, **131**, 3611-3620.

[56] O'Neill, A., U. Khan, P.N. Nirmalraj, J.J. Boland e J.N. Coleman (2011). Graphene dispersion and exfoliation in low boiling point solvents. J. Phys. Chem., **115**, 5422–5428.

[57] Lotya, M., P.J. King, U. Khan, S. De e J.N. Coleman (2010). High concentration, surfactant-stabilized graphene dispersions, ACS Nano, **4**, 3155–3162.

[58] Hao,R., W. Qian, L. Zhanga e Y. Hou (2008). Aqueous dispersions of TCNQ-anion-stabilized graphene sheets, Chem. Commun, 6576–6578.

[59] Vadukumpully, S., J. Paul, S. Valiyaveettil (2009). Cationic surfactant mediated exfoliation of graphite into graphene flakes, Carbon, **47**, 3288–3294.

[60] Ramanathan, T., A.A. Abdala, S. Stankovich, D.A. Dikin, M.H. Alonso, R.D. Piner, D. H. Adamson, H.C. Schniepp, X. Chen, R.S. Ruoff, S.T. Nguyen, I.A. Aksay, R.K. Prud'Homme e L.C. Brinson (2008). Functionalized graphene sheets for polymer nanocomposites. Nat. Nanotechnol., **3**, 327–331.

[61] Dikin, A.K., S. Stankovich, E.J. Zimney, R.D. Piner, G.H.B. Dommett, G. Evmenenko, , G. Evmenenko, S.T. Nguyen e R.S. Ruoff, (2007). Preparation and characterization of graphene oxide paper. Nature, **448**, 457–460.

[62] McAllister, M.J., J.L. Li, D.H. Adamson, H.C. Schniepp, A.A. Abdala, J. Liu, M.H. Alonso, D.L. Milius, R. Car, R.K. Prudhomme e I.A. Aksay (2007) Single sheet functionalized graphene by oxidation and thermal expansion of graphite. Chem.Mater, **19**, 4396–4404.

[63] Singh, V., D. Joung, L. Zhai, S.Das, S. I. Khondaker e S. Seal (2011). Graphene based materials: Past, present and future. *Progress in Materials Science*, **56**, 1178–1271.

[64] Kuilla, T., S. Bhadra, D. Yao, N.H. Kim, S. Bose e J.H.Lee (2010). Recent advances in graphene based polymer composites. *Progress in Polymer Science*, **35**,1350–1375.

[65] Das, T.K. e S. Prusty (2013). Graphene-Based Polymer Composites and Their Applications. *Polymer-Plastics Technology and Engineering*, **52**,319-331.

[66] Potts, J.R., D.R. Dreyer, C.W. Bielawski e R.S. Ruoff (2011). Graphene-based polymer nanocomposites. *Polymer*, **52**, 5-25.

Acknowledgements

I would first like to thank my parents for the financial and moral support in all these long years of university.
I thank Prof. Michele Modesti for giving me the opportunity to do this work and all those who helped me in the realization of the thesis: the university "The Petroleum Institute" to allow this internship, defining the technical objectives and making available the resources needed to achieve them. In particular, I would like to thank Prof. Vikas Mittal and Mr. Gigi George for their supervision and responsibility.
Finally, I thank all the people I met in these months at the laboratory with whom I spent a pleasant time, and all the friends with whom I shared the university experience.